NEUROPROSTHETIC DEVICES: INPUTS AND OUTPUTS

by

Kip A. Ludwig

A dissertation submitted in partial fulfillment
of the requirements for the degree of
Doctor of Philosophy
(Biomedical Engineering)
in The University of Michigan
2009

Doctoral Committee:
Professor Daryl R. Kipke, Chair
Professor David C. Martin
Emeritus Professor David J. Anderson
Assistant Professor Michael Mayer

DEDICATION

For my brother, Christopher Patrick Ludwig (1962-2006); perhaps the first science project I've completed without his guidance.

ACKNOWLEDGMENTS

Daryl Kipke has allowed me the freedom and resources to pursue my own scientific ideas unfettered. I am grateful for the understanding he displayed during several traumatic family events that occurred during the course of my research, forcing me to leave the lab for weeks and even months at a time to deal with these issues. His advice during each of these events: "Don't even think about lab; just take care of your family. We can take care of your research when you get back." In addition I'd like to thank my committee, Dr. Martin, Dr. Anderson, and Dr. Mayer, for their time and effort.

There are many individuals in the Neural Engineering Lab I would like to thank, but none more so than Nick Langhals. Nick has been my sounding board for the last six years, helping me refine my ideas, and always supplementing them with ideas of his own. Nick is always there to help with an experiment, a review of your paper, a computer problem… the list is truly endless. Most importantly, he has been a stalwart friend through some of the most trying experiences of my life. I don't know how I would have gotten this done without him, and in that respect, my PhD is also partially his.

My mentors in lab were Kevin Otto and Rio Vetter. Both have always taken an interest in my development, and were always there with advice when I needed it - and a cold beer when I didn't. I couldn't have been more fortunate to work in the same lab with Kevin

and Rio.

Rachel Miriani also deserves special thanks. Rachel has worked with me on most of my experiments – and lord knows I can be stubborn about experiments. She has been a good friend and a good lab partner, and has always been there to help with the experiment, the paper, the paper work, or the latest family emergency.

I'd like to thank all of the members of the Kipke mafia: John Seymour, Matt Johnson, Jeff Uram, Greg Gage, Tim Marzullo, Hirak Parikh, Erin Purcell, Elizabeth Nunamaker-Otto, Jey Subbaroyan, Taegyun Moon, and Brooks Gross. Each of you contributed in ways both large and small, and helped me keep my sanity during the bad times. I wish I could go into more detail here, but the way in which all of you helped has been enormous.

More recently, I'd like to specifically thank Mike Joseph, Matt Gibson, Mohammad Abidian, and Sarah Richardson-Burns. Mike - thanks for your experimental help, your editing, and giving me motivation to get back in lab. Matt – you are an incredibly impressive scientist, and just a good person. I've appreciated all of our conversations, and all of the time you've spent thoughtfully reviewing my work. I have high hopes for the future of our lab thanks to you and Mike. Mohammad – thank you for all of your advice regarding my dissertation, papers, and future plans. Sarah Richardson-Burns – I've truly enjoyed working with you on the Biotectix contract; your conversations have helped me refine my thoughts on the future of microelectrode recording technology.

Finally, I'd like to acknowledge the loving support of my family and my girlfriend Sarah Moyer (hopefully soon fiancée). Sometimes it's hardest to properly thank those that are closest to you, simply because the list of ways they've helped is too long.

TABLE OF CONTENTS

LIST OF FIGURES

LIST OF APPENDICES

ABSTRACT

Prior studies have demonstrated that the firing rate of cortical neurons can be volitionally modulated by a subject to generate a controllable output signal; this neural output signal can then be manipulated to direct a robotic arm, a cursor on a computer screen, or other interface device. The burgeoning field of neural control has led to a number of innovative applications, known more commonly as neuroprosthetic devices. Neuroprosthetic devices have the potential to return some degree of functionality to the over 250,000 Americans with incapacitating spinal cord injuries, or allow healthy subjects to control electronic devices in their everyday lives. The research presented here consists of three studies focused on improving the current generation of neuroprosthetic devices.

In the first study, we introduced and evaluated a Bayesian maximum-likelihood estimation (bMLE) strategy to identify optimized training data for neuroprosthetic devices. By limiting initial decoding assumptions and training only on relevant neural data, accurate neural-control was possible with as few as two neurons, using minimal training data and no *a-priori* movement measurements for calibration. Moreover, implanted subjects obtained useful prosthetic control using local field potentials and neurons from cingulate cortex as input.

In the second study, we refined a method to electrochemically deposit surfactant-templated ordered poly(3,4-ethylenedioxythiophene) (PEDOT) films on the recording sites of standard "Michigan" probes, and evaluated the *in vivo* efficacy of these modified sites in recording chronic neural activity. PEDOT sites were found to outperform control sites in terms of signal-to-noise ratio and number of viable unit potentials - thereby improving the quality of neural input sources to the neuroprosthetic device.

In the third study, we evaluated a technique known as common average referencing (CAR) to generate a more ideal reference electrode for microelectrode recordings. CAR was found to drastically outperform standard types of electrical referencing, reducing noise by more than 30 percent. As a result of the reduced noise floor, arrays referenced to a CAR yielded almost 60 percent more discernible neural units than traditional methods of electrical referencing – again improving the quality of neural input sources to a neuroprosthetic device.

CHAPTER 1
INTRODUCTION

Implantable cortical electrodes designed to record both action potentials from individual neurons as well as aggregate synaptic potentials are integral to a number of clinical and research applications (Brown et al. 1998; Dobelle 2000; Fetz and Finocchio 1975; Gage et al. 2005; Georgopoulos et al. 1986; Kargo and Nitz 2003; Nicolelis et al. 1995; Schwartz and Moran 2000; Taylor et al. 2002a). Studies have demonstrated that variations in the cortical neural firing rates recorded from an implanted subject can be used to predict characteristics of a subject's motor movement (Georgopoulos et al. 1986; Moran and Schwartz 1999b; Nicolelis et al. 1995; Paninski et al. 2004; Schwartz and Moran 2000; 1999), delivered somatosensory stimuli (Cattaneo et al. 1981a; b; Eggermont 1976; 1979; Eggermont et al. 1981; Epping and Eggermont 1986; Furukawa et al. 2000; Hermes et al. 1982; Middlebrooks et al. 1980; Middlebrooks and Knudsen 1984; Prijs and Eggermont 1981; Xu et al. 1999), or a subject's location in space (Barbieri et al. 2005; Brown et al. 2002; O'Keefe and Dostrovsky 1971). Moreover, the firing rate of cortical neurons can be volitionally modulated by a subject to generate a controllable output signal (Anderson et al. 2004; Carmena et al. 2003; Gage et al. 2005; Kennedy et al. 2000; Schwartz 2004; Serruya et al. 2002; Taylor et al. 2002a; Wolpaw et al. 2002); this neural output signal can then be manipulated to direct a robotic arm, a

cursor on a computer screen, or other interface device. The burgeoning field of neural control has led to a number of innovative applications, more commonly known as neuroprosthetic devices (NPDs). NPDs have the potential to return some degree of functionality to the over 250,000 Americans with incapacitating spinal cord injuries, or allow healthy subjects to control electronic devices in their everyday lives (Barnes et al. 2003).

Overview

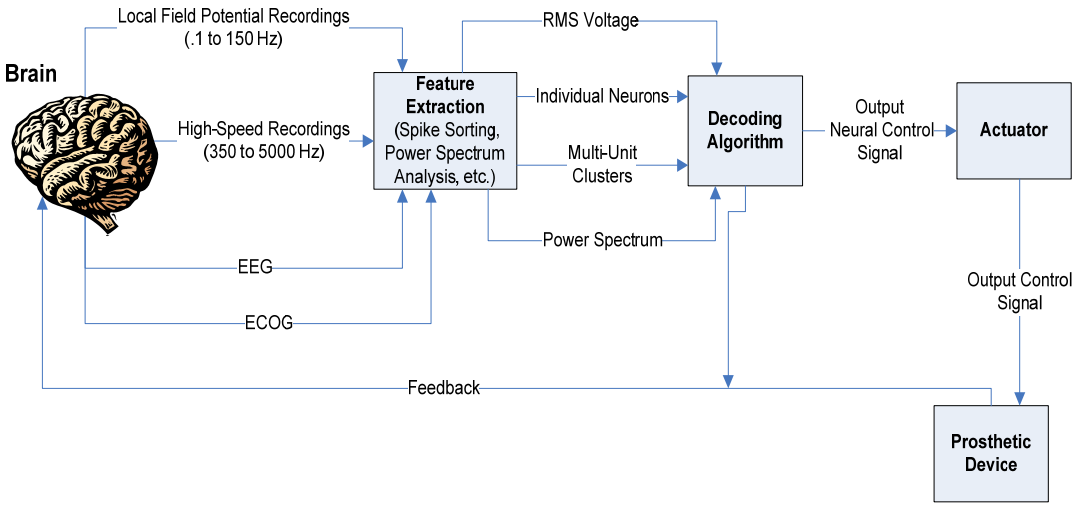

Figure 1.1: Taxonomy of a Standard Neuroprosthetic Device (NPD)

The ultimate goal of the work outlined for this dissertation is to increase the effectiveness of current generation neuroprosthetic devices (NPD). A standard NPD can be divided into four separate stages (See Figure 1.1). First, the neural activity from various sources in the brain is translated into a recorded electrical signal through a microelectrode. Next, the recordings are sent through a Feature Extraction Algorithm to reduce the neural recordings into input parameters considered relevant to a NPD. High-speed recordings

are typically reduced to individual or multi-unit neuronal firing rates, whereas local field potentials, ECoG, and EEG recordings are primarily translated into RMS voltage or segmented into power across specific frequency bands. Third, the extracted neuronal features of interest are decoded into a neural output control signal, most commonly by obtaining an *a priori* map of the linear relationship between the extracted neural features and a movement parameter. Finally, the neural output control signal is transformed into an electrical signal suitable for driving a neural prosthetic device. Improvements to NPDs are generally made by making modifications at one of these four stages.

Historical Development of Microelectrode Technology

In practice, chronic intracellular recording is difficult due to the small size of neurons and the motion of the brain. In the 1950s, a long-term extracellular recording technique was developed that allowed the electrode to remain in the extracellular fluid surrounding the neuron and record local micro-fluctuations in potential due to action potential propagation (Strumwasser 1958). Consequently, there was reduced difficulty in neural recordings because extracellular recordings do not require precise contact with a neuron, and therefore cause less disruption to the neuron in chronic preparations.

Numerous surgical implantation techniques have enabled long-term recording from multiple neurons. The first successful chronic electrode arrays consisted of many insulated microwires, cut to expose the cross-sectional surface area of the end of the wire (Olds et al. 1972), or etched to a sharpened tip (Burns et al. 1974; Marg and Adams 1967). Due to the inherent variability in the manufacture of microwires, this technology is ill-suited for systematic investigation into which electrode electrical characteristics

influence chronic recording performance. Moreover, the long-term capabilities are limited for microwires, as their recordings have been found to deteriorate after only a couple of weeks post-implantation (Williams et al. 1999).

Wise et al. introduced photoengraved microelectrodes for single unit recording in 1970 (Wise et al. 1970). These devices had several advantages over microwire technology, including the ability to span and record from multiple cortical layers simultaneously. Due to the ease of photolithography techniques, many different device geometries and parameters could be reliably reproduced (Bragin et al. 2000; Johnson et al. 2005; Kewley et al. 1997; Maynard et al. 1999; Selim Suner 2005; Vetter et al. 2004a).

At present, there are three primary microelectrode technologies used to obtain the neural recordings that drive modern day neuroprosthetic devices: microwire arrays, microelectrode arrays, and the 'Michigan' probe (Figure 1.2) (Polikov et al. 2005; Schwartz 2004). Current microwire arrays do not deviate much from their predecessors of the 1950's and 60's, typically consisting of multiple insulated stainless steel or tungsten wires with a small area at the tip stripped of insulation to act as the recording electrode (Figure 1.2a). Locating the recording site at the tip of the electrode has been speculated to increase the viewing radius of the site, as well as place the recording site in the area of least tissue damage (Polikov et al. 2005; Schwartz 2004). Microwires are perhaps the easiest and least expensive to manufacture, and have the longest history of experimental use. However, microwires cannot be manufactured with reliable consistent geometries and recording site locations, and their large size relative to other available

recording technologies (typically 30-50 microns in diameter) can cause additional damage upon implantation.

Silicon microelectrode arrays, such as the ones developed at the University of Utah, have many similarities to microwire arrays (Figure 1.2b). Instead of consisting of spaced microwires, the Utah arrays consists of 100 evenly spaced microneedles extending 1.0-1.5 millimeters from a 4x4 square base. Like microwires, recording sites – typically platinum or iridium – are located at the tip of each needle. Unlike microwires, the silicon fabrication process allows for greater specificity in manufacturing site spacings, geometries, and electrical characteristics.

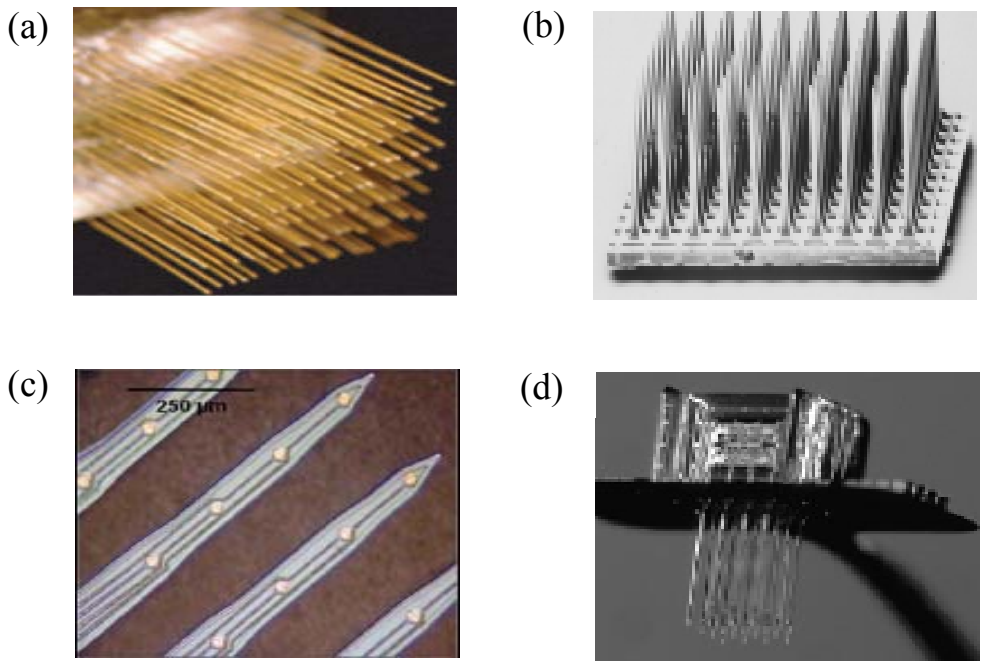

Figure 1.2: Current Microelectrode Designs. Examples of (a) a microwire array (Nicolelis et al. 2003), (b) The Utah array (Rousche and Normann 1998), (c) the 'Michigan' array (Vetter et al. 2004b) and (d) a three-dimensional silicon array (Bai et al. 2000)

Perhaps the most flexible of the three modern recording technologies is the 'Michigan' probe (Figure 1.2c). Based off of the earlier work of Ken Wise, photolithographic

techniques developed at the University of Michigan can be used to specify probe geometries, spacings, site sizes, and electrical characteristics with a remarkable degree of precision (Wise et al. 1970; Drake et al. 1988; Vetter et al. 2004b). Using these techniques, probes have been constructed which can densely sample at multiple cortical depths (Blanche et al. 2005), minimize the size of the implanted probe to decrease tissue damage (Seymour and Kipke 2007), or manufacture a three-dimensional assembly capable of sampling neural tissue across multiple cortical depths and locations simultaneously (Figure 1.2d) (Bai et al. 2000; Hoogerwerf and Wise 1994).

Basic Electrode Theory

Electrodes intended to stimulate and record neural activity in the brain must efficiently transduce ionic current of brain tissue to the electric current generated by the movement of charge through wiring. To accomplish this feat, electrodes are made of metals which undergo two primary chemical reactions immediately upon being placed in an ionic solution. First, metal atoms from the electrode dissociate into positively charged metal cations and free electrons at the electrode/electrolyte interface. Secondly, ions in the tissue pick up these free electrons to become negatively charged anions (Bard and Faulkner 1980; Gileadi et al. 1975; Merrill et al. 2005; Randles 1947). Through these two reversible reactions, electric charge from the electrode is delivered to the ionic medium of the brain, and vice-versa (Figure 1.3).

Depending on the concentration of cations already in the tissue and the activity of the metal, one of these two reactions becomes dominant until an equilibrium condition is established. The dominant reaction causes the local concentration of both cations and

anions to change with respect to distant tissue. A local charge gradient develops, known as a half-cell or open circuit potential. Bioelectric potentials, such as those generated by

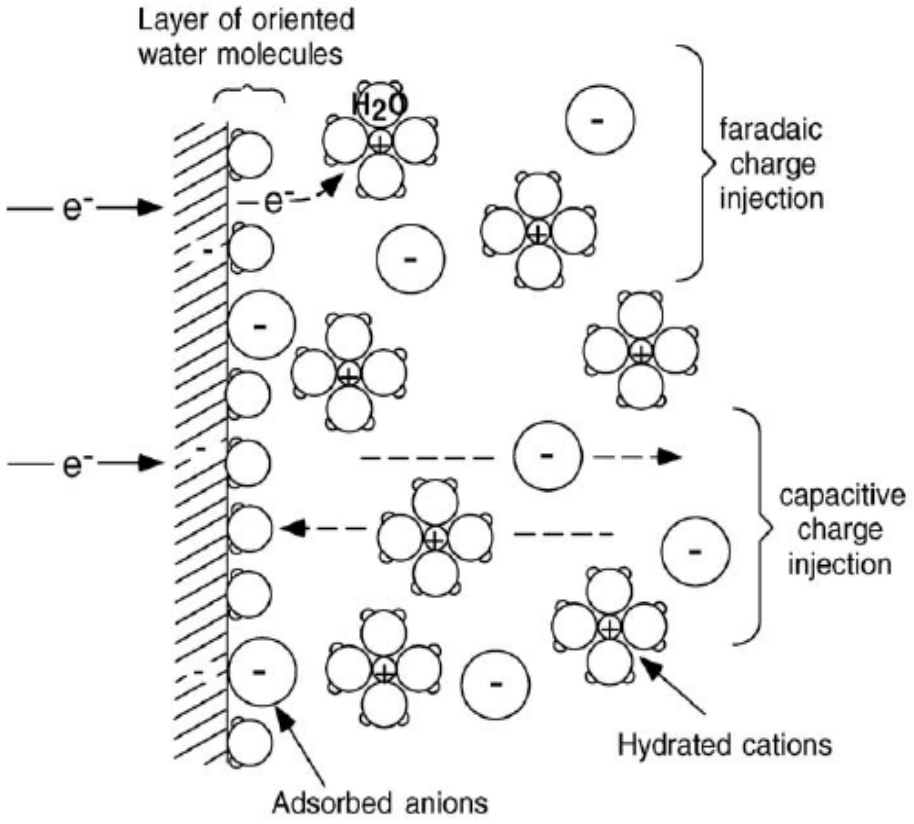

Figure 1.3: The Electrode/Electrolyte Interface, Illustrating Faradaic Charge Transfer (top) and Non-Faradaic Charge Transfer (bottom) (Merrill et al. 2005). Non-Faradaic capacitive charge transfer refers to the reversible redistribution of charge. Faradaic charge transfer refers to the transfer of electrons from the metal electrode, reducing hydrated cations in solution.

neuron action potentials, cause a change in the established equilibrium potential of the metal-ion interface, which in turn causes electric current to flow to the electrode instrumentation (recording) (Merrill et al. 2005; Webster 1978). Similarly, applying voltage perturbs this equilibrium condition, causing ionic current to flow into the surrounding tissue (stimulation).

Modeling the reactions occurring at the electrode/tissue interface has been researched extensively and a common basic circuit model has been widely accepted. This basic circuit model can be compartmentalized into three separate modules, the electrode/electrolyte interface, the shunt pathways, and the tissue response.

The electrode-electrolyte interface existing between the tissue and metal electrode is commonly modeled using five circuit components, as shown in Figure 1.4a (McAdams et al. 1995). The first component is a half-cell, E_{hc}, representing the equilibrium potential of the metal/electrolyte interface. The second component, C_d, represents the Helmholtz double layer. The Helmholtz layer consists of one layer of charge present at the electrode surface, and a separate opposing layer of charge generated at the electrolyte – and is therefore modeled as a capacitor (Figure 1.3). Some small charge does manage to leak across the electrode/electrolyte interface due to electrochemical reactions. Resistance to this transfer of charge is modeled as the third component, 'R_d' (Figure 1.3). The fourth component, a constant phase element (CPE), represents a) the fractal dimensions of the electrode surface, b) the non-linear impedance to current flow through the electrode system resulting from a finite rate of ion flow from the bulk of the electrolyte to the interface, and c) the frequency dependence of slow reactions. Finally, the fifth component is the resistance of the electrolyte solution, denoted as R_s.

The second module, representing the shunt pathway, accounts for the loss of signal from the electrode and measurement system to ground. The shunt pathway can be separated into three distinct circuit elements (Figure 1.4b). There is assumed a capacitive loss from the metal traces on the microelectrode to the surrounding electrolyte (brain tissue)

(Robinson 1968). A resistive element is used to model the loss of signal from the inherent resistivity of the metal wiring from the electrode to the measurement system (Robinson 1968). Finally, there is a third capacitive element that models the capacitive signal loss in the measurement system (Robinson 1968).

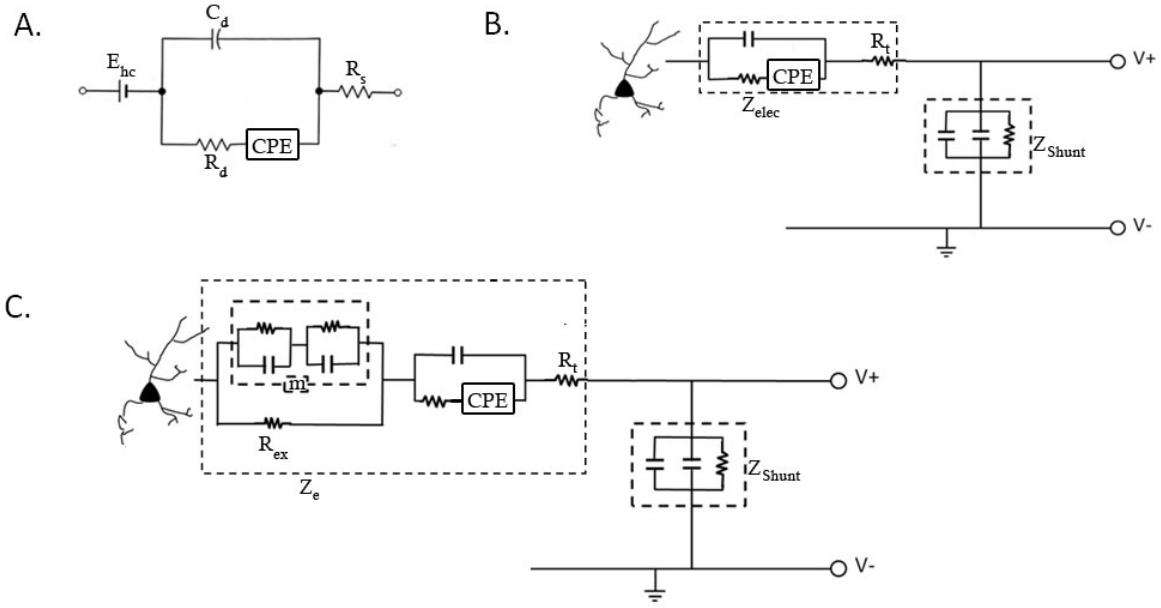

Figure 1.4: *In vivo* Electrode Model. (a) Basic Model of the Electrode Electrolyte Interface. (b) Basic Model with Shunt Pathways. (c) Full Model Including Encapsulation.

The third module of the circuit model for *in-vivo* electrode performance represents the foreign body response to the implant (Figure 1.5). Inserting a microelectrode into brain tissue elicits a reactive foreign body response, which produces a fibrous encapsulation of the array, effectively creating a high impedance barrier between the microelectrode and the neuron population (Buitenweg et al. 1998; Grill and Mortimer 1994; Liu et al. 1999; Stein et al. 1978; Szarowski et al. 2003; Turner et al. 1999). A well-described theoretical circuit model of this phenomenon has been widely accepted (Buitenweg et al. 1998; Grill and Mortimer 1994; Johnson et al. 2005; Otto et al. 2006; Williams 2001; Williams et al.

2007). The tissue encapsulation of the array can be characterized by a sealing resistance, describing protein adsorption and in some cases a layer of connective tissue (Buitenweg et al. 1998; Grill and Mortimer 1994; Stein et al. 1978). In addition, the model incorporates adjacent cellular layers of glia and macrophages given by a membrane capacitance, a membrane conductance resistance, and a membrane area scaling term, *m*, related to encapsulation thickness and cell-to-cell adhesion within the cellular layer (See Figure 1.5) (Buitenweg et al. 1998; Johnson et al. 2005; Otto et al. 2006). The extracellular pathway between cells is defined as a resistance (Buitenweg et al. 1998; Johnson et al. 2005; Otto et al. 2006). A full circuit model, encompassing all three modules can be seen in Figure 1.4c.

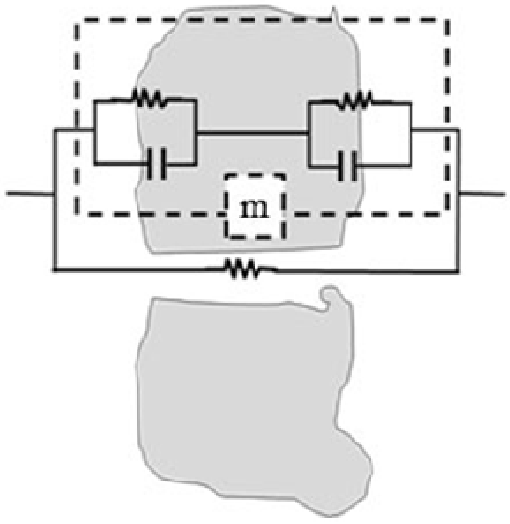

Figure 1.5: One Individual Element of the Lumped Circuit Model for Encapsulation. The model incorporates adjacent cellular layers of glia and macrophages given by a membrane capacitance, a membrane conductance resistance, and a membrane area scaling term, *m*, related to encapsulation thickness and cell-to-cell adhesion within the cellular layer ((Buitenweg et al. 1998; Johnson et al. 2005; Otto et al. 2006). The extracellular pathway between cells is defined as a resistance (Buitenweg et al. 1998; Johnson et al. 2005; Otto et al. 2006).

Neuroprosthesis and Signal Decoding Background

In a conference paper published in 1965, James Olds observed that single unit neuronal recordings could be operantly conditioned (Olds 1965). Although Olds' study did not have a large impact at the time of publication, his original work led to a number of innovative experiments using cortical activity as a direct control signal. Building upon Olds' original 1965 experiments, four year later Eberhart Fetz demonstrated that "after sufficient training sessions, (macaque) monkeys consistently and rapidly increased the firing rate of newly isolated (cortical) cells" when given a food reward for significantly increased firing rates (Fetz 1969). In 1977, Ed Schmidt went beyond requiring a monkey

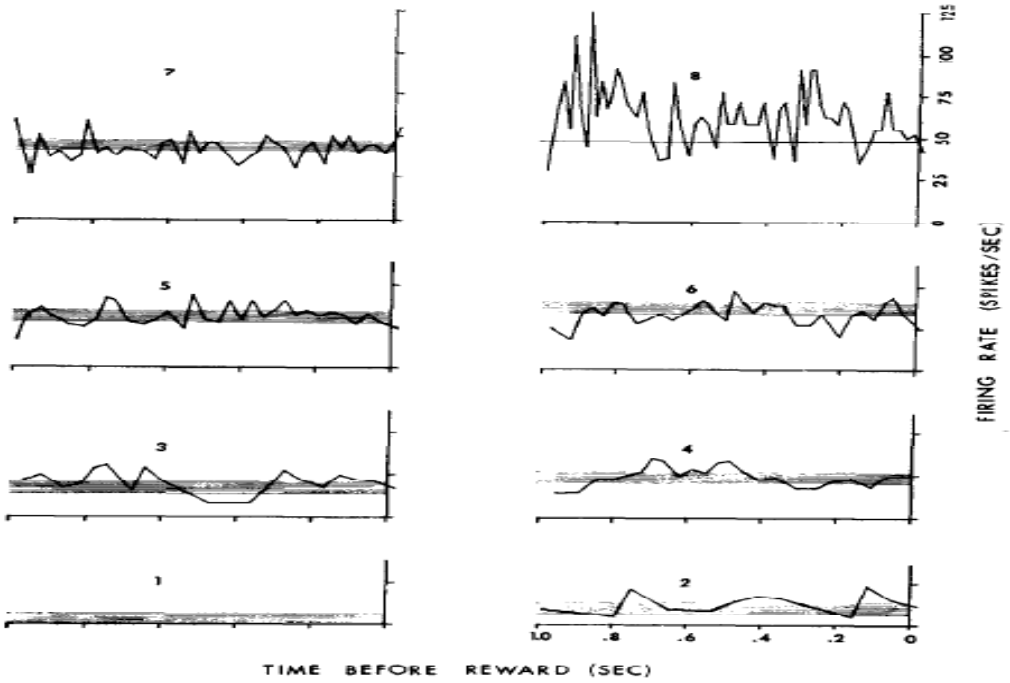

Figure 1.6: Instantaneous Firing Rate of a Conditioned Cortical Pyramidal Tract Neuron for Eight Different Targets (Schmidt et al. 1977). The animal was required to hold the firing rate of an individual neuron continuously within one of eight 'bands' for 0.76 seconds to receive a reward. Each trace shows a neurons firing rate one second prior to receiving a reward for each of the eight bands. For band 8 (top right), the animal was required to keep the firing rate of the neuron above 47.5 spikes per second.

to simply increase or decrease the firing rate of individual cortical neurons for a food reward, and instead trained his monkeys to successfully "fire a cortical neuron within a restricted frequency range and on command change to a new frequency range (Figure 1.6) (Schmidt et al. 1977)." When viewed in total, these three seminal studies strongly suggested that not only could individual neurons be operantly conditioned, they could also provide a reliable and robust control signal.

In spite of the promising results of these early experiments, very little research focused on the viability of cortical control signals until the late 1990's. Instead, the majority of studies investigated the relationship between the discharge of neurons in motor cortex and concurrent motor activities. In 1982, Apostolos Georgopoulos discovered an underlying bell-shaped directional tuning curve for neuronal firing rates in motor cortex with respect to a novel "center-out" task (Figure 1.7) (Georgopoulos et al. 1982).

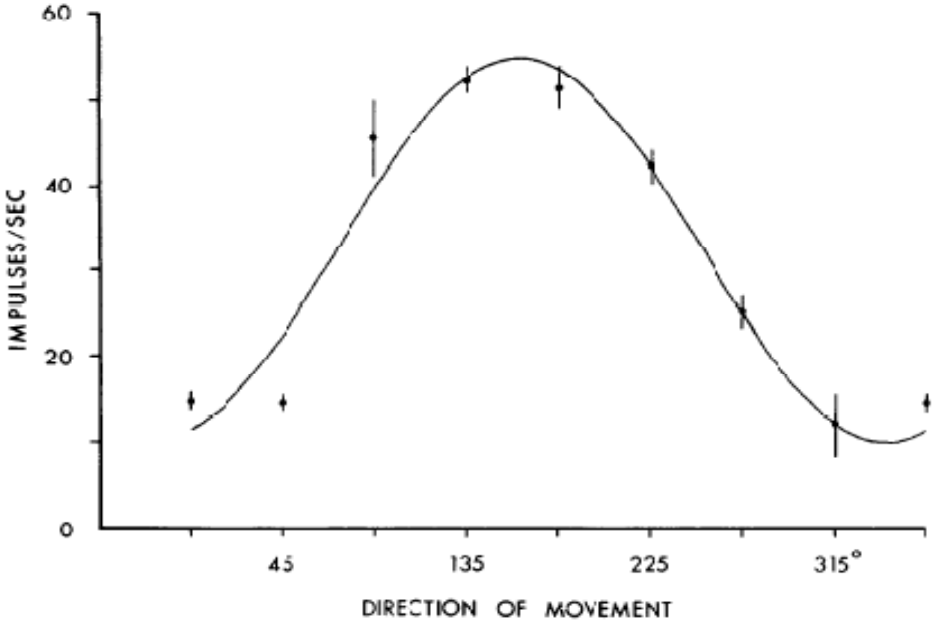

Figure 1.7: Bell-Shaped Directional Tuning Curve for One Neuron in Motor Cortex (Georgopoulos et al. 1986). Note the orderly variation in the firing rate of the recorded cell in response to movement direction. The regression equation for this curve is $D = 32.37 + 7.281 \sin\theta - 21.343 \cos\theta$, where D is the frequency of discharge and θ is the direction of movement.

Moreover, Georgopoulos and colleagues showed that a population vector constructed from the firing rates of multiple cortical neurons points in the direction of hand movement (Georgopoulos et al. 1986). Further work during this period demonstrated a strong relationship between neuronal activity in motor cortex and the force and velocity of a volitional arm movement (Moran and Schwartz 1999a; b).

The study of the relationship between neural firing rates and related motor activities in the 1980's and early 90's has led to a number of groundbreaking neural control experiments - known commonly as neuroprosthetic devices - in recent years. John Chapin and coworkers trained a rat to gain neural control of a lever in order to obtain a water reward using neural network decoding in 1999 (Chapin et al. 1999). One year later, Phil Kennedy *et al* demonstrated neural control of a cursor for communication in a human patient by implanting a unique electrode in neo-cortex of a "locked-in" subject (Kennedy et al. 2000). Later the same year, Andrew Schwartz used a fixed neural decoding algorithm calibrated on previously measured movements from a monkey in order to give the monkey reasonable real-time neural control of a robotic arm (Schwartz and Moran 2000). In 2002, Taylor and Schwartz presented a real-time adaptive decoding algorithm that could account for the inherent drift of single neuron preferred directions over time. Using this novel adaptive filter, Taylor and Schwartz were able to train monkeys to generate high accuracy neural control of a robotic arm in real-time (Taylor et al. 2002b). More recently, Velliste and Schwartz have trained a monkey implanted in motor cortex to feed itself using a neural controlled robotic arm (Velliste et al. 2008).

Building upon the considerable success of monkey work, neural recordings from the motor cortex of tertraplegic humans have now been used to control robotic devices and computer interfaces in real-time (Donoghue et al. 2007; Hochberg et al. 2006). Although these studies verified neural prosthetic control based off of calibration with *imagined* movements, the long-term efficacy of these neuroprosthetic devices remains limited.

Figure 1.8: Matthew Nagle, First Human Neuroprosthetic Patient (Martin 2005)

Initial human implants demonstrated limited electrode longevity; in the first human patient Matthew Nagle, the implanted electrodes failed to record neurological activity after 10 months (Figure 1.8) (Hochberg et al. 2006). Even prior to device failure, the control was described as 'crude' and 'limited' by lead scientist John Donoghue (Martin 2005).

Bayesian Maximum Likelihood Estimation Based on *A-Priori* Measurements

Despite the success of mapping the linear relationship between neuronal firing rates and real, observed, or imagined movements, this technique is dependent on a number of assumptions (Kettner et al. 1988) that can be difficult to achieve in practice (Hochberg et al. 2006; Kemere et al. 2004; Lebedev and Nicolelis 2006; Rickert et al. 2005; Santhanam et al. 2006; Wahnoun et al. 2006; Wu et al. 2003). In order to generate an effective neural map, the recorded sample of neurons must be sufficient to fully define the movement parameter space (Kemere et al. 2004; Santhanam et al. 2006; Schwartz 2004; Wu et al. 2003). However, often only a small number of stable neuronal units can be recorded under chronic conditions due to technological limitations and the chronic immune response (Hochberg et al. 2006; Ludwig et al. 2006; Nicolelis et al. 2003; Rennaker et al. 2007; Santhanam et al. 2006; Schwartz 2004; Selim Suner 2005; Seymour and Kipke 2007; Vetter et al. 2004b; Williams et al. 1999; Wu et al. 2003). Moreover, the firing rates of many neurons recorded in motor cortex have no identifiable relationship to movement parameters (Georgopoulos et al. 1986; Lebedev and Nicolelis 2006; Wahnoun et al. 2006), and the firing rates of neurons that are related to movement are only approximately linear during precisely defined stereotypical movements (Kemere et al. 2004; Lebedev and Nicolelis 2006; Wu et al. 2003). In addition, accurately isolating individual neurons can be difficult given low signal-to-noise recordings (Lewicki 1998; Wood et al. 2004; Wu et al. 2003). Consequently, multi-unit clusters are often used as the input for neural prosthetic applications. The inclusion of multi-unit clusters and individual neurons without a precisely defined linear relationship to a movement parameter act as sources of noise in predictions of movement intent, and can

negatively affect the performance of linear decoding algorithms (Lebedev and Nicolelis 2006; Wahnoun et al. 2006; Wu et al. 2003). As a result of these non-idealities, fully defining a movement parameter space outside of a controlled experimental situation is often problematic (Ali et al. 2007; Lebedev and Nicolelis 2006).

Using Maximum-Likelihood techniques, Santhanam *et al* found that the information transfer rate of neural prosthetic devices can be greatly enhanced by eliminating the prediction of unnecessary movement parameters (for example continuous trajectory) (Santhanam et al. 2006). Building upon the work of Santhanam, the decoding work in this dissertation was based on non-linear Bayesian Maximum Likelihood Estimation (bMLE) schemes (Achtman et al. 2007; Kemere et al. 2004; Santhanam et al. 2006; Shenoy et al. 2003). A non-linear decoding scheme was selected as prior studies have indicated that there is significant non-linear information present in the neural recordings (Brockwell et al. 2004; Chapin et al. 1999; Gao et al. 2003; Kemere et al. 2004; Kim et al. 2006; Wessberg et al. 2000).

Bayesian Maximum Likelihood Estimation Review

Bayesian maximum likelihood prediction of stimuli is dependent upon determining the probability distribution of neuronal responses for each delivered stimulus (Barbieri et al. 2005; Geisler and Albrecht 1995; Lehky 2004; Lehmkuhle et al. 2005; Oram et al. 1998; Sanger 1996). For purposes of this discussion, a stimulus may also include a measured movement parameter. Given the past history of neuronal responses with respect to different stimuli, observed neural responses can then be used to predict which stimulus is presently being delivered.

As a simple example, assume that the mean firing rate for a specific neuron when a subject's arm remained stationary was previously determined to be 40 Hz. The probability of this neuron firing n times over a short interval Δt while the arm remains stationary is given by the following Poisson statistic (See Figure 1.9):

$$P(n \text{ spikes}|\text{stationary}) = (40\Delta\text{t})^n \text{e}^{-(40\Delta\text{t})}/n! \qquad (1)$$

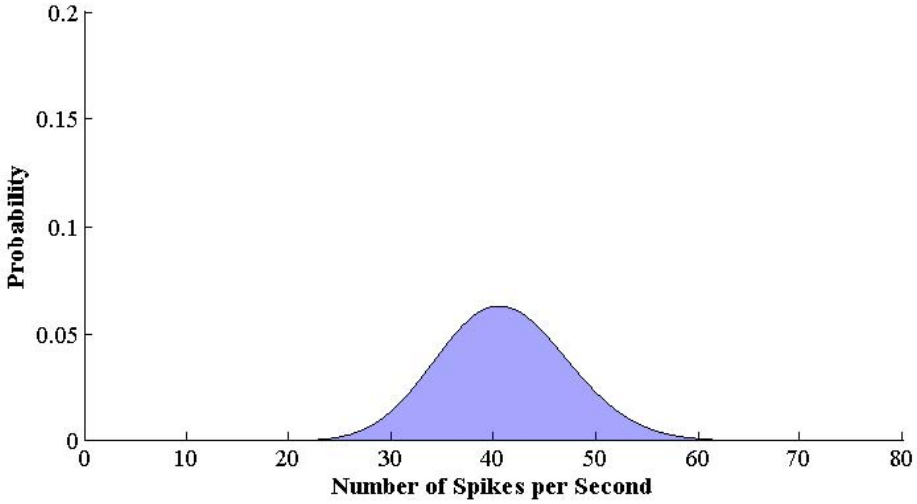

Figure 1.9: Probability Density Function of a Single Neuron with a Mean Firing Rate of 40 Hz Based on a Poisson Distribution. Note that over a 1 second interval, there is only a 6.3 percent chance of observing exactly 40 spikes from this neuron.

A Poisson distribution of spike counts was assumed in this work, as a Poisson distribution has been demonstrated to be a more accurate model of neural firing rates than standard Gaussian distributions (Barbieri et al. 2005; Gao et al. 2003; Lehky 2004; Santhanam et al. 2006).

Furthermore, assume that the firing rate of the same neuron during a subject's arm movement to the right was previously determined to be 80 Hz. The probability of this

neuron firing n times over a short interval Δt while a subject's arm moves to the right is given by the following Poisson statistic:

$$P(n \text{ spikes}|\text{right}) = (80\Delta\text{t})^{n}\text{e}^{-(80\Delta\text{t})}/n! \qquad (2)$$

Using Bayes' law, the present firing rate of the neuron can then be used to predict whether the subject's arm is currently stationary or moving to the right (See Figure 1.10).

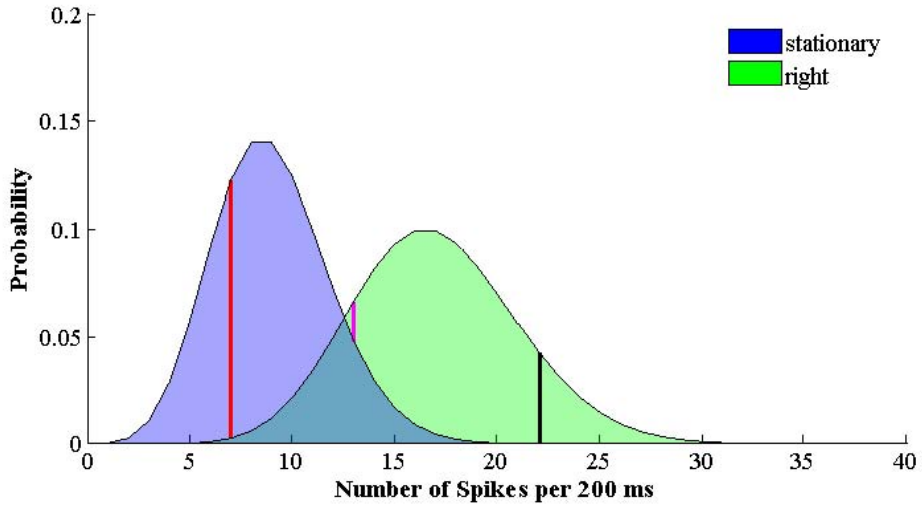

Figure 1.10: Probability Density Function of a Single Neuron's Firing Rate when the Subject's Arm Remains Stationary or Moves to the Right. The red line is located at 7 spikes over a 200 ms interval, the magenta line is located at 13 spikes, and the black line is located at 22 spikes. Note that the probability of 7 spikes occurring during a 200 ms interval is much greater when the subject's arm remains stationary than when the subject's arm moves right. In terms of a neuroprosthetic, an observed firing rate of 7 spikes per 200 ms indicates the device should remain stationary. Conversely, an observed firing rate of 22 spikes per 200 ms would indicate the prosthetic device should move to the right. An observed firing rate of 13 spikes per 200 ms would not yield a useable prediction, as this firing rate is approximately equally likely when the subject's arm remains stationary or moves to the right.

Given an observed firing rate of 7 spikes over 200 ms, equation 1 becomes:

$$P(7 \text{ spikes over } 200 \text{ ms}|\text{stationary}) = (40\text{Hz} * 0.2\text{s})^{7 \text{ spikes}}\text{e}^{-(40 \text{ Hz}*0.2\text{s})}/7 \text{ spikes!}$$

$$= 0.1396$$

Similarly, equation 2 becomes:

$$P(\text{7 spikes over 200 ms}|\text{right}) = (80\text{Hz} * 0.2\text{s})^{7\text{ spikes}} e^{-(80\text{ Hz} * 0.2\text{s})} / 7\text{ spikes!}$$
$$= 0.0060$$

Assuming that the subject's arm remaining stationary or moving to the right is equally likely, Bayes' law states that the probability of the subject's arm remaining stationary given an observed firing rate of 7 spikes over 200 ms can be calculated as follows:

$$P(\text{stationary}|\text{7 spikes over 200 ms}) = \frac{\text{P(7 spikes over 200 ms} \mid \text{stationary)}}{\text{P(7 spikes over 200 ms|stationary)+P(7 spikes over 200 ms|right)}}$$

$$= 0.1396/(0.1396 + 0.0060) = 0.9588, \text{or approximately 96 percent}$$

Note that this formula is simply the ratio of the probability of observing 7 spikes while the subject's arm remains stationary over the total probability of observing 7 spikes.

Likewise, the probability of the subject's arm moving to the right given an observed firing rate of 7 spikes over 200 ms is given by:

$$P(\text{right}|\text{7 spikes over 200 ms}) = \frac{\text{P(7 spikes over 200 ms} \mid \text{right)}}{\text{P(7 spikes over 200 ms|stationary)+P(7 spikes over 200 ms|right)}}$$

$$= 0.0060/(0.1396 + 0.0060) = 0.0412, \text{or approximately 4 percent}$$

In terms of a neuroprosthetic interface, a threshold of 95 percent probability can be used to determine a significant prediction. If the observed firing rate from a group of neurons predicts a movement to the right with a probability of greater than 95 percent, the neuroprosthetic device is then moved to the right. For this one neuron example, a firing rate of 7 spikes per 200 ms indicates that the neural prosthetic device should remain stationary (See Figure 1.10). Conversely, an observed firing rate of 22 spikes per 200 ms indicates the prosthetic device should move to the right [*P*(stationary | 22 spikes per 200 ms) <.0.001, *P*(right | 22 spikes per 200 ms) > 0.999]. An observed firing rate of 13 spikes per 200 ms does not yield a useable prediction, as this firing rate is likely to occur

when the subject's arm remains stationary or moves to the right [*P*(stationary | 13 spikes per 200 ms) <.0.2668, *P*(right | 13 spikes per 200 ms) > 0.7332].

This methodology can easily be extended to incorporate multiple neurons and multiple stimulus parameters. Assuming that the previously determined mean firing rate of a group of neurons with respect to a specific stimulus s_j is defined as the vector $\mathbf{M}_j$:

$$\mathrm{M}_j = \{\mu_{j1}, \mu_{j2}, \ldots \mu_{jn}\}$$

Where n is the total number of recorded neurons and $\boldsymbol{\mu_{j1}}$ is the mean firing rate of neuron 1 during stimulus s_j.

Given a vector of observed neuronal responses R from this group of neurons, where r_1 is the observed firing rate from neuron 1 of n neurons:

$$\mathrm{R} = \{r_1, r_2, \ldots r_n\}$$

The probability of an observed response vector R during the specific stimulus s_j is:

$$P(\mathrm{R}|s_j) = \prod_{i=1}^{\mathrm{n}} (\mu_{ji}\Delta\mathrm{t})^{r_i}\, \mathrm{e}^{-(\mu_{ji}\Delta\mathrm{t})}/r_i! \qquad (3)$$

If s is one of a set of n possible stimuli, then the set of possible stimuli S is given by:

$$\mathrm{S} = \{s_1, s_2, \ldots s_n\}$$

Assuming the delivery of all stimuli in set S are equally probable, the probability of any specific stimuli s_j based on observed response vector R can be computed as follows:

$$P(s_j|\mathrm{R}) = P(\mathrm{R}|s_j) \Big/ \sum_{i=1}^{n} P(\mathrm{R}|s_i) \qquad (4)$$

As in the one neuron example, a response vector R that predicts a specific movement s_j with a confidence level greater than 95 percent indicates that the neuroprosthetic device should also perform movement s_j. This basic Bayesian framework is often extended to include movement kinematics (previous position, velocity, and acceleration, for example) to further refine instantaneous movement predictions[1] (Barbieri et al. 2005; Brockwell et al. 2004; Kemere et al. 2004; Lehky 2004; Schwartz 2004).

Dissertation Organization

This dissertation includes three studies which are either in press, submission, or preparation for submission to peer-review journals. The first chapter is intended to introduce the reader to the relevant concepts and history not explicitly covered in each of the three studies. The last chapter of the dissertation summarizes the findings of all three studies as a whole, and discusses future work and preliminary results stemming directly from these initial studies. All studies in this dissertation are focused on improving the quality of current neuroprosthetic devices, primarily by improving the quality of neuronal inputs to the device.

---

[1] As a simple example, if a subject's arm at time t = 0 is located at horizontal position of 1 m, and is moving at a horizontal velocity of 1 m/s without any measurable acceleration, the arm is exceedingly unlikely to have reached a horizontal position of 10 meters by time t = 1 s. The probability density function relating the current prediction of movement to recent movement parameters can be used to refine the instantaneous prediction of a subject's movement based on neural firing rates. Unfortunately, a probability density function based on the history of a subject's real movements may not be fully or even partially applicable to neuroprosthetic device control. Furthermore, predictions using prior movement parameters are typically based on a random walk model, which does not apply for any movement that proceeds in a directed manner (Kemere 2004).

In Chapter 2, a Bayesian Maximum Likelihood strategy to isolate quality training data for a free-paced neuroprosthetic device is introduced and evaluated. By eliminating neural data unrelated to control tasks, neural control was possible using as few as two neurons and very limited initial training data. Moreover, by limiting initial assumptions, neural sources without a known linear relationship to a movement parameter - for example local field potential recordings or neurons in cingulate cortex - were used to successfully complete a neural control task. Finally, this decoding strategy was capable of identifying periods of 'No-Control', and neither trained or created control output during these periods. Chapter 2 is in preparation for submission to the *Journal of Neural Engineering*.

In Chapter 3, we refined a method to electrochemically deposit surfactant-templated ordered poly(3,4-ethylenedioxythiophene) (PEDOT) films on the recording sites of 'Michigan' probes, and evaluated the efficacy of these modified sites in recording chronic neural activity. PEDOT sites were found outperform controls in terms of number of units recorded, noise levels, and artifact evident in local field potential recordings. Increasing the signal-to-noise ratio at the input stage of the neuroprosthetic device (NPD) in turn increases both the quality and quantity of neural information sources. As a result, the overall efficacy of NPD devices predicated on these neuronal input sources should improve. Chapter 3 was published in the *Journal of Neural Engineering,* and was also included in the year-end highlights edition of the journal in 2006.

In Chapter 4, a technique known as common average referencing (CAR) to generate a more ideal electrode reference for single-unit neural recordings is introduced and evaluated. Sites referenced to a CAR were found to have over 30 percent less noise than

standard electrical referencing techniques, resulting in 60 percent more isolated units. Noise is expected to be an even greater confounding factor in the implementation of real-world pragmatic neuroprosthetic systems. Chapter 4 has been recently accepted as an Innovative Method to the *Journal of Neurophysiology*.

Chapter 5 summarizes the conclusions from the previous chapters, and places these results in the context of neuroprosthetic devices as a whole. In addition, early results from future work stemming from these earlier studies are described.

This dissertation provides several novel improvements to the current neuroprosthetic device, which have been evaluated in long-term chronic conditions. The results presented here not only impact the field of practical neuroprosthetic devices, but contributes to the fundamental understanding of microelectrode theory as a whole.

References

Achtman N, Afshar A, Santhanam G, Yu BM, Ryu SI, and Shenoy KV. Free-paced high-performance brain-computer interfaces. *J Neural Eng* 4: 336-347, 2007.

Ali B, Steve GM, Jaimie FB, Rabab KW, and Gary EB. A Comparative Study on Generating Training-Data for Self-Paced Brain Interfaces. *Neural Systems and Rehabilitation Engineering, IEEE Transactions on [see also IEEE Trans on Rehabilitation Engineering]* 15: 59-66, 2007.

Anderson RA, Burdick JW, Musallam S, Pesaran B, and Cham JG. Cognitive Neural Prosthetics. *Science Direct* 8: 2004.

Bai Q, Wise KD, and Anderson DJ. A high-yield microassembly structure for three-dimensional microelectrode arrays. *IEEE Trans Biomed Eng* 47: 281-289, 2000.

Barbieri R, Wilson MA, Frank LM, and Brown EN. An analysis of hippocampal spatio-temporal representations using a Bayesian algorithm for neural spike train decoding. *IEEE Trans Neural Syst Rehabil Eng* 13: 131-136, 2005.

Bard AJ, and Faulkner L. *Electrochemical methods: fundamentals and applications*. New York: Wiley, 1980.

Barnes PM, Adams PF, and Schiller JS. Summary Health Statistics for the U.S. Population: National Health Interview Survey, 2001. *Vital Health and Statistics* 10: 2003.

Bashashati A, Fatourechi M, Ward RK, and Birch GE. A survey of signal processing algorithms in brain;computer interfaces based on electrical brain signals. *Journal of Neural Engineering* 4: 2007.

Blanche TJ, Spacek MA, Hetke JF, and Swindale NV. Polytrodes: High-Density Silicon Electrode Arrays for Large-Scale Multiunit Recording. *J Neurophysiol* 93: 2987-3000, 2005.

Bragin A, Hetke J, Wilson CL, Anderson DJ, Engel J, and Buzsáki G. Multiple site silicon-based probes for chronic recordings in freely moving rats: implantation, recording and histological verification. *Journal of Neuroscience Methods* 98: 77-82, 2000.

Brockwell AE, Rojas AL, and Kass RE. Recursive bayesian decoding of motor cortical signals by particle filtering. *J Neurophysiol* 91: 1899-1907, 2004.

Brown EN, Frank LM, Tang D, Quirk MC, and Wilson MA. A statistical paradigm for neural spike train decoding applied to position prediction from ensemble firing patterns of rat hippocampal place cells. *J Neurosci* 18: 7411-7425, 1998.

Brown P, Kupsch A, Magill PJ, Sharott A, Harnack D, and Meissner W. Oscillatory local field potentials recorded from the subthalamic nucleus of the alert rat. *Exp Neurol* 177: 581-585, 2002.

Buitenweg JR, Rutten WL, Willems WP, and van Nieuwkasteele JW. Measurement of sealing resistance of cell-electrode interfaces in neuronal cultures using impedance spectroscopy. *Medical & biological engineering & computing* 36: 630-637, 1998.

Burns BD, Stean JP, and Webb AC. Recording for several days from single cortical neurons in completely unrestrained cats. *Electroencephalography and Clinical Neurophysiology* 36: 314-318, 1974.

Carmena JM, Lebedev MA, Crist RE, O'Doherty JE, Santucci DM, Dimitrov DF, Patil PG, Henriquez CS, and Nicolelis MAL. Learning to Control a Brain-Machine Interface for Reaching and Grasping by Primates. *PLoS Biology* 1: e42, 2003.

Cattaneo A, Maffei L, and Morrone C. Patterns in the discharge of simple and complex visual cortical cells. *Proc R Soc Lond B Biol Sci* 212: 279-297, 1981a.

Cattaneo A, Maffei L, and Morrone C. Two firing patterns in the discharge of complex cells encoding different attributes of the visual stimulus. *Exp Brain Res* 43: 115-118, 1981b.

Chapin JK, Moxon KA, Markowitz RS, and Nicolelis MA. Real-time control of a robot arm using simultaneously recorded neurons in the motor cortex. *Nat Neurosci* 2: 664-670, 1999.

Cooper R, Binnie CD, Osselton JW, Prior PF, and Wisman T. EEG, paediatric neurophysiology, special techniques and applications. In: *Clinical Neurophysiology Vol 2*, edited by Cooper R, Mauguiere F, Osselton JW, Prior PF, and Tedman BM. Amsterdam: Elsevier B.V, 2003, p. 8-103.

Dobelle WH. Artificial vision for the blind by connecting a television camera to the visual cortex. *Asaio Journal* 46: 3-9, 2000.

Donoghue JP, Nurmikko A, Black M, and Hochberg LR. Assistive technology and robotic control using motor cortex ensemble-based neural interface systems in humans with tetraplegia. *J Physiol* 579: 603-611, 2007.

Drake KL, Wise KD, Farraye J, Anderson DJ, and BeMent SL. Performance of planar multisite microprobes in recording extracellular single-unit intracortical activity. *IEEE Trans Biomed Eng* 35: 719-732, 1988.

Eggermont JJ. Analysis of compound action potential responses to tone bursts in the human and guinea pig cochlea. *J Acoust Soc Am* 60: 1132-1139, 1976.

Eggermont JJ. Compound action potentials: tuning curves and delay times. *Scand Audiol Suppl* 129-139, 1979.

Eggermont JJ, Aertsen AM, Hermes DJ, and Johannesma PI. Spectro-temporal characterization of auditory neurons: redundant or necessary. *Hear Res* 5: 109-121, 1981.

Epping WJ, and Eggermont JJ. Sensitivity of neurons in the auditory midbrain of the grassfrog to temporal characteristics of sound. I. Stimulation with acoustic clicks. *Hear Res* 24: 37-54, 1986.

Fetz E. Operant conditioning of cortical unit activity. *Science* 163: 955–958, 1969.

Fetz EE, and Finocchio DV. Correlations between activity of motor cortex cells and arm muscles during operantly conditioned response patterns. *Exp Brain Res* 23: 217-240, 1975.

Furukawa S, Xu L, and Middlebrooks JC. Coding of sound-source location by ensembles of cortical neurons. *J Neurosci* 20: 1216-1228, 2000.

Gage GJ, Ludwig KA, Otto KJ, Ionides EL, and Kipke DR. Naive coadaptive cortical control. *J Neural Eng* 2: 52-63, 2005.

Gao Y, Black MJ, Bienenstock E, Wu W, and Donoghue JP. A quantitative comparison of linear and non-linear models of motor cortical activity for the encoding and decoding of arm motions. In: *1st International IEEE/EMBS Conference on Neural Engineering*. Capri, Italy: 2003, p. 189-192.

Geisler WS, and Albrecht DG. Bayesian analysis of identification performance in monkey visual cortex: nonlinear mechanisms and stimulus certainty. *Vision Res* 35: 2723-2730, 1995.

Georgopoulos AP, Kalaska JF, Caminiti R, and Massey JT. On the relations between the direction of two-dimensional arm movements and cell discharge in primate motor cortex. *J Neurosci* 2: 1527-1537, 1982.

Georgopoulos AP, Schwartz AB, and Kettner RE. Neuronal population coding of movement direction. *Science* 233: 1416-1419, 1986.

Gileadi E, Kirowa-Eisner E, and Penciner J. *Interfacial electrochemistry: an experimental approach*. United States: Addison-Wesley Publishing Co., Inc.,Reading, MA, 1975, p. Pages: 540.

Grill WM, and Mortimer JT. Electrical properties of implant encapsulation tissue. *Annals of biomedical engineering* 22: 23-33, 1994.

Hermes DJ, Eggermont JJ, Aertsen AM, and Johannesma PI. Spectro-temporal characteristics of single units in the auditory midbrain of the lightly anaesthetised grass frog (Rana temporaria L.) investigated with tonal stimuli. *Hear Res* 6: 103-126, 1982.

Hochberg LR, Serruya MD, Friehs GM, Mukand JA, Saleh M, Caplan AH, Branner A, Chen D, Penn RD, and Donoghue JP. Neuronal ensemble control of prosthetic devices by a human with tetraplegia. *Nature* 442: 164, 2006.

Hoogerwerf AC, and Wise KD. A three-dimensional microelectrode array for chronic neural recording. *IEEE Trans Biomed Eng* 41: 1136-1146, 1994.

Johnson MD, Otto KJ, and Kipke DR. Repeated voltage biasing improves unit recordings by reducing resistive tissue impedances. *Neural Systems and Rehabilitation Engineering, IEEE Transactions on [see also IEEE Trans on Rehabilitation Engineering]* 13: 160-165, 2005.

Kargo WJ, and Nitz DA. Early skill learning is expressed through selection and tuning of cortically represented muscle synergies. *J Neurosci* 23: 11255-11269, 2003.

Kemere C, Shenoy KV, and Meng TH. Model-based neural decoding of reaching movements: a maximum likelihood approach. *IEEE Trans Biomed Eng* 51: 925-932, 2004.

Kennedy P, Andreasen D, Ehirim P, King B, Kirby T, Mao H, and Moore M. Using human extra-cortical local field potentials to control a switch. *J Neural Eng* 1: 72-77, 2004a.

Kennedy PR, Bakay RA, Moore MM, Adams K, and Goldwaithe J. Direct control of a computer from the human central nervous system. *IEEE Trans Rehabil Eng* 8: 198-202, 2000.

Kennedy PR, Kirby MT, Moore MM, King B, and Mallory A. Computer control using human intracortical local field potentials. *IEEE Trans Neural Syst Rehabil Eng* 12: 339-344, 2004b.

Kettner RE, Schwartz AB, and Georgopoulos AP. Primate motor cortex and free arm movements to visual targets in three- dimensional space. III. Positional gradients and population coding of movement direction from various movement origins. *J Neurosci* 8: 2938-2947, 1988.

Kewley DT, Bower JM, Hills MD, Borkholder DA, Opris IE, Maluf NI, Storment CW, and Kovacs GTA. Plasma-etched neural probes. *Sensors and Actuators A: Physical* 58: 27-35, 1997.

Kim KH, Kim SS, and Kim SJ. Superiority of nonlinear mapping in decoding multiple single-unit neuronal spike trains: A simulation study. *Journal of Neuroscience Methods* 150: 202, 2006.

Lebedev MA, and Nicolelis MAL. Brain-machine interfaces: past, present and future. *Trends in Neurosciences* 29: 536-546, 2006.

Lee D, Port NL, Kruse W, and Georgopoulos AP. Variability and correlated noise in the discharge of neurons in motor and parietal areas of the primate cortex. *J Neurosci* 18: 1161-1170, 1998.

Lehky SR. Bayesian estimation of stimulus responses in Poisson spike trains. *Neural Comput* 16: 1325-1343, 2004.

Lehmkuhle MJ, Normann RA, and Maynard EM. Trial-by-Trial Discrimination of Three Enantiomer Pairs by Neural Ensembles in Mammalian Olfactory Bulb. *J Neurophysiol* 2005.

Lewicki MS. A review of methods for spike sorting: the detection and classification of neural action potentials. *Network-Computation in Neural Systems* 9: R53-R78, 1998.

Liu X, McCreery DB, Carter RR, Bullara LA, Yuen TG, and Agnew WF. Stability of the interface between neural tissue and chronically implanted intracortical microelectrodes. *IEEE transactions on rehabilitation engineering* 7: 315-326, 1999.

Ludwig KA, Miriani R, Langhals NB, Joseph MD, and Kipke DR. Employing a Common Average Reference to Improve Cortical Neuron Recordings from Microelectrode Arrays. *in preparation* 2008.

Ludwig KA, Uram JD, Yang J, Martin DC, and Kipke DR. Chronic neural recordings using silicon microelectrode arrays electrochemically deposited with a poly(3,4-ethylenedioxythiophene) (PEDOT) film. *Journal of Neural Engineering* 3: 59, 2006.

Magill PJ, Sharott A, Bevan MD, Brown P, and Bolam JP. Synchronous unit activity and local field potentials evoked in the subthalamic nucleus by cortical stimulation. *J Neurophysiol* 92: 700-714, 2004.

Marg E, and Adams JE. Indwelling multiple micro-electrodes in the brain. *Electroencephalogr Clin Neurophysiol* 23: 277-280, 1967.

Martin R. Mind Control. In: *Wired*2005.

Marzullo TC, Miller CR, and Kipke DR. Suitability of the Cingulate Cortex for Neural Control. *Neural Systems and Rehabilitation Engineering, IEEE Transactions on [see also IEEE Trans on Rehabilitation Engineering]* 14: 401-409, 2006.

Mason SG, and Birch GE. A brain-controlled switch for asynchronous control applications. *Biomedical Engineering, IEEE Transactions on* 47: 1297-1307, 2000.

Maynard EM, Hatsopoulos NG, Ojakangas CL, Acuna BD, Sanes JN, Normann RA, and Donoghue JP. Neuronal interactions improve cortical population coding of movement direction. *J Neurosci* 19: 8083-8093, 1999.

McAdams ET, Lackermeier A, McLaughlin JA, Macken D, and Jossinet J. The linear and non-linear electrical properties of the electrode-electrolyte interface. *Biosensors and Bioelectronics* 10: 67-74, 1995.

Mehring C, Rickert J, Vaadia E, Cardosa de Oliveira S, Aertsen A, and Rotter S. Inference of hand movements from local field potentials in monkey motor cortex. *Nat Neurosci* 6: 1253-1254, 2003.

Merrill DR, Bikson M, and Jefferys JGR. Electrical stimulation of excitable tissue: design of efficacious and safe protocols. *Journal of Neuroscience Methods* 141: 171-198, 2005.

Middlebrooks JC, Dykes RW, and Merzenich MM. Binaural response-specific bands in primary auditory cortex (AI) of the cat: topographical organization orthogonal to isofrequency contours. *Brain Res* 181: 31-48, 1980.

Middlebrooks JC, and Knudsen EI. A neural code for auditory space in the cat's superior colliculus. *J Neurosci* 4: 2621-2634, 1984.

Moran DW, and Schwartz AB. Motor cortical activity during drawing movements: population representation during spiral tracing. *J Neurophysiol* 82: 2693-2704, 1999a.

Moran DW, and Schwartz AB. Motor cortical representation of speed and direction during reaching. *J Neurophysiol* 82: 2676-2692, 1999b.

Nicolelis MAL, Baccala LA, Lin RCS, and Chapin JK. Sensorimotor Encoding by Synchronous Neural Ensemble Activity at Multiple Levels of the Somatosensory System. *Science* 268: 1353-1358, 1995.

Nicolelis MAL, Dimitrov D, Carmena JM, Crist R, Lehew G, Kralik JD, and Wise SP. Chronic, multisite, multielectrode recordings in macaque monkeys. *Proceedings of the National Academy of Sciences of the United States of America* 100: 11041-11046, 2003.

O'Keefe J, and Dostrovsky J. The hippocampus as a spatial map. Preliminary evidence from unit activity in the freely-moving rat. *Brain Res* 34: 171-175, 1971.

Olds J. Operant Conditioning of Single Unit Responses. In: *Proc XXIII Int Congress Physiol Sci*. Tokyo: 1965, p. 372–380.

Olds J, Disterhoft JF, Segal M, Kornblith CL, and Hirsh R. Learning centers of rat brain mapped by measuring latencies of conditioned unit responses. *J Neurophysiol* 35: 202-219, 1972.

Oram MW, Foldiak P, Perrett DI, and Sengpiel F. The 'Ideal Homunculus': decoding neural population signals. *Trends Neurosci* 21: 259-265, 1998.

Otto KJ, Johnson MD, and Kipke DR. Voltage pulses change neural interface properties and improve unit recordings with chronically implanted microelectrodes *Biomedical Engineering, IEEE Transactions on* 53: 333-340, 2006.

Paninski L, Fellows MR, Hatsopoulos NG, and Donoghue JP. Spatiotemporal tuning of motor cortical neurons for hand position and velocity. *J Neurophysiol* 91: 515-532, 2004.

Paxinos G, Watson CR, and Emson PC. AChE-stained horizontal sections of the rat brain in stereotaxic coordinates. *J Neurosci Methods* 3: 129-149, 1980.

Polikov VS, Tresco PA, and Reichert WM. Response of brain tissue to chronically implanted neural electrodes. *J Neurosci Methods* 148: 1-18, 2005.

Prijs VF, and Eggermont JJ. Narrow-band analysis of compound action potentials for several stimulus conditions in the guinea pig. *Hear Res* 4: 23-41, 1981.

Randles J. Rapid electrode reactions. *Discuss Faraday Soc* 1: 11-19, 1947.

Rennaker RL, Miller J, Tang H, and Wilson DA. Minocycline increases quality and longevity of chronic neural recordings. *Journal of Neural Engineering* 4: 2007.

Rickert J, Oliveira SC, Vaadia E, Aertsen A, Rotter S, and Mehring C. Encoding of movement direction in different frequency ranges of motor cortical local field potentials. *J Neurosci* 25: 8815-8824, 2005.

Robinson DA. The electrical properties of metal microelectrodes. *Proceedings of the IEEE* 56: 1065, 1968.

Rousche PJ, and Normann RA. Chronic recording capability of the Utah Intracortical Electrode Array in cat sensory cortex. *Journal of Neuroscience Methods* 82: 1-15, 1998.

Sanger TD. Probability density estimation for the interpretation of neural population codes. *J Neurophysiol* 76: 2790-2793, 1996.

Santhanam G, Linderman MD, Gilja V, Afshar A, Ryu SI, Meng TH, and Shenoy KV. HermesB: a continuous neural recording system for freely behaving primates. *IEEE Trans Biomed Eng* 54: 2037-2050, 2007.

Santhanam G, Ryu SI, Yu BM, Afshar A, and Shenoy KV. A high-performance brain computer interface. *Nature* 442: 195, 2006.

Schmidt EM, Bak MJ, McIntosh JS, and Thomas JS. Operant conditioning of firing patterns in monkey cortical neurons. *Exp Neurol* 54: 467-477, 1977.

Schwartz AB. Cortical neural prosthetics. *Annu Rev Neurosci* 27: 487-507, 2004.

Schwartz AB, and Moran DW. Arm trajectory and representation of movement processing in motor cortical activity. *Eur J Neurosci* 12: 1851-1856, 2000.

Schwartz AB, and Moran DW. Motor cortical activity during drawing movements: population representation during lemniscate tracing. *J Neurophysiol* 82: 2705-2718, 1999.

Selim Suner MRF, Carlos Vargas-Irwin, Kenji Nakata, and John P. Donoghue. Reliability of Signals from a Chronically Implanted, Silicon-based Electrode Array in Non-human Primate Primary Motor Cortex. *Submitted to IEEE* 2005.

Serruya MD, Hatsopoulos NG, Paninski L, Fellows MR, and Donoghue JP. Instant neural control of a movement signal. *Nature* 416: 141-142, 2002.

Seymour JP, and Kipke DR. Neural probe design for reduced tissue encapsulation in CNS. *Biomaterials* 28: 3594-3607, 2007.

Shenoy KV, Meeker D, Cao S, Kureshi SA, Pesaran B, Buneo CA, Batista AP, Mitra PP, Burdick JW, and Andersen RA. Neural prosthetic control signals from plan activity. *Neuroreport* 14: 591-596, 2003.

Stein RB, Charles D, Gordon T, Hoffer JA, and Jhamandas J. Impedance properties of metal electrodes for chronic recording from mammalian nerves. *IEEE transactions on bio-medical engineering* 25: 532-537, 1978.

Strumwasser F. Long-Term Recording from Single Neurons in Brain of Unrestrained Mammals. *Science* 127: 469-470, 1958.

Szarowski DH, Andersen MD, Retterer S, Spence AJ, Isaacson M, Craighead HG, Turner JN, and Shain W. Brain responses to micro-machined silicon devices. *Brain Research* 983: 23-35, 2003.

Taylor DM, Helms-Tillery SI, and Schwartz AB. Direct cortical control of 3D neuroprosthetic devices. *Science* 296: 1829-1832, 2002a.

Taylor DM, Tillery SI, and Schwartz AB. Direct cortical control of 3D neuroprosthetic devices. *Science* 296: 1829-1832, 2002b.

Turner JN, Shain W, Szarowski DH, Andersen M, Martins S, Isaacson M, and Craighead H. Cerebral astrocyte response to micromachined silicon implants. *Exp Neurol* 156: 33-49, 1999.

Velliste M, Perel S, Spalding MC, Whitford AS, and Schwartz AB. Cortical control of a prosthetic arm for self-feeding. *Nature* 453: 1098-1101, 2008.

Vetter RJ, Williams JC, Hetke JF, Nunamaker EA, and Kipke DR. Chronic neural recording using silicon-substrate microelectrode arrays implanted in cerebral cortex. *IEEE transactions on bio-medical engineering* 51: 896-904, 2004a.

Vetter RJ, Williams JC, Hetke JF, Nunamaker EA, and Kipke DR. Spike recording performance of implanted chronic silicon-substrate microelectrode arrays in cerebral cortex. *IEEE Transactions on Neural Systems and Rehabilitation Engineering* 52: 2004b.

Wahnoun R, He J, and Tillery SIH. Selection and parameterization of cortical neurons for neuroprosthetic control. *Journal of Neural Engineering* 3: 162, 2006.

Webster JG. *Medical Instrumentation: Application and Design*. 1978.

Wessberg J, Stambaugh CR, Kralik JD, Beck PD, Laubach M, Chapin JK, Kim J, Biggs SJ, Srinivasan MA, and Nicolelis MA. Real-time prediction of hand trajectory by ensembles of cortical neurons in primates. *Nature* 408: 361-365, 2000.

Williams J, Rennaker R, and Kipke D. Long-term neural recording characteristics of wire microelectrode arrays implanted in cerebral cortex. *Brain Res Brain Res Protocol* 4: 303–313, 1999.

Williams JC. Performance of chronic neural implants: measurement, modeling and intervention strategies. 2001.

Williams JC, Hippensteel JA, Dilgen J, Shain W, and Kipke DR. Complex impedance spectroscopy for monitoring tissue responses to inserted neural implants. *J Neural Eng* 4: 410-423, 2007.

Wolpaw JR, Birbaumer N, McFarland DJ, Pfurtscheller G, and Vaughan TM. Brain-computer interfaces for communication and control. *Clin Neurophysiol* 113: 767-791, 2002.

Wood F, Black MJ, Vargas-Irwin C, Fellows M, and Donoghue JP. On the variability of manual spike sorting. *Ieee Transactions on Biomedical Engineering* 51: 912-918, 2004.

Wu W, Black MJ, Mumford D, Gao Y, Bienenstock E, and Donoghue JP. A Switching Kalman Filter Model for the Motor Cortical Coding of Hand Motion. *Proc IEEE Engineering in Medicine and Biology Society* 2083-2086, 2003.

Xu L, Furukawa S, and Middlebrooks JC. Auditory cortical responses in the cat to sounds that produce spatial illusions. *Nature* 399: 688-691, 1999.

CHAPTER 2
BAYESIAN MLE CLASSIFIER FOR GENERATING TRAINING DATA

Abstract

In order to quickly translate the initial promise of neuroprosthetic studies into a practical clinical device, decoding algorithms need to be predicated on assumptions that are easily met outside of an experimental setting. Given present technology limitations, a low number of potentially unstable neuronal units must be assumed from day to day, driving a need for decoding algorithms which a) are not dependent upon a large number of neurons for control, b) are adaptable to alternative sources of neuronal input such as local field potentials, and c) require only marginal training data for day to day calibrations. Moreover, practical decoding algorithms must be able to recognize and eliminate poor training data, as well as when the user is not intending to generate a control output.

In this study, we introduce and evaluate a Bayesian maximum-likelihood estimation (bMLE) strategy to address the issues of isolating quality training data and self-paced control. Simulation and *in vivo* results using this method demonstrate that the standard eight-state center out task can be accomplished with as little as two neurons, while requiring as few as eight trials for algorithm training. In addition, untrained animals could quickly obtain accurate neuroprosthetic control using local field potentials and neurons in cingulate cortex – two neuronal sources not known to have a linear relationship to a movement parameter. Finally, this algorithm successfully recognized

segments of 'No Control', and did not generate training data or a control output during these segments.

Introduction

The study of the relationship between neural firing rates and related motor activities in the 1980's and early 90's has led to a number of groundbreaking neural control experiments, known more commonly as neuroprosthetic devices, over the last ten years (Anderson et al. 2004; Carmena et al. 2003; Chapin et al. 1999; Gage et al. 2005; Schwartz 2004; Taylor et al. 2002a; Wolpaw et al. 2002). Typical neuroprostheses use previously measured movements from a subject to map a linear relationship between a subject's recorded neural firing rates and each movement parameter, and then apply this map directly to the control of a device (Bashashati et al. 2007; Schwartz 2004; Taylor et al. 2002a; Velliste et al. 2008; Wahnoun et al. 2006; Wessberg et al. 2000; Wu et al. 2003). This approach has the advantage of being both simple and intuitive, while still yielding insights into the relationship between cortical neurons and natural movement.

Unfortunately, generating training data from which to derive a linear relationship between neuronal firing rates and movement parameters can be problematic in practical application. Neuroprosthetic devices are typically designed for use by patients with severe motor disabilities, and are therefore unable to make movements for calibration purposes. In a recent study, Wahnoun *et al* addressed this issue by mapping cortical neural activity to *observed* movements (Velliste et al. 2008; Wahnoun et al. 2006). Similarly, Hochberg *et al* successfully mapped neural activity to *imagined* movements (Hochberg et al. 2006) Although calibrating a neuroprosthetic device based on observed

or imagined movement presents a promising alternative to *a priori* movement measurements, the exact relationship between observed/imagined movements and neuronal firing rates is ill-defined (Bashashati et al. 2007). There is no obvious indicator of when the neural activity related to the observed/imagined movement begins or ends, or if any relationship is present at all on a particular trial (Bashashati et al. 2007). Consequently, neural data unrelated to any movement parameter may unintentionally be used to train the neural decoding algorithm, degrading device performance (Bashashati et al. 2007).

Another issue which needs to be addressed before the experimental promise of neuroprosthetic systems can be translated to practical application is self-paced control (Achtman et al. 2007; Bashashati et al. 2007; Mason and Birch 2000). According to Bashashati *et al*, in a self-paced system the user directs the neuroprosthetic device by intentionally changing neural activity (Bashashati et al. 2007). Between periods of intentional control (IC), the subject is not actively attempting to use the neuroprosthetic device (No-Control, NC) (Bashashati et al. 2007). Current cortical control paradigms, however, operate under the assumption that the subject is always intentionally attempting to control the output device. This methodology presents two problems, a) the output device responds when the user is not intending to generate a control signal, and b) neural activity unrelated to observed/imagined movement parameters is intermittently used to train the system (Bashashati et al. 2007; Lebedev and Nicolelis 2006; Wahnoun et al. 2006).

For neuroprosthetic devices to translate to real clinical applications, decoding algorithms need to be based on assumptions that are easily met outside of an experimental setting. Given present technology limitations, a low number of potentially unstable neuronal units must be assumed from day to day, driving a need for decoding algorithms which a) are not dependent upon a large number of neurons for control, b) are adaptable to alternative sources of neuronal input such as local field potentials, and c) require only marginal training data for day to day calibrations. Moreover, practical decoding algorithms must be able to recognize and eliminate poor training data, and operate without initial movement measurements for calibration.

In this study we introduce and evaluate a Bayesian Maximum-Likelihood Estimation (bMLE) strategy to identify optimized training data for neuroprosthetic devices, in order to address the issues of isolating quality training data and self-paced control. Using simulated neural data based on the standard eight-state center-out task (Georgopoulos et al. 1986), we demonstrate that the center-out task can be consistently performed at above 95 percent performance levels with as few as two neurons intermittently providing information relevant to predicting movement parameters out of a set of one hundred noisy neuronal sources. In addition, we show that this decoding scheme correctly identifies periods of No-Control (NC), and neither operates nor generates training data during these periods. All of this is accomplished without any *a priori* movement information, using very small training data sets.

In an accompanying proof of concept experiment, we implanted six Sprague Dawley rats and employed our modified bMLE scheme to allow the subjects to build their own

neuronal output classes to accomplish an auditory variant of the standard center-out task. Subjects were able to quickly adapt to the bMLE scheme and generate neuronal control sufficient to reliably complete a useful neuroprosthetic task, despite limited training data and no external movement information. By limiting the initial assumptions in our decoding strategy, we also demonstrate that useful neuroprosthetic control is possible using local field potentials and neurons in cingulate cortex, two prospective neuronal information sources without a clearly defined linear relationship to typical movement parameters.

Experimental Design and Methods

In order to develop a classification strategy aimed at identifying significantly separable neural states from real-time recordings, we chose to base our work on previous non-linear Bayesian Maximum Likelihood Estimation schemes (Achtman et al. 2007; Kemere et al. 2004; Santhanam et al. 2006; Shenoy et al. 2003). A non-linear decoding scheme was selected as prior studies have indicated that there is significant non-linear information present in the neural recordings (Brockwell et al. 2004; Chapin et al. 1999; Gao et al. 2003; Kemere et al. 2004; Kim et al. 2006; Wessberg et al. 2000). In addition, Santhanam *et al* found that the information transfer rate of neural prosthetic devices can be greatly enhanced by eliminating the prediction of unnecessary movement parameters (for example continuous trajectory) using MLE techniques (Santhanam et al. 2006).

Auditory Variant of the Standard Eight State Center-Out Task

One goal of this study was to allow implanted subjects to build a catalog of the separable neural states that they could reliably generate in real-time neural recordings; these states would then be mapped to the control of a neuroprosthetic device. As Sprague-Dawley rats were used as test subjects in this study, an auditory neuroprosthetic task was developed that parallels the standard center-out task in order to cater to the rat's heavy reliance on auditory cues.

In the standard center-out task, subjects are trained to reach out and press red buttons that have been lit. A center button is typically placed directly in front of the subject, and eight target buttons are placed equidistant from the target button at regular angular intervals. In a given trial, first the center button is lit, and the subject is required to press and hold the center button for one second. Next, the center light turns off, and one of the eight target buttons is randomly selected to be lit. For a successful trial, a subject is required to move their hand to touch the illuminated target button (Georgopoulos et al. 1982; Shenoy et al. 2003).

In our auditory variant of the center-out task, an audio cursor was represented by 200 ms tone pips corresponding to a location on a two-dimensional axis with frequency and intensity as the individual axes (See Figure 2.1). Subjects were given neural control of the auditory cursor through our bMLE scheme (Details Later in Methods). In order to start a trial, subjects were required to hold the auditory cursor in the center of the two axes for one second. Each trial began with the random presentation of one of eight target tones. The eight target tones were selected to be equidistant from the center of both axes, and spaced at regular angular intervals (See Figure 2.1). After the presentation of the

target tone, subjects were given a ten second response window to match the audio cursor to the selected target tone by adjusting their neural state in order to obtain a food reward. If the subject failed to accomplish this task in ten seconds, or matched the audio cursor to one of the other eight possible target tones, the trial ended and no reward was given.

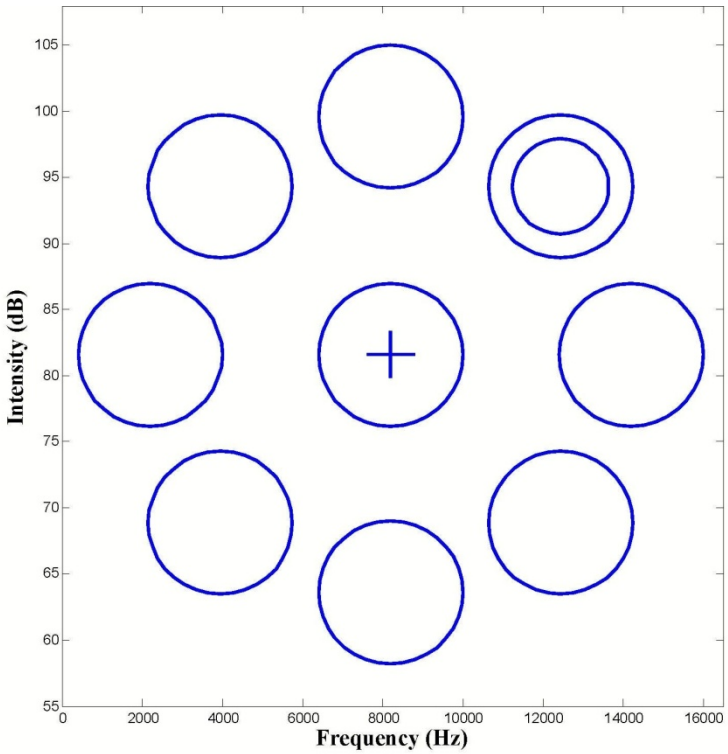

Figure 2.1: Auditory Variant of the Standard Center-Out Task (Visual Representation). The center of each circle on the periphery represents the frequency and intensity of each of the eight target tones. The center of the middle circle represents the frequency and intensity of the baseline tone. The subject was given neural control of the auditory cursor, the frequency and intensity of which is represented by the cross-hairs. On a given trial, the subject was required to first match the auditory cursor to the frequency and intensity indicative of the baseline state for one second. A goal tone was then presented, denoted by the smaller interior circle. During the response window, the subject was required to match the auditory cursor to the frequency and intensity of the goal tone for one second in order to obtain a food reward. Matching the auditory cursor to a target tone not presented resulted in an incorrect trial. All target tone frequencies and intensities were easily distinguishable by the human ear.

Bayesian MLE Classification Scheme to Isolate Quality Training Data

Similar to the work of Bashashati, the methodology used to identify neural data for training was based on external knowledge of the "approximate" time of intended control (IC) (Bashashati et al. 2007). During the IC response window, IC may or may not be present, and the timing of IC is unknown. Neural data during the IC response window may belong to either the IC or No Control (NC) class.

Pre-Experiment Set-up: Developing Separable Neural States for each Target

The auditory center-out task required the subject to first develop a distinct neural class for the tone at the center position on the 2-D auditory axis, and each of the eight possible target tones. After developing a separable neural class for each tone, real-time control proceeded according to the standard MLE scheme. To successfully complete a trial, subjects were required to match their current neural state to the neural class associated with the center position on the 2-D axis for one second, and then match their current neural state to the neural class associated with a random target tone for one second.

At the beginning of an experimental run, baseline neural recordings were taken for twenty seconds to establish a mean neural class for the subject representative of the No Control (NC) class. The firing rate of each recorded neuron was calculated in 200 ms non-overlapping windows (also known as 'bins"), and then averaged over the twenty seconds of baseline recordings to determine the mean firing rate of each neuron during the baseline NC window. This NC neural class was then mapped to the center of the 2-D auditory axis (See Appendix A for details on how each observed neural response was

translated into an auditory cursor for feedback based on current probability). In order to start a trial, subjects were required to match their current neural state to the NC class with a confidence level of greater than 95 percent for five consecutive 200 ms bins (See Chapter 1, Equation 4).

At the start of each trial, one of the eight target tones was randomly selected to be presented to the subject. On the first presentation of a target tone, there was no previous neural history from which to generate a neural class for the tone. As a result, the subject could not match their current neural state to the neural class associated with the target tone, and the first presentation of any target tone always resulted in an incorrect trial. After all incorrect trials, the neural activity over the ten second response window was inspected for candidate neural classes to be added to the history for the target tone in subsequent trials.

Candidate neural classes were selected on the basis of 'separability' from the neural classes already assigned to baseline and prior target tones. A 'separable' neural class can be statistically distinguished from the neural classes already associated with baseline and other target tones using a bMLE classification scheme, and therefore can be effectively used to predict an additional target tone in the future. To identify 'separable' neural classes, the intended control (IC) response window was inspected for neural states that were unlikely to have been generated by fluctuations around the mean neural firing rates already associated with previous tones. Using a simple one neuron example, a neuron with a mean firing rate of 40 Hz during the baseline NC class and a mean firing rate of 45 Hz after the presentation of target tone one would have low separability, as this neuron's

probability density functions for the NC and tone 1 classes largely overlap, providing little information to distinguish between these two classes (see Figure 2.2). Conversely, a neuron with a mean firing rate of 20 Hz during the NC class and 80 Hz after the presentation of tone 1 provides information to distinguish between these two classes, as the probability density function for each state is separate and distinct (See Figure 6), and therefore has high separability. The process to determine if any of the neural states during the IC response window were separable from the neural classes already associated with baseline and other target tones was as follows:

First, the firing rate of each neuron was calculated in 200 ms non-overlapping bins to create the vector R_k, a C x 1 vector containing the firing rates of C observed neurons for bin k (where k = 1 indicates the 200 ms bin immediately following the presentation of the target tone, k = 2 indicates the bin starting at 200 ms after target tone presentation and ending at 400 ms, etc; see Figure 2.3 Step 1 for an example). The vectors for each bin were then grouped into overlapping blocks of five bins (where block 1 consists of vectors $R_{1..5}$, block 2 consists of $R_{2..6}$, etc…), and a C x 1 mean vector for each block was determined (See Figure 2.3 Step 2 for an example).

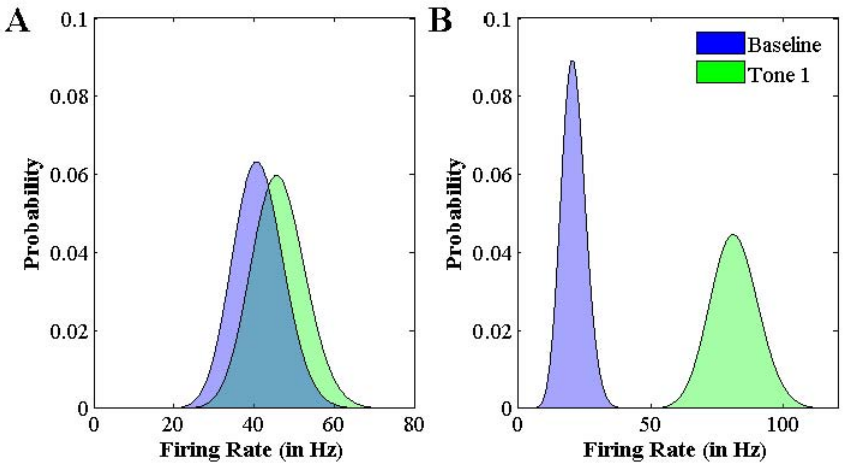

Figure 2.2: Separability of Neural Classes. (a) Single neuron with a mean firing rate of 40 Hz for the baseline class and a mean firing rate of 45 Hz for the tone 1 class. Notice that even an observed neuron firing rate of exactly 40 Hz cannot be used to distinguish between the baseline and tone 1 class, as the probability of the neuron firing at exactly 40 Hz for both states is similar. Therefore, these two neural classes are considered to have low separability. (b) Single neuron with a mean firing rate of 20 Hz for the baseline class and a mean firing rate of 80 Hz for the tone 1 class. The observed neuron firing rate can easily be used to distinguish between the baseline and tone 1 classes, as the respective probability density functions for these states have very little overlap. Therefore, an observed neuron firing rate of 28 Hz strongly indicates that the current neural state is from the baseline class, and an observed firing rate of 94 Hz is very likely attributable to the tone 1 class.

Next, the mean vector for each block was tentatively assigned as $\mathbf{M}_j$, a C x 1 vector to be examined as a possible new neural state for target tone j. From a practical neuroprosthetic perspective, a subject cannot consistently generate a neural response state exactly matching a mean vector; there is an inherent variability in the observed firing rate of a neuron around a given mean (Lee et al. 1998; Maynard et al. 1999). For a new neural class to be useful in the context of a neuroprosthetic task, expected fluctuations around the mean firing rates for the class must be differentiable from the neural classes already assigned to other tones. To account for this, one thousand artificially generated 'variance' vectors, drawn from the probability distribution resulting from the expected

variance centered around $\mathbf{M}_j$ (See Section: Testing the Classifier – Simulations, Equation 6 for details), were tested as observed responses. Equation 4 (Chapter 1) was then used to calculate the probability of target tone *j* given each observed response, using $\mathbf{M}_j$ as the vector mean for the neural class representing target tone *j*. For $\mathbf{M}_j$ to be considered 'separable', 95 percent of the 'variance' vectors were required to predict target tone *j* (as compared to the neural classes for baseline and the other target tones) with a probability of greater than 99 percent (See Figure 2.3 Step 3 for an example).

If a 'separable' block was evident in the response window, this block was appended to the history for target tone *j*. If multiple blocks were separable, the block with the greatest number of 'variance' vectors accurately predicting target tone *j* was appended to the history for target tone *j*. If no 'separable' block was evident during the IC response window, no block was appended to the history for the target tone. This distinction was important, as adding data to the history for the target tone when no useful neural modulation was present would significantly alter the mean firing rates for the neural class associated with the target tone, and therefore negatively impact performance. The mean of all the individual vectors in the history for target tone *j* was used to generate the mean for the neural class for target tone *j*, $\mathbf{M}_j$, for future trials.

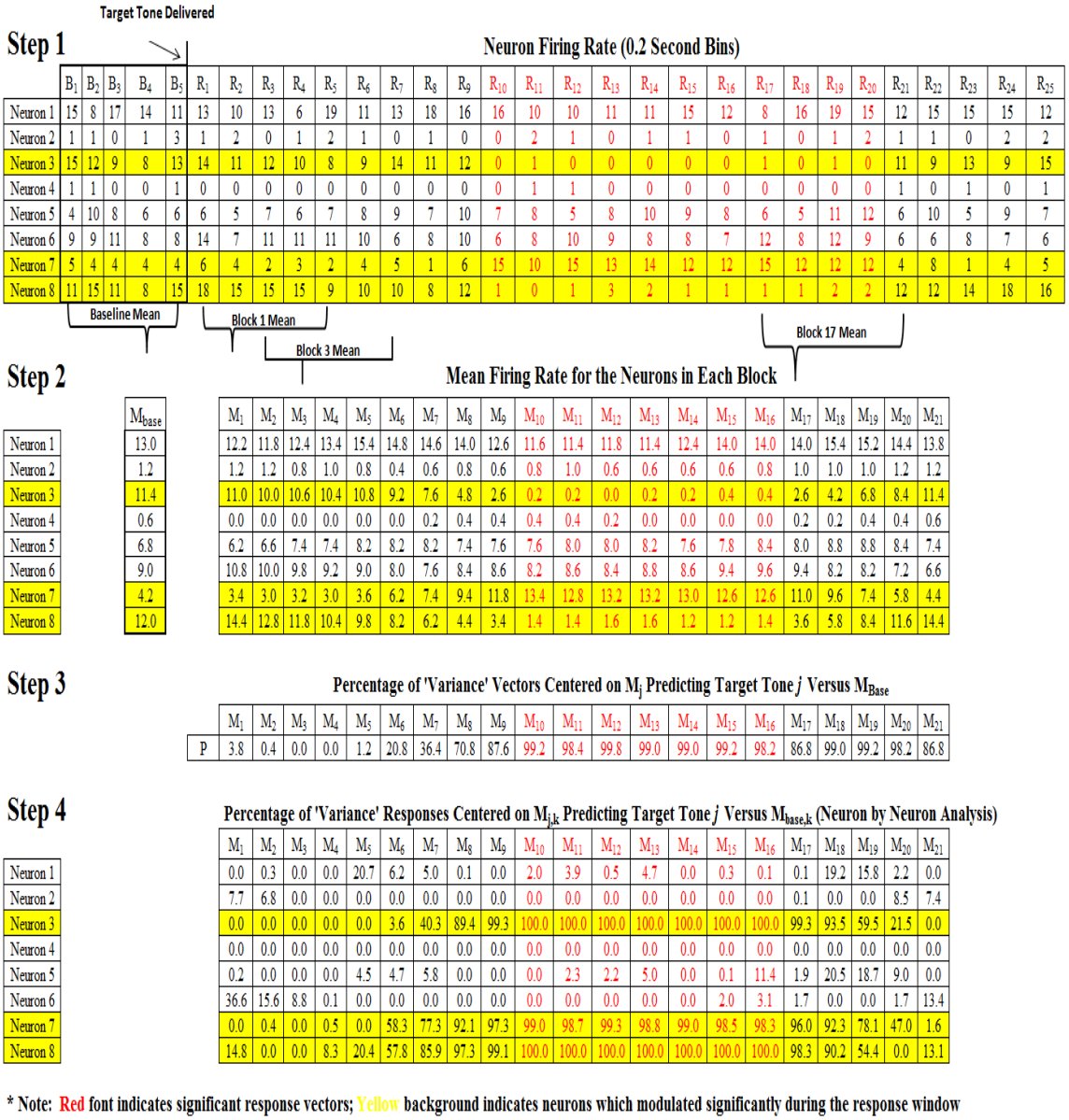

Figure 2.3: Analyzing the Response Window for a New Neural State. The response window for each trial began immediately after the target tone, *j*, was presented. The firing rates of individual neurons during the response window were binned every 0.2 seconds to generate an observed response vector R_i (Step 1). The vectors for each bin were then grouped into overlapping blocks of five bins, and a mean vector for each block, $\mathbf{M}_j$, was determined (Step 2). Using $\mathbf{M}_j$ as the mean neural state for the presented target tone, one thousand 'variance' vectors were generated around $\mathbf{M}_j$ and tested as observed responses (Step 3). For a block to be included in the history for the target tone *j*, 95 percent of the 'variance' vectors were required to predict target tone *j* (as compared to the mean neural state for baseline and the other target tones) with a probability of greater than 99 percent. In Step 4, Steps 1 through 3 were repeated on a neuron by neuron basis to determine which neurons (if any) were modulating significantly during the response window.

The size of the history for each target tone was adjusted based on the percentage of correct trials for the presentation of each tone (See Appendix B for details). The prior history for a given tone was shortened during periods of poor performance and lengthened during periods of strong performance. This strategy was implemented to allow the subject to quickly generate new neural classes for a target tone while performing poorly, but minimize the influence of occasional aberrant responses during periods of strong performance.

Subsequent Trials

After a history for each tone was built to establish the neural class for each tone, prediction of the current tone based on the present neural firing rate proceeded identically to Bayesian MLE classification based on *a priori* measurements (See Chapter 1). Defining the mean firing rate based on the history of *n* neurons with respect to the target tone *j* as the vector $\mathbf{M}_j$:

$$\mathrm{M}_j = \{\mu_{j1}, \mu_{j2}, \ldots \mu_{jn}\}$$

The real-time observed response R can be used to predict the probability of the baseline tone and each target tone by Equation 4.

In order to start a trial, the observed response vector R generated by the subject was required to predict the No Control (NC) class with a greater than 99 percent probability for five consecutive bins. If the subject failed to start a trial, a twenty second recording was taken to establish a new mean vector for the baseline NC class. Upon starting a trial, a random target tone was presented to the subject, and the subject was required to

generate an observed response vector R that predicted the neural class for that target tone with a greater than 99 percent probability for five consecutive bins to receive a food reward. The five 'correct' bins were then appended to the history for the target tone. Failing to accomplish this task, or generating an observed response vector R that predicted a target tone other than the one presented, resulted in an incorrect trial. After all incorrect trials, the response window was inspected for candidate neural states to be appended to the history for the target tone. During the response window, an auditory feedback tone (cursor) was presented to the subject such that as the subject's current neural state approached the neural state attributed to a target tone, the feedback tone approached the target tone (See Appendix A for details).

Refining the Analyzed Neuronal Sample

Including neurons in the sample used to predict a target tone which do not modulate with respect to at least one target tone detracts from neural control performance, as these neurons act as additional noise sources (Wahnoun et al. 2006). The neuronal sample for a Bayesian MLE classifier is normally pared down to include only the neurons positively contributing to performance by iterating through all possible combinations of neurons as input to the classifier. Due to the time constraints of a real-time application, this strategy was not technically feasible. Therefore, an alternative methodology to eliminate neurons failing to positively contribute to completing the neuroprosthetic task was implemented. Using the procedure outlined earlier to locate separable neural states in the response window, neurons were analyzed on an individual basis to locate neurons generating a differential response during the intended control (IC) response window. A neuron, *k,* was

deemed to generate a significant response to a tone if 90 percent of the artificially generated noise responses centered around the neuron's mean for a block in the response window, $\mathbf{M}_{j,k}$, were sufficient to differentiate a new target tone from baseline with greater than 95 probability (See Figure 2.3 Step 4). For a neuron to be included in the Bayesian MLE analysis, it was required to exhibit one significant response to at least one of the target tones in the trial history. This strategy ensured that every neuron included in the real-time analysis significantly modulated to at least one tone.

Local Field Potentials

The basic MLE methodology presented here can easily be extended to include Local Field Potentials (LFPs) as a potential neural input source. After being relayed from the Multichannel Neuron Acquisition System (Plexon, Inc., Dallas, TX), LFPs were additionally filtered in MatLab using a 4th order Butterworth filter with a pass band between 10 and 40 Hz. The RMS voltage of the filtered LFP signal for each channel was calculated over non-overlapping 200 ms bins and used as the input to the MLE filter. The mean μ and standard deviation σ of the recorded RMS was then calculated for each channel. Similar to other LFP studies, the probability distribution for the RMS for each channel was assumed to be Gaussian (Mehring et al. 2003; Rickert et al. 2005). The previously determined RMS mean for each channel with respect to a specific stimulus s_j was defined as the vector $\mathbf{M}_j$:

$$\mathrm{M}_j = \{\mu_{j1}, \mu_{j2}, \ldots \mu_{jn}\}$$

Where n is the total number of recorded LFP channels and $\boldsymbol{\mu}_{j1}$ is the RMS mean for channel 1 during stimulus s_j.

Given a vector of observed RMS responses R from each channel where r_1 is the observed RMS from channel 1 of *n* channels:

$$\mathrm{R} = \{r_1, r_2, \ldots r_n\}$$

Under the Gaussian assumption for RMS voltages, Equation 3 becomes:

$$P(\mathrm{R}|s_j) = \frac{1}{\sqrt{2\pi}}\sum_{i=1}^{\mathrm{n}} \frac{e^{-(r_i-\mu_{ji})^2/(2\sigma_i^2)}}{\sigma_i} \qquad (5)$$

Bayesian MLE analysis after this modification proceeded identically to single neuron analysis.

Behavioral Testing

Six Sprague-Dawley rats were implanted with standard Michigan 4x4 arrays to test the MLE classifier under practical neuroprosthetic conditions. Surgical procedures were identical to those performed in Chapter 3, with the following exceptions. Five of the animals were implanted in motor cortex (See Chapter 3: Surgical Techniques for Details). One animal was implanted in cingulate cortex using coordinates 1.5-2.5 mm anterior to bregma, 0.3-0.7 mm lateral from bregma, and 1.6-2.5 mm deep from the surface of the brain (Paxinos et al. 1980). The cingulate animal was used to assess the suitability of the naïve MLE classifier for use with cortical areas not known to have a linear relationship between neuronal firing rates and movement parameters.

Electrophysiology and Behavior System

Units were sorted via a Multichannel Neuron Acquisition System (Plexon, Inc., Dallas, TX) and spike times were relayed with nominal delays via TCP/IP to a dual 1.25 GHz

Dell Dimension Computer (Dell, Inc., Austin, TX) that both analyzed the spike activity using in-house designed software (Mathworks, Inc., Natick, MA) and controlled the behavioral box (Coulborne Instruments, Inc., Allentown, PA). During each experimental session neural electrophysiological data from the 16 electrode channels sampled at 40 kHz were simultaneously amplified and bandpass filtered (450 – 5000 Hz). Manual spike sorting was conducted prior to each experimental session. Autocorrelograms were generated for each sorted unit and visually inspected for an obvious absolute and relative refractory period. Local field potential recordings from all 16 channels were sampled at 1000 Hz and initially bandpass filtered from 3-90 Hz. Auditory stimuli were delivered via a speaker (Yamaha NS-10M Studio, Yamaha Corporation, Buena Park, CA) located 35 cm directly above the test box. The system delivered a near-flat frequency response between 500 Hz and 32 kHz. The system was calibrated to a position at the food delivery tray; although calibration measurements indicated that the test box approximated a free field.

Behavioral Training

All rats entering training were deprived to 85% of their free-feeding weight to provide motivation to receive a food reward. For each behavioral session, the rats were plugged into the headstage and commutator cables and placed into the behavioral box.

Testing the Classifier – Simulations

For useful neuroprosthetic control, a practical adaptive neuroprosthetic system needs to be able to separate neural data relevant to completing a neuroprosthetic task from periods

of inactivity. This is necessary to a) avoid training on neural data without useful predictive value, and b) prevent neural activity unrelated to the control task from generating unwanted device movement. In order to test our Bayesian MLE classifier, simulated neural data based on reasonable assumptions appropriate for cortical neurons engaged in a motor center-out task were used to model the classifier's performance under a variety of realistic experimental conditions. Using this methodology, the classifier's performance could easily be compared to the known expected performance from the simulated neural data.

To investigate the utility of the naïve MLE classifier in a realistic situation, we simulated the spike trains of 100 neurons as the neural input into the classifier. The no-control (NC) firing rate for each neuron was randomly selected based on physiological norms for cortical neurons (between 1-150 Hz). As the variance in experimentally derived neuronal data often exceeds that predicted by a Poisson spike count (Lee et al. 1998; Maynard et al. 1999), the following experimentally derived equation was used to generate the variability, SD, in neural firing rates around the mean M (Lee et al. 1998; Maynard et al. 1999):

$$SD = 1.44\mathrm{M}^{0.50} \qquad (6)$$

For each experimental run, a small subset of the 100 simulated neurons was selected to consistently modulate to a new mean firing rate for each target tone. The modulated firing rate for each neuron in the subset was randomly selected within physiological norms (1-150 Hz). The size of the subset was systematically varied between two and

twenty neurons to determine the impact of the number of actively engaged neurons on task performance. The mean firing rates for each tone were required to be differentiable from NC and other target tone class means with greater than 99 percent probability (See Chapter 1 Equation 4). Given the variance from Equation 6, a single neuron by itself was unable to generate the nine differentiable neural classes representing the no-control (NC) and the eight target tones.

Upon the presentation of a target tone, the subset neurons were modulated to their mean firing rates for the target tone for two seconds, beginning at a random time during the intentional control (IC) response window. This strategy was employed to test the ability of the classifier to identify new candidate neural classes generated by a small number of neurons, presented at short random locations in time during the IC response window. NC and modulated firing rates were reselected after each experimental run for a given subset size. Five hundred experimental runs, consisting of 300 trials each, were simulated for each subset size.

After running these initial simulations, attempts were made to deliberately confound the bMLE classifier by mimicking self-paced neuroprosthetic control. Instead of modulating to the correct response 100 percent of the time, the percentage of trials in which the neurons modulated correctly was also systematically varied. These additional simulations were performed to test the bMLE classifier performance during periods in which the subject is not generating a neural control signal. For the classifier to perform well under these conditions, it must recognize and omit neural data for training during

periods of no-control (NC). Moreover, the classifier output should direct a neuroprosthetic device to remain motionless during stretches of NC.

Results

Simulation Results

When the simulated input neural activity modulated to correctly perform the eight-state center-out task for 100 percent of all experimental trials, the bMLE classifier generated an output signal that completed the eight-state center out task with nearly 100 percent accuracy (See Figure 2.4). As no history was used at the beginning of each experimental run, the classifier had to first quickly locate and adopt new neural classes generated only briefly during the response window for each of the target tones. Therefore, the output signal from the classifier could not successfully predict a presented target tone until the second time that tone was encountered. Consequently, there were at least eight - and typically only eight – incorrect trials for each experimental run, indicating how quickly the classifier was able to identify and adopt a new neural class for each tone. The classifier output performance accurately mimicked the performance of the simulated input neural signal, even with as few as two neurons out of 100 generating all nine neural classes (eight target tones and baseline/No Control). The performance of the output signal deteriorated only slightly with fewer neurons (See Figure 2.4); the fewer the number of neurons used to generate all of the neural classes, the less distinct/separable these neural classes become.

When the simulated input neural activity was modified to include trials of No-Control (See Methods), the bMLE classifier was able to successfully identify these trials; the bMLE classifier did not generate training data during these trials, and the bMLE output signal successfully identified these trials as No-Control (See Figure 2.4). When the simulated input neural signal only modulated to generate intentional control for 75

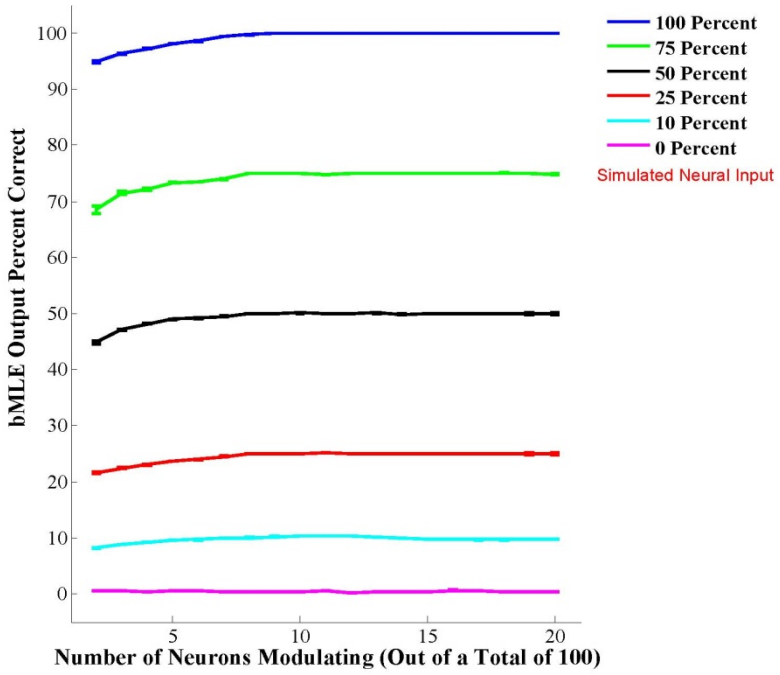

Figure 2.4: Simulated Data - Identifying Neural States Useful for Completing the Auditory Center-Out Task. The bars denote standard error, n = 500. For each experimental run, a subset of the 100 simulated neurons was selected to consistently modulate to a new mean firing rate for each of the eight target tones. Upon the presentation of a target tone, the subset neurons were modulated to their mean firing rates for that target tone for two seconds, beginning at a random time during the response window. Five hundred experimental runs, consisting of 300 trials each, were simulated for each subset size. The actual performance of the simulated neurons was systematically varied (See Legend) to represent more realistic subject performance expectations. The y-axis denotes the average percent correct according to the classifier based on the simulated input. The x-axis denotes the total number of neurons modulating out of the initial 100. The performance predicted by the classifier accurately reflected the simulated performance, even with as few as two neurons generating the eight separate neural states needed to complete the center-out task. Moreover the classifier was able to accurately predict low levels of simulated performance, indicating the classifier was able to identify neural data useful for generating separable neural states while ignoring extraneous data that would negatively impact classifier performance.

percent of the trials, the output signal from the bMLE classifier correctly performed the eight-state center out task at almost 75 percent accuracy. As the simulated input neural

performance varied, the performance of the bMLE classifier output signal also varied. When the simulated input neural signal completely failed to modulate during the response window; the bMLE classifier output signal correctly indicated a period of No-Control for the entire experimental run, and never generated any training data.

In-vivo Performance

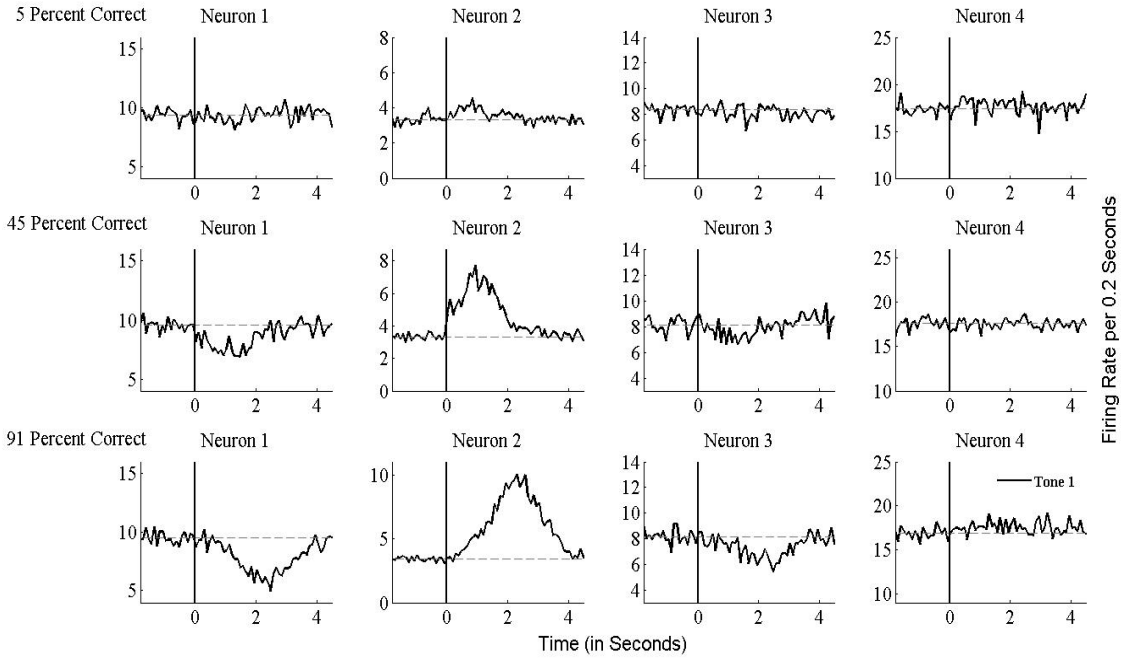

Figure 2.5: Building a Distinct Neural Class for a Tone. Each row depicts the same four neurons recorded from one animal, across the same recording day. The dotted line denotes the mean firing rate for each neuron during the baseline window. The dark black line centered at 0 seconds indicates the presentation of a target tone. Row 1 depicts the first 200 trials for the animal, where the subject successfully completed the 1-state center-task on only 5 percent of the trials. Row 2 depicts the second set of 200 trials for this animal, where 45 percent of the trials were successfully completed. Row 3 depicts the third set of 200 trials for this animal, where 91 percent of the trials were successfully completed. Note that as performance improves, the animal progressively learns to decrease the firing rates of Neurons 1 and 3, while increasing the firing rate of Neuron 2, in response to the presentation of the target tone.

All six animals in this study were first started on a one-state detection task, where the same target tone was presented each trial. This task requires the animal to generate a 2nd neural class, different than the baseline/No-Control state, on command after the target

tone was presented. Figure 2.5 depicts a representative example of one animal progressively learning to generate a 2nd distinct neural class in response to the presentation of a tone. All six animals were able to use the bMLE classifier to complete this task at a 90 percent or greater level within three days of the first experimental run (See Table 2.1).

After learning the one-state task, four animals - three implanted in motor cortex, the other implanted in cingulate cortex - were moved to a two-state discrimination task where only two of the possible eight target tones were randomly presented to the animal. Again, animals were typically able to complete this task above chance within three days of training (See Table 2.1). Figure 2.6 depicts a Peri-Stimulus Time Histogram (PSTHs) of an experimental run from a subject successfully completing this task well above random chance. When first exposed to the task, the animal generated only one neural response state different than the baseline/NC class, presumably a hold-over response from training with the one-state detection task. Hold-over behavior was evident every time an animal was switched to a more difficult/new task. After only three days of training (100-trial sessions, 7 sessions per day), subjects were able to consistently perform the two state discrimination above chance. In contrast, un-implanted Sprague Dawley rats trained on a two-state tone discrimination task in our lab - where subjects are simply required to press one of two levers to indicate which tone was presented – can take over a month of training to achieve this level of performance.

After reaching a two-state task performance level of greater than 80 percent, two of the animals were anesthetized for a 300 trial experimental run. In both cases, the anesthetized animal performance level was under 2 percent. Under anesthetized conditions, the bMLE classifier rarely generated training data, and almost never deviated from the baseline/No-Control condition.

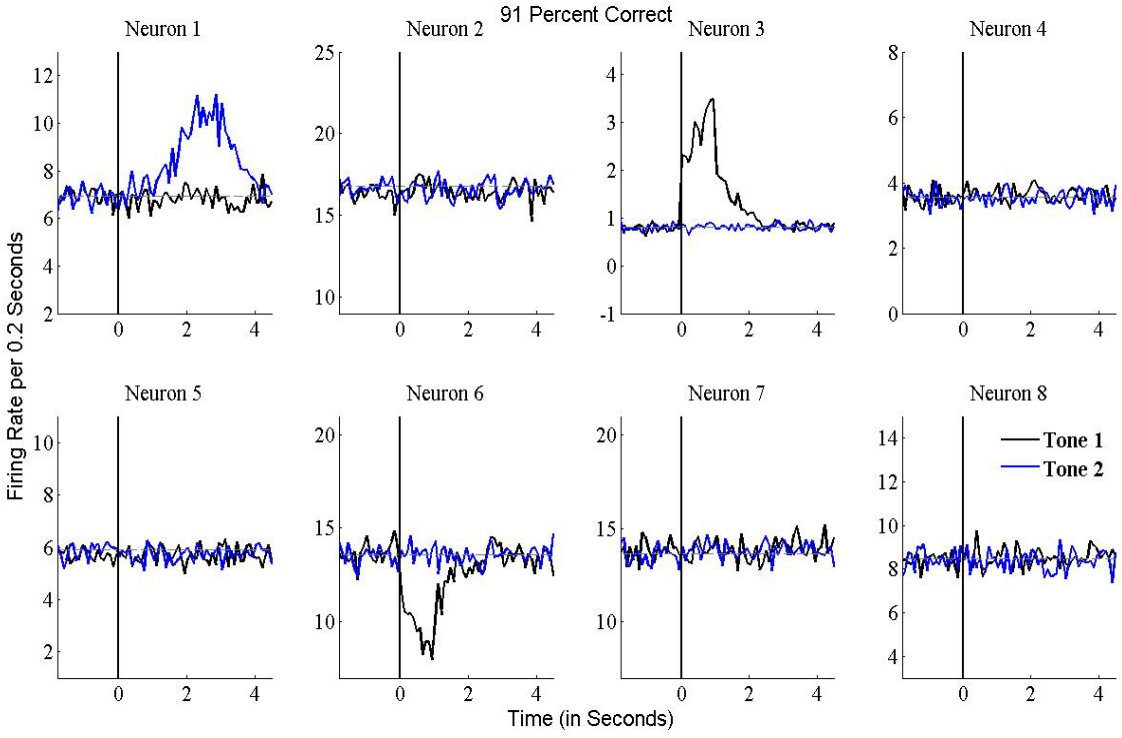

Figure 2.6: Representative Example, Two-State Center-Out Task. The dotted line denotes the mean firing rate for each neuron during the baseline window. The dark black line centered at 0 seconds indicates the presentation of a target tone. Data set depicts a 200 trial interval in which one subject (KMI 5) successfully completed 91 percent of trials (Significant, $p < 0.001$). Note that for Tone 1, the subject modulates Neuron 3 while demodulating Neuron 5. For Tone 2, the subject only modulates Neuron 1. In a forced choice paradigm, random chance would be fifty percent.

After learning the two-state task, two animals - one implanted in motor cortex, the other implanted in cingulate cortex - were moved to a four-state discrimination task, where four of the possible eight target tones were randomly presented to the animal. Both subjects were able to successfully complete the four-state task significantly above random chance

after one week (See Table 2.1).

Figure 2.7 depicts a Peri-Stimulus Time Histograms (PSTHs) of an experimental run from a subject (KMI 5) successfully completing this task well above random chance. Note that KMI 5 retained the same neural classes for Tone 1 and 2 as generated for the two-state task (See Figure 2.6). However, for Tone 3, the KMI 5 modulated Neuron 3

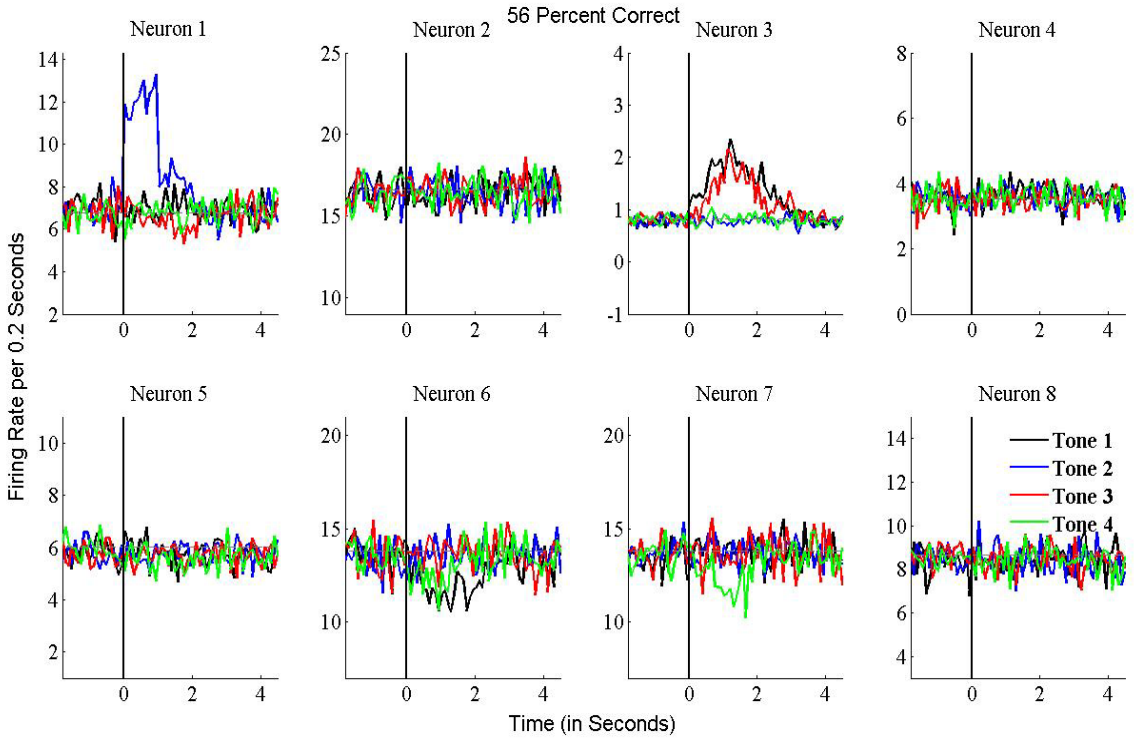

Figure 2.7: Representative Example, Four-State Center-Out Task. The dotted line denotes the mean firing rate for each neuron during the baseline window. The dark black line centered at 0 seconds indicates the presentation of a target tone. Data set depicts a 200 trial interval in which one subject (KMI 5) successfully completed 56 percent of trials (Significant, $p < 0.001$). Note that for Tone 1 and Tone 2, KMI 5 has retained approximately the same neural classes as those adopted for the 2-state center-out task (Figure 10). However, for Tone 3, the subject modulates Neuron 3 *without* demodulating Neuron 6, therefore creating a neural class distinct from Tone 2. For Tone 4, the subject demodulated Neuron 7 slightly without changing the firing pattern for the other neurons. As subjects progressed from the one-state task to the four-state task, they typically retained neural classes associated with previous tones, and added new neural classes for additional tones. Percent correct for each tone: Tone 1 = 85 Percent, Tone 2 = 74 Percent, Tone 3 = 38 Percent, Tone 4 = 28 Percent. In a forced choice paradigm, random chance would be twenty-five percent.

without demodulating Neuron 6, therefore creating a neural class distinct from Tone 2. For Tone 4, the subject demodulated Neuron 7 slightly without changing the firing pattern for the other neurons. Both animals' performance for Tone 1 and Tone 2 presentation was superior to subject performance for Tone 3 and Tone 4, presumably because of previous training.

Performance using Local Field Potentials

As noted in other studies, recorded unit activity for animals in this study typically diminished substantially over the three weeks following surgery (Ludwig et al. 2008; Ludwig et al. 2006; Santhanam et al. 2007; Schwartz 2004). When fewer than two well-isolated neuronal units[2] were evident, animals were transitioned to a single-state center-out task using their recorded local field potentials (LFPs) as the input to the classifier (see Methods). All six animals were able to generate a second neural class sufficient to complete the 1-state task on the first day of LFP training (See Table 2.1). Subjects typically retained the same stereotyped motor responses noted when performing the 1-state unit task, which may explain how quickly the animals were able to generate viable LFP responses. Subjects tended to increase the RMS voltage across the entire array in response to a presented tone. Subject performance increased significantly ($p < 0.01$) over the first week of LFP training.

[2] Units were sorted by hand, and the autocorrelogram was visually inspected for an obvious absolute and relative refractory period.

Table 2.1: Summary of *In Vivo* Results

Neural Input Source	Number of Target Tones	Number of Animals	Average Day 1 Performance	Average Day 3 Performance	Average Day 7 Performance	Forced Choice Random Chance
Units	1	6, 5 Motor 1 Cingulate	16.8 ± 7%	92.8± 5%*	N.A.	N.A.
	2	4, 3 Motor 1 Cingulate	32.5 ± 11%	64 ± 10%*$^{+}$	73.3 ± 9%*$^{+}$	50%
	4	2, 1 Motor 1Cingulate	15 ± 8%	26 ± 8%	53 ± 13%*$^{+}$	25%
LFPs	1	6, 5 Motor 1 Cingulate	67 .4± 13%	75.2 ±10%	83 ± 14%*	N.A.
	2	2, 1 Motor 1 Cingulate	37.5± 9%	51± 9%*	65± 6%*$^{+}$	50%

*** Significant improvement over Day 1 Performance (p <0.01)**

$^{+}$ Significant Improvement over Forced Choice Random Chance (p <0.01)

After learning the one-state LFP task, two animals - one implanted in motor cortex, the other implanted in cingulate cortex - were moved to a two-state LFP discrimination task. Both animals were able to successfully complete the two-state task significantly above random chance for a 2-state forced choice paradigm ($p< 0.01$). As with the one-state LFP task, both subjects tended to increase the RMS voltage in the 10-40 Hz frequency band

across the entire array in response to Tone 1. In response to Tone 2 presentation, however, both subject increased the RMS voltage across only the upper half of the array.

Discussion

Animal Behavior during Task Performance

In the process of developing new neural classes, animals implanted in motor and cingulate cortex often developed specific stereotyped movements for each of the target tones. This result is not surprising, as the animal is likely learning a new movement/behavior for each target tone which incidentally changes the firing rates of recorded neurons, as opposed to deliberately modulating neural activity. Behaviors associated with a specific target would often carry over as the number of targets was increased. In cases where the neurons recorded across the array changed dramatically from one day to the next, animals would often learn a new behavior for each target in order to generate the separate neural classes necessary to complete the task.

Algorithm Performance

By isolating and training on only useful neural data, an improvement in algorithm decoding performance in comparison to other bMLE classification schemes was expected. Simulation results demonstrate that the full center-out task can be performed at greater than 95% accuracy using our bMLE classification scheme, with as few as two active neurons out of 100. Moreover, typically only one training trial was necessary for each of the eight targets. At first glance, these results are a marked improvement over other bMLE neuroprosthetic paradigms, which can require as many as 120 neurons to

achieve an asymptotic performance level of approximately 90 percent, and require in excess of 400 training trials (Achtman et al. 2007; Santhanam et al. 2006; Shenoy et al. 2003). However, alternative bMLE studies use real neural data taken from previous experiments to arrive at these performance metrics. In addition, these studies typically utilize a single decoding time window of 200 ms to improve information transfer rates, as opposed to requiring five consecutive correct 200 ms bins to actuate the neuroprosthetic device (Achtman et al. 2007; Santhanam et al. 2006; Shenoy et al. 2003). Consequently, a direct comparison is difficult, and simulated data in this study should only be viewed as a theoretical maximum for self-paced bMLE performance.

Results from implanted animals utilizing our bMLE algorithm in real-time to develop neural control also indicate an improvement in number of neurons necessary to complete the center-out task, as well as number of trials necessary to train the algorithm. Animals well-trained in a particular task typically required only one trial for each target to establish a useable neural class. Moreover, animals performing the 2-state and 4-state tasks used fewer than five total neurons to generate the neural classes necessary to perform these tasks[3]. Finally, the speed in which animals were able to successfully perform new tasks above chance – typically within a week – suggests the self-paced bMLE decoding strategy presented in this study is easy to use.

Algorithm Parameters

Algorithm parameters – window size, number of consecutive 'correct' bins, required

[3] The number of neurons actively engaged in the task out of the total number of neurons isolated on a given day was determined as noted in Methods: Refining the Analyzed Neuronal Sample.

degree of statistical separability of neural classes, etc - were initially determined from relevant literature, and then modified through systematic trial and error to optimize animal performance. Depending on specific requirements for a particular neuroprosthetic device, these parameters can be modified to tailor device performance. For example, the required *p* value to specify a particular target from a No-Control state can be decreased to reduce accidental movements. Similarly, the required percentage of noise vectors (See Methods) around a prospective neural class indicating a new target can be varied to decrease the probability of training on poor data. Window size can be decreased to increase information transfer rates, but at the expense of accuracy. In clinical applications, these parameters would need to be determined based off the preferences of the patient.

Limiting Decoding Assumptions

Only two assumptions were necessary for the bMLE classifier presented in this study to work: 1) the approximate time of intended control, and 2) the probability distribution of the neural input source (Poisson or Gaussian for individual neurons and Local Field Potentials, respectively). In contrast the linear mapping of neural firing rates to prosthetic control is dependent on a number of assumptions (Kettner et al. 1988) that can be difficult to achieve in practice (Hochberg et al. 2006; Kemere et al. 2004; Lebedev and Nicolelis 2006; Rickert et al. 2005; Santhanam et al. 2006; Wahnoun et al. 2006; Wu et al. 2003). In order to generate an effective neural map, the recorded sample of neurons must be sufficient to fully define the movement parameter space (Kemere et al. 2004; Santhanam et al. 2006; Schwartz 2004; Wu et al. 2003). However, often only a small

number of stable neuronal units can be recorded under chronic conditions due to technological limitations and the chronic immune response (Hochberg et al. 2006; Ludwig et al. 2006; Nicolelis et al. 2003; Rennaker et al. 2007; Santhanam et al. 2006; Schwartz 2004; Selim Suner 2005; Seymour and Kipke 2007; Vetter et al. 2004b; Williams et al. 1999; Wu et al. 2003). Moreover, the firing rates of many neurons recorded in motor cortex have no identifiable relationship to movement parameters (Georgopoulos et al. 1986; Lebedev and Nicolelis 2006; Wahnoun et al. 2006), and the firing rates of neurons that are related to movement are only approximately linear during precisely defined stereotypical movements (Kemere et al. 2004; Lebedev and Nicolelis 2006; Wu et al. 2003). In addition, accurately isolating individual neurons can be difficult given low signal-to-noise recordings (Lewicki 1998; Wood et al. 2004; Wu et al. 2003). Consequently, multi-unit clusters are often used as the input for neural prosthetic applications, which can negatively affect the performance of linear decoding algorithms (Lebedev and Nicolelis 2006; Wahnoun et al. 2006).

Calibrating a neural control system based on previously determined relationships between neural firing rates and measured movement parameters may also ignore the subject's ability to adapt neural firing patterns in order to generate a greater number of usable output states. Studies which use decoding algorithms that can incorporate transient changes in neural ensemble firing patterns have indicated that animal subjects can learn to adapt their firing patterns in order to improve performance in neural control tasks (Carmena et al. 2003; Kennedy et al. 2000; Serruya et al. 2002; Taylor et al. 2002). In these studies, neurons which had little or no previous relationship to a known movement parameter often adapted over time to provide information relevant to completing the

neural control task (Carmena et al. 2003; Kennedy et al. 2000; Serruya et al. 2002; Taylor et al. 2002).

By limiting the initial assumptions used in our decoding algorithm, subjects were allowed to utilize neuronal sources without a known linear relationship to a movement parameter to create an output signal for neural control. Specifically, neurons from cingulate cortex and local field potentials were effectively used as neuronal input sources to the bMLE algorithm in real-time (See Results). In a previous study, rats were able to modulate single neurons from cingulate cortex on command (Marzullo et al. 2006). By successfully completing a 4-state center-out task significantly above chance levels, the cingulate animal in this study demonstrated an even more refined neural control signal, demonstrating that cortical areas outside of motor cortex can be used to generate effective neural control. As an added benefit, by limiting the initial decoding assumptions, the bMLE classification scheme presented in this study should be less dependent upon experimental environment and set-up for practical clinical use.

Local Field Potential Recordings

Although prior studies have investigated the utility of the recorded local field potentials (LFPs) to predict observed movements off-line (Mehring et al. 2003; Rickert et al. 2005), real-time control of a neuronal output signal utilizing LFPs has only been demonstrated in one study (Kennedy et al. 2004a; Kennedy et al. 2004b). LFPs could represent the optimal input signal for neuroprosthetic systems, as LFPs exhibit greater spatial and temporal resolution than electroencephalograms (EEGs) (Anderson et al. 2004; Mehring et al. 2003; Rickert et al. 2005), and are presumed to be easier to obtain and more stable

than single unit recordings for chronic implantations (Anderson et al. 2004; Rickert et al. 2005).

In this study, animals were able to modulate the RMS voltage of LFPs in the 10-40 Hz band to generate a real-time control signal sufficient to complete the 1-state and 2-state center-out tasks above random chance (See Table 2.1). However, there is no way to determine if the animals were manipulating their LFPs through neurological mechanisms, or by inducing artifact into the system. As noted in many other studies (Ludwig et al. 2006; Mehring et al. 2003; Rickert et al. 2005; Santhanam et al. 2007), obvious artifact was intermittently apparent during animal motion, which would on occasion create a perturbation in the RMS voltage of the LFP between 10-40 Hz. Not surprisingly, despite the self-paced architecture of the bMLE classifier, these noise perturbations could generate occasional unwanted control outputs. Unlike other studies which removed periods of extensive noise during *post-hoc* analysis (Magill et al. 2004; Mehring et al. 2003; Rickert et al. 2005), the constraints of real-time decoding preclude this option. In order to generate more refined real-time control with local field potentials in a self-paced context, techniques drawn from EEG (electroencephalography) control tasks to isolate signal from noise should be applied in future experiments (Cooper et al. 2003; Wolpaw et al. 2002).

Conclusions

In this study, we developed and tested a non-linear Bayesian Maximum Likelihood Estimator classification (bMLE) scheme to identify statistically separable neural states evident in real-time neural recordings, and then mapped these states to generate self-

paced neural control of a neuroprosthetic interface suitable for accomplishing a useful task. By limiting initial decoding assumptions and training only on relevant neural data, accurate neural-control was possible with as few as two neurons, using minimal training data and no *a-priori* movement measurements for calibration. In addition, we expanded our pool of possible neuronal input sources to include neurons in motor cortex without a detectable linear relationship to movement parameters, neurons from non-motor cortical areas, multi-unit clusters, and local field potentials. This decoding scheme was sufficient to identify periods of No-Control in the data set, and neither generated training data nor control output during these periods. Finally, as the methodology proposed here is both simple and adaptive, this framework should be more resistant to the inherent instability of the neuronal input source resulting from the chronic immune response.

Acknowledgements

The authors of this paper would like to acknowledge all of members of the Neural Engineering Laboratory at the University of Michigan for their assistance in this study Specific thanks go to Kevin Otto and Greg Gage for helpful advice and programming relating to the behavioral paradigm. This work was supported by the Center for Wireless Integrated Microsystems NSF EEC-9986866, the NIH P41 Center for Neural Communications Technology (EB002030), and the Whitaker Foundation.

References

Achtman N, Afshar A, Santhanam G, Yu BM, Ryu SI, and Shenoy KV. Free-paced high-performance brain-computer interfaces. *J Neural Eng* 4: 336-347, 2007.

Ali B, Steve GM, Jaimie FB, Rabab KW, and Gary EB. A Comparative Study on Generating Training-Data for Self-Paced Brain Interfaces. *Neural Systems and Rehabilitation Engineering, IEEE Transactions on [see also IEEE Trans on Rehabilitation Engineering]* 15: 59-66, 2007.

Anderson RA, Burdick JW, Musallam S, Pesaran B, and Cham JG. Cognitive Neural Prosthetics. *Science Direct* 8: 2004.

Bai Q, Wise KD, and Anderson DJ. A high-yield microassembly structure for three-dimensional microelectrode arrays. *IEEE Trans Biomed Eng* 47: 281-289, 2000.

Barbieri R, Wilson MA, Frank LM, and Brown EN. An analysis of hippocampal spatio-temporal representations using a Bayesian algorithm for neural spike train decoding. *IEEE Trans Neural Syst Rehabil Eng* 13: 131-136, 2005.

Bard AJ, and Faulkner L. *Electrochemical methods: fundamentals and applications*. New York: Wiley, 1980.

Barnes PM, Adams PF, and Schiller JS. Summary Health Statistics for the U.S. Population: National Health Interview Survey, 2001. *Vital Health and Statistics* 10: 2003.

Bashashati A, Fatourechi M, Ward RK, and Birch GE. A survey of signal processing algorithms in brain;computer interfaces based on electrical brain signals. *Journal of Neural Engineering* 4: 2007.

Blanche TJ, Spacek MA, Hetke JF, and Swindale NV. Polytrodes: High-Density Silicon Electrode Arrays for Large-Scale Multiunit Recording. *J Neurophysiol* 93: 2987-3000, 2005.

Bragin A, Hetke J, Wilson CL, Anderson DJ, Engel J, and Buzsáki G. Multiple site silicon-based probes for chronic recordings in freely moving rats: implantation, recording and histological verification. *Journal of Neuroscience Methods* 98: 77-82, 2000.

Brockwell AE, Rojas AL, and Kass RE. Recursive bayesian decoding of motor cortical signals by particle filtering. *J Neurophysiol* 91: 1899-1907, 2004.

Brown EN, Frank LM, Tang D, Quirk MC, and Wilson MA. A statistical paradigm for neural spike train decoding applied to position prediction from ensemble firing patterns of rat hippocampal place cells. *J Neurosci* 18: 7411-7425, 1998.

Brown P, Kupsch A, Magill PJ, Sharott A, Harnack D, and Meissner W. Oscillatory local field potentials recorded from the subthalamic nucleus of the alert rat. *Exp Neurol* 177: 581-585, 2002.

Buitenweg JR, Rutten WL, Willems WP, and van Nieuwkasteele JW. Measurement of sealing resistance of cell-electrode interfaces in neuronal cultures using impedance spectroscopy. *Medical & biological engineering & computing* 36: 630-637, 1998.

Burns BD, Stean JP, and Webb AC. Recording for several days from single cortical neurons in completely unrestrained cats. *Electroencephalography and Clinical Neurophysiology* 36: 314-318, 1974.

Carmena JM, Lebedev MA, Crist RE, O'Doherty JE, Santucci DM, Dimitrov DF, Patil PG, Henriquez CS, and Nicolelis MAL. Learning to Control a Brain-Machine Interface for Reaching and Grasping by Primates. *PLoS Biology* 1: e42, 2003.

Cattaneo A, Maffei L, and Morrone C. Patterns in the discharge of simple and complex visual cortical cells. *Proc R Soc Lond B Biol Sci* 212: 279-297, 1981a.

Cattaneo A, Maffei L, and Morrone C. Two firing patterns in the discharge of complex cells encoding different attributes of the visual stimulus. *Exp Brain Res* 43: 115-118, 1981b.

Chapin JK, Moxon KA, Markowitz RS, and Nicolelis MA. Real-time control of a robot arm using simultaneously recorded neurons in the motor cortex. *Nat Neurosci* 2: 664-670, 1999.

Cooper R, Binnie CD, Osselton JW, Prior PF, and Wisman T. EEG, paediatric neurophysiology, special techniques and applications. In: *Clinical Neurophysiology Vol 2*, edited by Cooper R, Mauguiere F, Osselton JW, Prior PF, and Tedman BM. Amsterdam: Elsevier B.V, 2003, p. 8-103.

Dobelle WH. Artificial vision for the blind by connecting a television camera to the visual cortex. *Asaio Journal* 46: 3-9, 2000.

Donoghue JP, Nurmikko A, Black M, and Hochberg LR. Assistive technology and robotic control using motor cortex ensemble-based neural interface systems in humans with tetraplegia. *J Physiol* 579: 603-611, 2007.

Drake KL, Wise KD, Farraye J, Anderson DJ, and BeMent SL. Performance of planar multisite microprobes in recording extracellular single-unit intracortical activity. *IEEE Trans Biomed Eng* 35: 719-732, 1988.

Eggermont JJ. Analysis of compound action potential responses to tone bursts in the human and guinea pig cochlea. *J Acoust Soc Am* 60: 1132-1139, 1976.

Eggermont JJ. Compound action potentials: tuning curves and delay times. *Scand Audiol Suppl* 129-139, 1979.

Eggermont JJ, Aertsen AM, Hermes DJ, and Johannesma PI. Spectro-temporal characterization of auditory neurons: redundant or necessary. *Hear Res* 5: 109-121, 1981.

Epping WJ, and Eggermont JJ. Sensitivity of neurons in the auditory midbrain of the grassfrog to temporal characteristics of sound. I. Stimulation with acoustic clicks. *Hear Res* 24: 37-54, 1986.

Fetz E. Operant conditioning of cortical unit activity. *Science* 163: 955–958, 1969.

Fetz EE, and Finocchio DV. Correlations between activity of motor cortex cells and arm muscles during operantly conditioned response patterns. *Exp Brain Res* 23: 217-240, 1975.

Furukawa S, Xu L, and Middlebrooks JC. Coding of sound-source location by ensembles of cortical neurons. *J Neurosci* 20: 1216-1228, 2000.

Gage GJ, Ludwig KA, Otto KJ, Ionides EL, and Kipke DR. Naive coadaptive cortical control. *J Neural Eng* 2: 52-63, 2005.

Gao Y, Black MJ, Bienenstock E, Wu W, and Donoghue JP. A quantitative comparison of linear and non-linear models of motor cortical activity for the encoding and decoding of arm motions. In: *1st International IEEE/EMBS Conference on Neural Engineering*. Capri, Italy: 2003, p. 189-192.

Geisler WS, and Albrecht DG. Bayesian analysis of identification performance in monkey visual cortex: nonlinear mechanisms and stimulus certainty. *Vision Res* 35: 2723-2730, 1995.

Georgopoulos AP, Kalaska JF, Caminiti R, and Massey JT. On the relations between the direction of two-dimensional arm movements and cell discharge in primate motor cortex. *J Neurosci* 2: 1527-1537, 1982.

Georgopoulos AP, Schwartz AB, and Kettner RE. Neuronal population coding of movement direction. *Science* 233: 1416-1419, 1986.

Gileadi E, Kirowa-Eisner E, and Penciner J. *Interfacial electrochemistry: an experimental approach*. United States: Addison-Wesley Publishing Co., Inc.,Reading, MA, 1975, p. Pages: 540.

Grill WM, and Mortimer JT. Electrical properties of implant encapsulation tissue. *Annals of biomedical engineering* 22: 23-33, 1994.

Hermes DJ, Eggermont JJ, Aertsen AM, and Johannesma PI. Spectro-temporal characteristics of single units in the auditory midbrain of the lightly anaesthetised grass frog (Rana temporaria L.) investigated with tonal stimuli. *Hear Res* 6: 103-126, 1982.

Hochberg LR, Serruya MD, Friehs GM, Mukand JA, Saleh M, Caplan AH, Branner A, Chen D, Penn RD, and Donoghue JP. Neuronal ensemble control of prosthetic devices by a human with tetraplegia. *Nature* 442: 164, 2006.

Hoogerwerf AC, and Wise KD. A three-dimensional microelectrode array for chronic neural recording. *IEEE Trans Biomed Eng* 41: 1136-1146, 1994.

Johnson MD, Otto KJ, and Kipke DR. Repeated voltage biasing improves unit recordings by reducing resistive tissue impedances. *Neural Systems and Rehabilitation Engineering, IEEE Transactions on [see also IEEE Trans on Rehabilitation Engineering]* 13: 160-165, 2005.

Kargo WJ, and Nitz DA. Early skill learning is expressed through selection and tuning of cortically represented muscle synergies. *J Neurosci* 23: 11255-11269, 2003.

Kemere C, Shenoy KV, and Meng TH. Model-based neural decoding of reaching movements: a maximum likelihood approach. *IEEE Trans Biomed Eng* 51: 925-932, 2004.

Kennedy P, Andreasen D, Ehirim P, King B, Kirby T, Mao H, and Moore M. Using human extra-cortical local field potentials to control a switch. *J Neural Eng* 1: 72-77, 2004a.

Kennedy PR, Bakay RA, Moore MM, Adams K, and Goldwaithe J. Direct control of a computer from the human central nervous system. *IEEE Trans Rehabil Eng* 8: 198-202, 2000.

Kennedy PR, Kirby MT, Moore MM, King B, and Mallory A. Computer control using human intracortical local field potentials. *IEEE Trans Neural Syst Rehabil Eng* 12: 339-344, 2004b.

Kettner RE, Schwartz AB, and Georgopoulos AP. Primate motor cortex and free arm movements to visual targets in three- dimensional space. III. Positional gradients and population coding of movement direction from various movement origins. *J Neurosci* 8: 2938-2947, 1988.

Kewley DT, Bower JM, Hills MD, Borkholder DA, Opris IE, Maluf NI, Storment CW, and Kovacs GTA. Plasma-etched neural probes. *Sensors and Actuators A: Physical* 58: 27-35, 1997.

Kim KH, Kim SS, and Kim SJ. Superiority of nonlinear mapping in decoding multiple single-unit neuronal spike trains: A simulation study. *Journal of Neuroscience Methods* 150: 202, 2006.

Lebedev MA, and Nicolelis MAL. Brain-machine interfaces: past, present and future. *Trends in Neurosciences* 29: 536-546, 2006.

Lee D, Port NL, Kruse W, and Georgopoulos AP. Variability and correlated noise in the discharge of neurons in motor and parietal areas of the primate cortex. *J Neurosci* 18: 1161-1170, 1998.

Lehky SR. Bayesian estimation of stimulus responses in Poisson spike trains. *Neural Comput* 16: 1325-1343, 2004.

Lehmkuhle MJ, Normann RA, and Maynard EM. Trial-by-Trial Discrimination of Three Enantiomer Pairs by Neural Ensembles in Mammalian Olfactory Bulb. *J Neurophysiol* 2005.

Lewicki MS. A review of methods for spike sorting: the detection and classification of neural action potentials. *Network-Computation in Neural Systems* 9: R53-R78, 1998.

Liu X, McCreery DB, Carter RR, Bullara LA, Yuen TG, and Agnew WF. Stability of the interface between neural tissue and chronically implanted intracortical microelectrodes. *IEEE transactions on rehabilitation engineering* 7: 315-326, 1999.

Ludwig KA, Miriani R, Langhals NB, Joseph MD, and Kipke DR. Employing a Common Average Reference to Improve Cortical Neuron Recordings from Microelectrode Arrays. *in preparation* 2008.

Ludwig KA, Uram JD, Yang J, Martin DC, and Kipke DR. Chronic neural recordings using silicon microelectrode arrays electrochemically deposited with a poly(3,4-ethylenedioxythiophene) (PEDOT) film. *Journal of Neural Engineering* 3: 59, 2006.

Magill PJ, Sharott A, Bevan MD, Brown P, and Bolam JP. Synchronous unit activity and local field potentials evoked in the subthalamic nucleus by cortical stimulation. *J Neurophysiol* 92: 700-714, 2004.

Marg E, and Adams JE. Indwelling multiple micro-electrodes in the brain. *Electroencephalogr Clin Neurophysiol* 23: 277-280, 1967.

Martin R. Mind Control. In: *Wired*2005.

Marzullo TC, Miller CR, and Kipke DR. Suitability of the Cingulate Cortex for Neural Control. *Neural Systems and Rehabilitation Engineering, IEEE Transactions on [see also IEEE Trans on Rehabilitation Engineering]* 14: 401-409, 2006.

Mason SG, and Birch GE. A brain-controlled switch for asynchronous control applications. *Biomedical Engineering, IEEE Transactions on* 47: 1297-1307, 2000.

Maynard EM, Hatsopoulos NG, Ojakangas CL, Acuna BD, Sanes JN, Normann RA, and Donoghue JP. Neuronal interactions improve cortical population coding of movement direction. *J Neurosci* 19: 8083-8093, 1999.

McAdams ET, Lackermeier A, McLaughlin JA, Macken D, and Jossinet J. The linear and non-linear electrical properties of the electrode-electrolyte interface. *Biosensors and Bioelectronics* 10: 67-74, 1995.

Mehring C, Rickert J, Vaadia E, Cardosa de Oliveira S, Aertsen A, and Rotter S. Inference of hand movements from local field potentials in monkey motor cortex. *Nat Neurosci* 6: 1253-1254, 2003.

Merrill DR, Bikson M, and Jefferys JGR. Electrical stimulation of excitable tissue: design of efficacious and safe protocols. *Journal of Neuroscience Methods* 141: 171-198, 2005.

Middlebrooks JC, Dykes RW, and Merzenich MM. Binaural response-specific bands in primary auditory cortex (AI) of the cat: topographical organization orthogonal to isofrequency contours. *Brain Res* 181: 31-48, 1980.

Middlebrooks JC, and Knudsen EI. A neural code for auditory space in the cat's superior colliculus. *J Neurosci* 4: 2621-2634, 1984.

Moran DW, and Schwartz AB. Motor cortical activity during drawing movements: population representation during spiral tracing. *J Neurophysiol* 82: 2693-2704, 1999a.

Moran DW, and Schwartz AB. Motor cortical representation of speed and direction during reaching. *J Neurophysiol* 82: 2676-2692, 1999b.

Nicolelis MAL, Baccala LA, Lin RCS, and Chapin JK. Sensorimotor Encoding by Synchronous Neural Ensemble Activity at Multiple Levels of the Somatosensory System. *Science* 268: 1353-1358, 1995.

Nicolelis MAL, Dimitrov D, Carmena JM, Crist R, Lehew G, Kralik JD, and Wise SP. Chronic, multisite, multielectrode recordings in macaque monkeys. *Proceedings of the National Academy of Sciences of the United States of America* 100: 11041-11046, 2003.

O'Keefe J, and Dostrovsky J. The hippocampus as a spatial map. Preliminary evidence from unit activity in the freely-moving rat. *Brain Res* 34: 171-175, 1971.

Olds J. Operant Conditioning of Single Unit Responses. In: *Proc XXIII Int Congress Physiol Sci*. Tokyo: 1965, p. 372–380.

Olds J, Disterhoft JF, Segal M, Kornblith CL, and Hirsh R. Learning centers of rat brain mapped by measuring latencies of conditioned unit responses. *J Neurophysiol* 35: 202-219, 1972.

Oram MW, Foldiak P, Perrett DI, and Sengpiel F. The 'Ideal Homunculus': decoding neural population signals. *Trends Neurosci* 21: 259-265, 1998.

Otto KJ, Johnson MD, and Kipke DR. Voltage pulses change neural interface properties and improve unit recordings with chronically implanted microelectrodes *Biomedical Engineering, IEEE Transactions on* 53: 333-340, 2006.

Paninski L, Fellows MR, Hatsopoulos NG, and Donoghue JP. Spatiotemporal tuning of motor cortical neurons for hand position and velocity. *J Neurophysiol* 91: 515-532, 2004.

Paxinos G, Watson CR, and Emson PC. AChE-stained horizontal sections of the rat brain in stereotaxic coordinates. *J Neurosci Methods* 3: 129-149, 1980.

Polikov VS, Tresco PA, and Reichert WM. Response of brain tissue to chronically implanted neural electrodes. *J Neurosci Methods* 148: 1-18, 2005.

Prijs VF, and Eggermont JJ. Narrow-band analysis of compound action potentials for several stimulus conditions in the guinea pig. *Hear Res* 4: 23-41, 1981.

Randles J. Rapid electrode reactions. *Discuss Faraday Soc* 1: 11-19, 1947.

Rennaker RL, Miller J, Tang H, and Wilson DA. Minocycline increases quality and longevity of chronic neural recordings. *Journal of Neural Engineering* 4: 2007.

Rickert J, Oliveira SC, Vaadia E, Aertsen A, Rotter S, and Mehring C. Encoding of movement direction in different frequency ranges of motor cortical local field potentials. *J Neurosci* 25: 8815-8824, 2005.

Robinson DA. The electrical properties of metal microelectrodes. *Proceedings of the IEEE* 56: 1065, 1968.

Rousche PJ, and Normann RA. Chronic recording capability of the Utah Intracortical Electrode Array in cat sensory cortex. *Journal of Neuroscience Methods* 82: 1-15, 1998.

Sanger TD. Probability density estimation for the interpretation of neural population codes. *J Neurophysiol* 76: 2790-2793, 1996.

Santhanam G, Linderman MD, Gilja V, Afshar A, Ryu SI, Meng TH, and Shenoy KV. HermesB: a continuous neural recording system for freely behaving primates. *IEEE Trans Biomed Eng* 54: 2037-2050, 2007.

Santhanam G, Ryu SI, Yu BM, Afshar A, and Shenoy KV. A high-performance brain computer interface. *Nature* 442: 195, 2006.

Schmidt EM, Bak MJ, McIntosh JS, and Thomas JS. Operant conditioning of firing patterns in monkey cortical neurons. *Exp Neurol* 54: 467-477, 1977.

Schwartz AB. Cortical neural prosthetics. *Annu Rev Neurosci* 27: 487-507, 2004.

Schwartz AB, and Moran DW. Arm trajectory and representation of movement processing in motor cortical activity. *Eur J Neurosci* 12: 1851-1856, 2000.

Schwartz AB, and Moran DW. Motor cortical activity during drawing movements: population representation during lemniscate tracing. *J Neurophysiol* 82: 2705-2718, 1999.

Selim Suner MRF, Carlos Vargas-Irwin, Kenji Nakata, and John P. Donoghue. Reliability of Signals from a Chronically Implanted, Silicon-based Electrode Array in Non-human Primate Primary Motor Cortex. *Submitted to IEEE* 2005.

Serruya MD, Hatsopoulos NG, Paninski L, Fellows MR, and Donoghue JP. Instant neural control of a movement signal. *Nature* 416: 141-142, 2002.

Seymour JP, and Kipke DR. Neural probe design for reduced tissue encapsulation in CNS. *Biomaterials* 28: 3594-3607, 2007.

Shenoy KV, Meeker D, Cao S, Kureshi SA, Pesaran B, Buneo CA, Batista AP, Mitra PP, Burdick JW, and Andersen RA. Neural prosthetic control signals from plan activity. *Neuroreport* 14: 591-596, 2003.

Stein RB, Charles D, Gordon T, Hoffer JA, and Jhamandas J. Impedance properties of metal electrodes for chronic recording from mammalian nerves. *IEEE transactions on bio-medical engineering* 25: 532-537, 1978.

Strumwasser F. Long-Term Recording from Single Neurons in Brain of Unrestrained Mammals. *Science* 127: 469-470, 1958.

Szarowski DH, Andersen MD, Retterer S, Spence AJ, Isaacson M, Craighead HG, Turner JN, and Shain W. Brain responses to micro-machined silicon devices. *Brain Research* 983: 23-35, 2003.

Taylor DM, Helms-Tillery SI, and Schwartz AB. Direct cortical control of 3D neuroprosthetic devices. *Science* 296: 1829-1832, 2002a.

Taylor DM, Tillery SI, and Schwartz AB. Direct cortical control of 3D neuroprosthetic devices. *Science* 296: 1829-1832, 2002b.

Turner JN, Shain W, Szarowski DH, Andersen M, Martins S, Isaacson M, and Craighead H. Cerebral astrocyte response to micromachined silicon implants. *Exp Neurol* 156: 33-49, 1999.

Velliste M, Perel S, Spalding MC, Whitford AS, and Schwartz AB. Cortical control of a prosthetic arm for self-feeding. *Nature* 453: 1098-1101, 2008.

Vetter RJ, Williams JC, Hetke JF, Nunamaker EA, and Kipke DR. Chronic neural recording using silicon-substrate microelectrode arrays implanted in cerebral cortex. *IEEE transactions on bio-medical engineering* 51: 896-904, 2004a.

Vetter RJ, Williams JC, Hetke JF, Nunamaker EA, and Kipke DR. Spike recording performance of implanted chronic silicon-substrate microelectrode arrays in cerebral cortex. *IEEE Transactions on Neural Systems and Rehabilitation Engineering* 52: 2004b.

Wahnoun R, He J, and Tillery SIH. Selection and parameterization of cortical neurons for neuroprosthetic control. *Journal of Neural Engineering* 3: 162, 2006.

Webster JG. *Medical Instrumentation: Application and Design*. 1978.

Wessberg J, Stambaugh CR, Kralik JD, Beck PD, Laubach M, Chapin JK, Kim J, Biggs SJ, Srinivasan MA, and Nicolelis MA. Real-time prediction of hand trajectory by ensembles of cortical neurons in primates. *Nature* 408: 361-365, 2000.

Williams J, Rennaker R, and Kipke D. Long-term neural recording characteristics of wire microelectrode arrays implanted in cerebral cortex. *Brain Res Brain Res Protocol* 4: 303–313, 1999.

Williams JC. Performance of chronic neural implants: measurement, modeling and intervention strategies. 2001.

Williams JC, Hippensteel JA, Dilgen J, Shain W, and Kipke DR. Complex impedance spectroscopy for monitoring tissue responses to inserted neural implants. *J Neural Eng* 4: 410-423, 2007.

Wolpaw JR, Birbaumer N, McFarland DJ, Pfurtscheller G, and Vaughan TM. Brain-computer interfaces for communication and control. *Clin Neurophysiol* 113: 767-791, 2002.

Wood F, Black MJ, Vargas-Irwin C, Fellows M, and Donoghue JP. On the variability of manual spike sorting. *Ieee Transactions on Biomedical Engineering* 51: 912-918, 2004.

Wu W, Black MJ, Mumford D, Gao Y, Bienenstock E, and Donoghue JP. A Switching Kalman Filter Model for the Motor Cortical Coding of Hand Motion. *Proc IEEE Engineering in Medicine and Biology Society* 2083-2086, 2003.

Xu L, Furukawa S, and Middlebrooks JC. Auditory cortical responses in the cat to sounds that produce spatial illusions. *Nature* 399: 688-691, 1999.

CHAPTER 3
PEDOT FILMS FOR IMPROVING NEURAL RECORDINGS

Abstract

Conductive polymer coatings can be used to modify traditional electrode recording sites with the intent of improving the long-term performance of cortical microelectrodes. These coatings can drastically decrease recording site impedance, which in turn is hypothesized to reduce thermal noise and signal loss through shunt pathways. Moreover, conductive polymers can be seeded with agents aimed at promoting neural growth towards the recording sites or minimizing the inherent immune response. The end aim of these efforts is to generate an ideal long-term interface between the recording electrode and surrounding tissue.

The goal of this study was to refine a method to electrochemically deposit surfactant-templated ordered poly(3,4-ethylenedioxythiophene) (PEDOT) films on the recording sites of standard "Michigan" probes, and to evaluate the efficacy of these modified sites in recording chronic neural activity. PEDOT coated site performance was compared to control sites over a six-week evaluation period in terms of impedance spectroscopy, signal-to-noise ratio, number of viable unit potentials recorded, and local field potential recordings. PEDOT sites were found to outperform control sites with respect to signal-to-noise ratio and number of viable unit potentials. The benefit of reduced initial

impedance, however, was mitigated by the impedance contribution of typical silicon electrode encapsulation. Coating sites with PEDOT also reduced the amount of low frequency drift evident in local field potential recordings. These findings indicate that electrode sites electrochemically deposited with PEDOT films are suitable for recording neural activity *in vivo* for extended periods. This study also provided a unique opportunity to monitor how neural recording characteristics develop over the six weeks following implantation.

Introduction

Implantable electrodes designed to record action potentials from individual neurons are integral to a number of clinical and research applications (Abbott and Salinas 1994; Beiko and Cain 1998; Brown et al. 1998; Carmena et al. 2003; Dobelle 2000; Serruya et al. 2002). The ability to record action potentials from individual neurons is dependent on a tradeoff between the geometric area of the recording site and the site's impedance, often referred to as the tradeoff between selectivity and sensitivity (Kovacs 1994; Paik et al. 2003). A recording site with small geometric area is required to isolate the action potential of an individual neuron from more distant neural sources (*selectivity*)[4] (Drake et al. 1988; Kovacs 1994; Paik et al. 2003; Schmidt and Humphrey 1990; Shoham and Nagarajan 2003). A low impedance recording site is necessary because impedance is

[4] The extracellular potential field of a neuron drops off steeply with respect to distance from the neuron. Large recording sites span multiple diminishing potential lines, and therefore average strong signal from near the neuron, with weaker, more distal signal. Moreover, large recording sites are more likely to be closer to additional neurons than small recording sites, and therefore measure unwanted competing signals. Finally, recording sites that are larger than the neurons they record from run the risk of recording from both poles of a dipole source at once, effectively shorting the measured potential.

proportional to both thermal noise and signal loss through shunt pathways (s*ensitivity*) (Kovacs 1994; Paik et al. 2003; Robinson 1968; Schmidt and Humphrey 1990; Shoham and Nagarajan 2003). Unfortunately, decreasing the geometric area of a recording site causes an increase in the impedance of the recording site (Kovacs 1994; Paik et al. 2003; Schmidt and Humphrey 1990).

A number of studies have explored methods to reduce the impedance of small recording sites in order to alleviate this tradeoff (Burke and Shannell 1984; Kovacs 1994; Paik et al. 2003; Schmidt and Humphrey 1990). Fabricating non-planar structures onto the surface of the recording site, iridium oxide deposition, and platinum black deposition have all been used to increase the surface area of a recording site by increasing its fractal dimensions (Burke and Shannell 1984; Kovacs 1994; Paik et al. 2003; Robinson 1968; Schmidt and Humphrey 1990). However, there are drawbacks to each of these methods. The fabrication of non-planar structures on the surface of a recording site is limited by photolithographic resolution and non-conformal metal deposition (Paik et al. 2003). Recording sites deposited with iridium oxide and platinum black have been reported to have unstable impedance, weak adherence to the underlying substrate, and can cause drift in the open circuit potential of the site (Burke and Shannell 1984; Kovacs 1994; Paik et al. 2003; Robinson 1968). Moreover, there has been no detailed investigation into how effective these methods are in improving the chronic performance of neural recording electrodes.

More recently, investigators have focused on the use of conductive polymers such as polypyrrole (PPy) to reduce the impedance of recording sites. The specificity attainable when electrochemically depositing conductive polymers facilitates the generation of conductive polymer films that maximize surface area over a given geometric space (Cui and Martin 2003; Cui et al. 2001; Yang et al. 2005). As a result, the capacitance of the recording site dramatically increases, creating a corresponding reduction in site impedance (Bobacka et al. 2000; Cui and Martin 2003; Cui et al. 2001; Yang et al. 2005). In addition, porous conductive polymer films promote effective ion exchange between the recording site and the surrounding tissue (Bobacka et al. 2000; Cui and Martin 2003; Cui et al. 2001; Yang et al. 2005). These films transduce ionic current into electronic current via an efficient redox reaction, minimizing the charge transfer resistance at the recording site, again lowering the impedance of the recording site (Bobacka et al. 2000; Cui and Martin 2003; Cui et al. 2001; Yang et al. 2005).

PPy can also be used to facilitate a number of innovative techniques intended to improve neural recordings. Studies have indicated that topographically modified surfaces are capable of enhancing axonal and dendritic growth (Craighead 2001; Dowell-Mesfin et al. 2004; Fan Y W 2002; St John et al. 1997). Electrical stimulation through oxidized PPy has also been demonstrated to significantly increase the neurite lengths in rat PC-12 cells *in vitro* (Schmidt et al. 1997). Furthermore, PPy can be electrochemically deposited on microelectrode arrays and seeded with various biomolecule combinations that improve the interface between tissue and recording site (Cui and Martin 2003; Cui et al. 2001).

These biomolecules can be selected to induce the attachment of cells onto coated recording sites or alleviate the inherent immune response.

Unfortunately, PPy is not well suited for chronic, long-term implantation (Beck et al. 1987; Hitoshi Yamato 1995; Schlenoff and Xu 1992). A study by Yamato *et al.* found that PPy/poly(styrene sulfonate) (PSS) retained only 5 percent of its original charge after polarization at 0.4 Volts for sixteen hours (Hitoshi Yamato 1995). A number of studies have suggested that a nucleophilic attack of OH^- on the α and β positions of the pyrrole rings may lead to a loss of conjugation, and consequently a loss of electrochemical activity (Beck et al. 1987; Schlenoff and Xu 1992; Wernet 1985).

Past studies have indicated that nodular poly(3,4-ethylenedioxythiophene) (PEDOT) can be used as a viable alternative to PPy for chronic, long-term implantations (Bobacka et al. 2000; Cui and Martin 2003; Hitoshi Yamato 1995; Yang et al. 2005). Unlike PPy, PEDOT has a dioxyethylene bridging group across the 3- and 4- positions of the heterocycle preventing α-β' coupling, and as a result is more electrochemically stable than PPy (Bobacka et al. 2000; Cui and Martin 2003; Hitoshi Yamato 1995). Yamato *et al.* reported that PEDOT/PSS retained eighty-nine percent of its original electrochemical activity when polarized at 0.4 V for sixteen hours (Hitoshi Yamato 1995). PEDOT has also been effectively used as a template to incorporate the bioactive peptide DCDPGYIGSR (Cui and Martin 2003). Preferential growth of neuronal cells was observed on the coated areas of standard acute "Michigan" probes coated with PEDOT/DCDPGYIGSR *in vitro* (Cui and Martin 2003). PEDOT/DCDPGYISR coated

sites were then used to obtain high-quality acute neural recordings (Cui and Martin 2003).

Surfactant-templated ordered PEDOT films have been shown to possess superior electrical characteristics to the more conventional nodular PEDOT (Yang et al. 2005). SEM micrographs indicate that surfactant-templated ordered PEDOT films have a larger surface area than nodular PEDOT or PPy films when grown under the same conditions (Yang et al. 2005). As a result, surfactant-templated ordered PEDOT films lower recording site impedance even further than nodular PEDOT or PPy films (Yang et al. 2005). Surfactant-templated ordered PEDOT films also demonstrate a larger charge carrying capacity than nodular PEDOT or PPy films (Yang et al. 2005). In addition, the charge carrying capacity of surfactant-templated ordered PEDOT films has been found to be more stable than nodular PEDOT or PPy films after 1000 cyclic voltammetry cycles (Yang et al. 2005).

The goal of the current study was to refine a method to electrochemically deposit surfactant-templated ordered PEDOT films on the recording sites of standard Michigan chronic probes, and to evaluate the efficacy of these modified sites in recording chronic neural activity (Yang et al. 2005). Eight male Sprague Dawley rats were implanted in motor cortex with standard 4x4, 16-channel probes and neural recordings were monitored over a six week period. The performance of PEDOT-coated sites was compared to control sites in terms of impedance spectroscopy, signal-to-noise ratio, number of viable unit potentials recorded, and local field potential recordings. This experiment also

provided a unique opportunity to systematically investigate how neural recording characteristics develop over the six weeks following implantation.

Methods

Silicon Probes

The micromachined silicon probes used in this experiment were provided by the University of Michigan Center for Neural Communications Technology. Design and fabrication of the probes have been described in detail elsewhere (Anderson et al. 1989; Drake et al. 1988). Sixteen-channel chronic probes with 703 μm^2 iridium recording sites were selected for use throughout this work as these probes are routinely used to record single-unit action potentials in motor cortex.

Electrochemical Deposition & Initial Evaluation

Electrochemical deposition of PEDOT in this study was accomplished using an electrochemical potentiostat/ galvanostat (Autolab PGSTAT12, Eco Chemie, Urtecht, The Netherlands) with associated General Purpose Electrochemical System (GPES) software. PEDOT doped with tetraethylammonium perchlorate and dissolved in 20 wt% surfactant poly(oxythylene)$_{10}$-oleyl ether was galvanostatically deposited onto the iridium sites of the neural probes (Yang et al. 2005). Test probes were first deposited with PEDOT in order to determine the optimum deposition characteristics for use in the chronic study. The deposition charge used on the test probes was varied from 50 to 1000

mC/cm^2 in order to generate a wide spectrum of coating morphologies and thicknesses (Yang et al. 2005). Coated sites were then visually inspected under a microscope and impedance spectroscopy measurements for each site were made. Next, each of the test probes was inserted and removed from a gelatin model of rat cortex (Shahriari 2001). After the insertion test, the test probes were again visually inspected under a microscope and impedance spectroscopy measurements for each site were retaken (Figure 3.1). Only PEDOT films that were grown using the largest two deposition charges, corresponding to a coating thickness of approximately 6 μm (Yang et al. 2005), detached partially from the electrode site upon insertion. Smaller film thicknesses appeared unchanged after insertion.

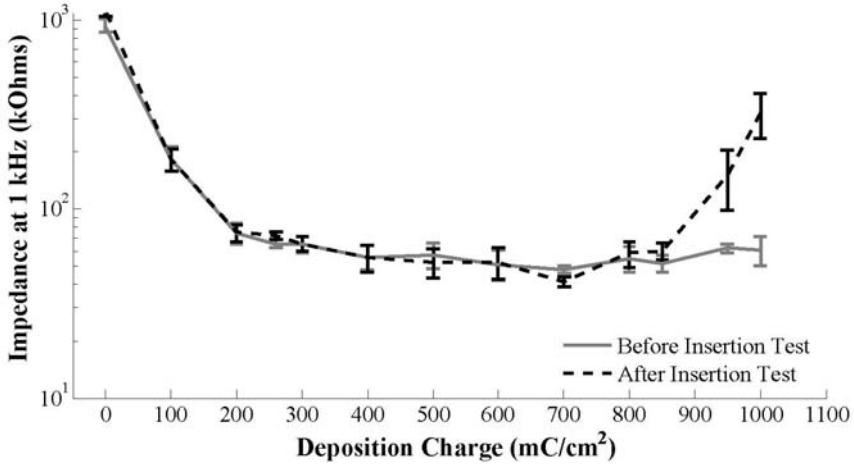

Figure 3.1: Average Recording Site Impedance versus Polymerization Charge. The bars denote standard error (n=4). Impedance at 1 kHz decreased up to a deposition charge of 260 mC/cm^2, and then remained relatively constant. Coatings made using the two larges deposition charges often delaminated during the insertion test, causing an increase in impedance post-insertion.

As a result of these preliminary tests, PEDOT films generated with a deposition charge of 260 mC/cm^2 were chosen for *in vivo* testing. Films created with a deposition charge of 260 mC/cm^2 were found to have an impedance drop comparable to the largest applied

deposition charges, as well as a porous morphology conducive to ion transfer (Figure 3.1). Moreover, PEDOT films generated using this deposition charge extend only 1 μm from the recording site (Yang et al. 2005), and therefore should mitigate the risk of delamination upon insertion, minimize the tissue displaced during insertion, and present less of a focal point for the concentration of mechanical stress on the electrode shank. For *in vivo* testing, eight sites on each probe testing were deposited with surfactant-templated ordered PEDOT film. The deposited sites were staggered in relative location to prevent bias due to specific shank location or cortical depth (Figure 3.2). The remaining eight sites on each probe were left uncoated as controls for comparison.

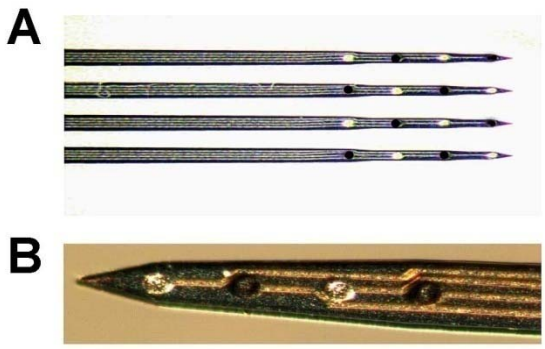

Figure 3.2: PEDOT Coating Protocol. (a) Snapshot of standard 16-site, 4-shank probe prior to deposition. The locations of electrode sites deposited with PEDOT have been artificially darkened for reference. (b) One shank of a probe after deposition. The darker sites have been electrochemically deposited with a PEDOT film.

Surgical Techniques

Eight male Sprague-Dawley rats were implanted in motor cortex with a 16-channel, chronic Michigan silicon microelectrode array using experimental procedures outlined previously (Vetter et al. 2004). Initial anesthesia was administered via intra-peritoneal

injections of a mixture of 50 mg/ml ketamine, 5 mg/ml xylazine, and 1 mg/ml acepromazine at an injection volume of 0.125 ml/100g body weight. Updates of 0.1 ml ketamine (50 mg/ml) were delivered as needed during the surgery to maintain anesthesia during the surgery. Animals were secured to a standard stereotaxic frame, and three stainless steel bone screws were inserted into the skull. The electrode connector was grounded to a bone screw over parietal cortex using a stainless steel ground wire. A craniotomy approximately 3 mm by 2 mm was made over motor cortex. Two incisions were made in the dura mater over the target area to create four flaps, and these flaps were subsequently folded back over the edge of the craniotomy. The electrodes were then hand inserted into the exposed target cortical area (location 3.0 mm anterior to bregma, 2.5 mm lateral from bregma, and 1.4 mm deep from the surface of the brain) (Donoghue et al. 1990). Next, NeuroSeal® (NeuroNexus Technologies, Inc., Ann Arbor, MI) was applied as a dural sealant, the silicon cable connector was wrapped with GelFoam® (Henry Schein, Inc., Miami, FL) for protection, and the entire assembly excluding the connector was enclosed using dental acrylic (Co-Oral-Ite, Dental Mfg. Co., Santa Monica, Ca). Finally, sutures were used to close the skin around the acrylic and triple-antibiotic ointment was applied. All procedures complied with the United States Department of Agriculture guidelines for the care and use of laboratory animals and were approved by the University of Michigan Animal Care and Use Committee.

Data Collection

After implantation, neural recordings and impedance spectroscopy for each animal were taken daily for the first two weeks, and every other day thereafter for the remainder of the

six weeks. Animals were either awake or kept lightly sedated throughout the data collection sessions.

Neural Recordings & Data Analysis

Recorded neural signals were acquired using a Multi-channel Neural Acquisition Processor (MNAP; Plexon Inc, Dallas, TX). Neural electrophysiological data for all 16 recording channels were amplified and bandpass filtered; single and multi-unit recordings were sampled at 40 kHz and bandpass filtered from 450-5000 Hz, while local field potentials were sampled at 1 kHz and bandpass filtered from 3-90 Hz. During recording sessions, animals were placed in an electrically shielded recording booth and multiple 30-second segments of continuous neural recordings were taken.

Neural recording segments were analyzed offline using custom automated MatLab (Mathworks Inc., MA) software. Candidate action potentials were discriminated from background noise based on the probability distribution of the samples in a 30-second segment. An amplitude threshold window was set 3.5 standard deviations above and below the mean of the sample distribution. For each peak exceeding the threshold window, a 2.4 ms candidate waveform snippet centered on the absolute minimum of the waveform was removed from the recorded segment and stored. The amplitude of the noise voltage for every recording site in each recorded segment was calculated after all candidate waveforms had been removed.

The store of candidate waveform snippets for a given channel was used to derive a set of orthogonal basis vectors ordered based on ability to represent the largest variation in the data set, a technique commonly known as Principal Component Analysis (Gerstein et al. 1983; Glaser 1971; Glaser and Marks 1968; Lewicki 1998). The first three principal components were used to generate the axes of a three dimensional component space. Each waveform in the store was transformed into a point in this three dimensional space based on its score for each of the component axes. Individual points were grouped into clusters using Fuzzy C-Means clustering (Bezdek 1981; Dunn 1974). When compared to hard clustering, fuzzy clustering reduces classification errors resulting from the synchronous firing of multiple neurons (Zouridakis and Tam 2000). In order to determine the optimum number of clusters, the number of clusters was iteratively increased until the value for the objective function calculated for k + 1 number of clusters was at least 55 percent of the value for the objective function calculated for k number of clusters (Karkkainen and Franti August 2002).

After clustering, waveforms with a cluster membership index of greater than 0.8 were used to determine a mean waveform for a cluster. Contributions of white noise and waveforms created by the simultaneous firing of multiple neurons generally do not have a membership index of greater than 0.8 for a particular cluster, and therefore were limited using this procedure (Zouridakis and Tam 2000). Signal amplitude for a cluster was defined as the peak-to-peak amplitude of the mean waveform for each cluster. The signal-to-noise ratio (SNR) for a given cluster was defined as follows:

SNR = Signal Amplitude / (2 * Calculated RMS Noise Voltage for Recording Site)

Clusters were then separated into one of four categories based on calculated SNR. Clusters with an SNR of greater than 4 were categorized as quality units. Clusters with an SNR between 3 and 4 were categorized as moderate units. Clusters with an SNR between 2 and 3 were categorized as poor units, while clusters with an SNR of less than 2 were not considered units. These four categories correspond well with observations of unit quality based on signal-to-noise ratio made in similar recording studies (Henze et al. 2000; Selim Suner 2005).

As noted elsewhere, isolating action potentials from a specific neuron using only a single recording site as a reference is prone to classification errors (Harris et al. 2000; Lewicki 1998). Although classification errors are inevitable, the number of neurons detected using the methodology presented here should accurately parallel the true underlying number of neural sources. This methodology also compared favorably with conservative manual clustering performed by experienced researchers on the same data sets, but with the advantage of being both objective and automated.

Impedance Spectroscopy Measurements

Impedance spectroscopy measurements were made using an Autolab potentiostat PGSTAT12 (Eco Chemie, Utrecht, The Netherlands) with associated frequency response analyzer (Brinkmann, Westbury, NY). Impedance measurements were made by applying a 25 mV RMS sine wave with frequencies varied logarithmically from 10 Hz to 10 kHz (Johnson et al. 2005). Prior to implantation, measurements were made by immersing the electrode recording sites in 0.1 M phosphate buffer saline (PBS) and a

platinum foil was used as the reference electrode. After implantation, a distant stainless steel (316-SS grade) bone screw was used as the reference electrode.

Statistical Analysis

For this study, comparative statistical significance between groups was determined using standard analysis of variance techniques (ANOVA). There were 64 PEDOT modified sites and 64 control sites on any specific day in the experiment. The factors used in initial comparative ANOVA calculations for any given metric were coated vs. control, and day number. A significant difference across days was noted ($p<0.001$), but no *post-hoc* test to separate specific days was performed, as there was an obvious day to day trend in the data. Instead, the data sets were grouped into three time segments (Day 0-2 after surgery, Day 3-15 after surgery, and Day 16-42 after surgery), and a one factor ANOVA (coated vs. control) was performed. These three periods of time were chosen based on the time course of initial trauma, early reactive response, and sustained immune response evident in other experiments (Schmidt et al. 1993; Szarowski et al. 2003; Turner et al. 1999; Vetter et al. 2004). The associated calculated standard deviation has been included in text with all average measurements.

Results

Impedance Spectroscopy Measurements

The impedance of electrode recording sites at 1 kHz is often used to evaluate recording probes because action potentials have a characteristic frequency band centered at 1 kHz (Kuffler 1976). Three distinct periods of time are evident in the chart of recording site impedance at 1 kHz over time (Figure 3.3). Over the course of the first three days following surgery, the 1 kHz impedance for the electrode recording sites remained relatively stable. During this first period, the mean 1 kHz impedance for the uncoated sites was 0.98 MΩ ± 0.08 MΩ while the mean 1 kHz impedance for the PEDOT

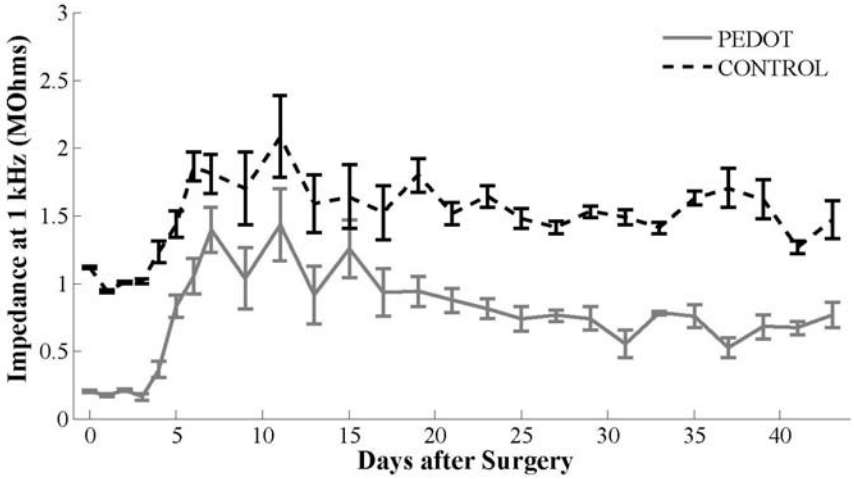

Figure 3.3: Average Site Impedances at 1 kHz over Time. The bars denote standard error of the data set on the given day (n=64). Day 0 measurements were taken immediately after surgery. The 1 kHz impedance for both PEDOT and control sites increased an average of 70 kΩ immediately upon implantation. Impedances increased dramatically the third day after implantation, up to a maximum value at the one week mark. Two weeks after implantation, 1 kHz impedance for PEDOT and control sites settled. This trend in 1 kHz impedance is highly correlated between PEDOT and control sites, suggesting a global immune response equally affecting both PEDOT and control sites.

recording sites was 0.13 MΩ ± 0.06 MΩ, a ratio of over 7 to 1 (p<0.001). The variability in 1 kHz impedance from PEDOT site to PEDOT site and control site to control site was

small. The second period of time, spanning from day three to day fifteen, was notable for an increase in both impedance magnitude and site to site variability. Across this second time segment, the mean 1 kHz impedance for the control sites was 1.7 MΩ ± 0.9 MΩ while the mean 1 kHz impedance for the PEDOT sites was 1.1 MΩ ± 0.8 MΩ, a ratio of approximately 1.5 to 1 (p<0.001). The third period of time, spanning from day 15 to the end of the experiment, was marked by a settling of impedance magnitude and site to site variability. During this third segment of time the mean 1 kHz impedance for control recording sites was 1.5 MΩ ± 0.3 MΩ while the mean 1 kHz impedance for the PEDOT sites was 0.81 MΩ ± 0.3 MΩ, a ratio of roughly 2 to 1 (p<0.001). The three distinct segments of time noted in the data set correspond well to the time course of initial trauma, early reactive response, and sustained immune response evident in other experiments studying the immune response of cortical tissue to an implanted silicon probe (Schmidt et al. 1993; Szarowski et al. 2003; Turner et al. 1999; Vetter et al. 2004). An increase in impedance at 1 kHz over the two weeks following implantation was also noted in another study of Michigan probe performance conducted at the University of Michigan (Vetter et al. 2004).

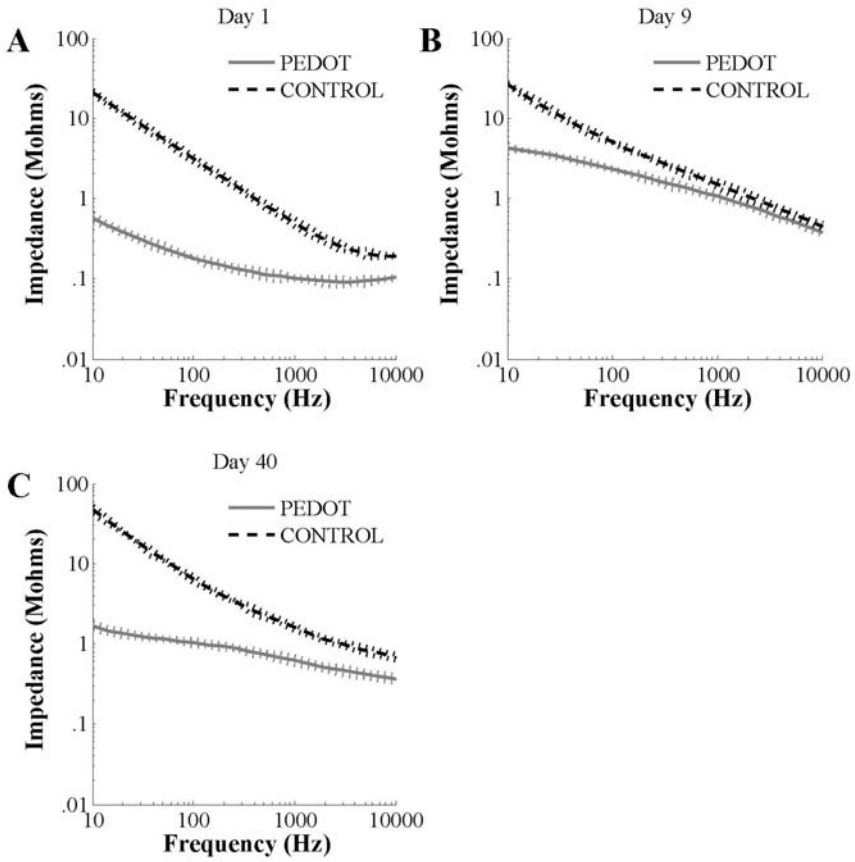

Figure 3.4: Bode Plot of Average Measured Impedance Versus Frequency. The dotted lines denote standard error of the data set on the given day (n=64). (a) Day 1 post-implantation. (b) Day 9 post-implantation. (c) Day 40 post-implantation. Initially, there was a large difference in impedance between PEDOT and control sites at both 1 kHz and low frequencies (10-40 Hz). On day 9, the difference in impedance at 1 kHz was much smaller, whereas a large difference in impedance at low frequencies was still evident. By day 41, 1 kHz and low frequency impedance for both PEDOT and control sites had settled. A large difference in impedance at low frequencies between PEDOT and control sites remained, however, the difference in impedance at 1 kHz was not as dramatic as seen initially.

Bode plots of the impedance magnitude from 10 Hz to 10 kHz during the three distinct time periods yield additional insight into the developing electrical characteristics of the recording sites over time (Figure 3.4). Ions can more effectively infiltrate the porous PEDOT at lower frequencies, creating a larger accessible interfacial area, and therefore reducing low frequency impedance by increasing recording site capacitance and lowering charge transfer resistance (Cui et al. 2001). On day 1 after the surgery, the mean impedance magnitude of the PEDOT sites at very low frequencies (≤40 Hz) was more

than 30 times smaller than the uncoated sites (Figure 3.4). On day 9 during the peak of the early reactive response, the mean impedance magnitude of the PEDOT sites at very low frequencies was still more than 10 times smaller than the uncoated sites (Figure 3.4). On day 40, the mean impedance magnitude of the PEDOT sites returned to almost 30 times smaller than the uncoated sites (Figure 3.4). The trend in impedance of the PEDOT sites over time at low frequency also parallels the time course of initial trauma, early reactive response, and sustained immune response.

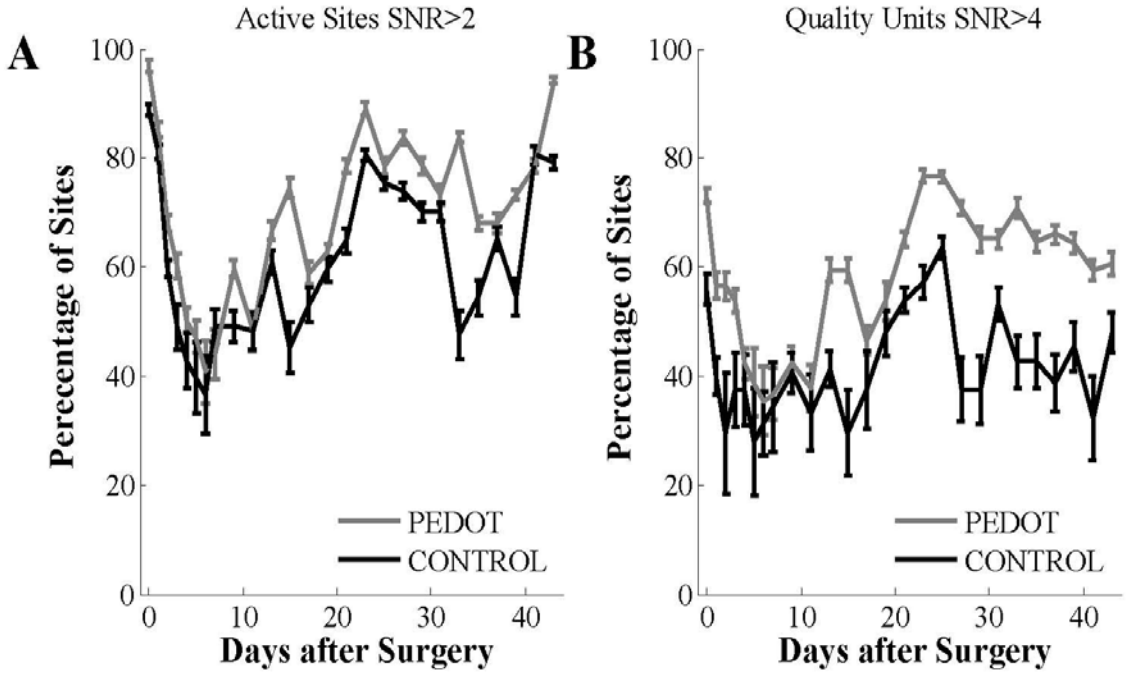

Figure 3.5: Percentage of Sites Recording Low and High Quality Units on a Given Day. The bars denote standard error of the data set on the given day (n=8). (a) Units with SNR > 2. (b) Quality units with SNR > 4. Unit recordings tended to be unstable over the first two weeks after implantation. During these two weeks, a noticeable drop in measurable units occurred on both PEDOT and control sites. After two weeks unit recordings stabilized, and the recordable number of units became more constant on a day to day basis. Throughout the course of the study, sites electrochemically deposited with PEDOT films on average registered both more low and high quality units than control sites (p<0.001).

Unit Recordings

Over the course of the experiment, signals that regularly exceeded the 3.5 standard deviation threshold were evident on all 128 recording sites. On average, 70 percent of the PEDOT sites recorded waveforms categorized as poor or better (SNR>2), compared to 59 percent for the uncoated sites ($p<0.001$) (Figure 3.5). After day 15, 78 percent of the PEDOT sites recorded waveforms categorized as poor or better, in contrast to 68 percent for the control sites ($p<0.001$). The overall percentage of sites recording poor or better unit recordings was high initially, markedly lower for the two weeks following the surgery, and then returned to prior levels after the two week mark. Multiple units were evident on a number of both PEDOT and uncoated recording sites. An average of 1.2 ± 0.3 units of poor or better quality were identified on PEDOT sites over the course of the experiment, while an average of 1.0 ± 0.3 units of poor or better quality identified on control sites ($p<0.001$).

A more dramatic difference in performance between PEDOT and uncoated sites over the length of the study is evident in the percentage of sites recording high quality units (SNR>4) (Figure 3.5). Over the six week study, an average of 41 percent of the uncoated recording sites at any given time registered at least 1 quality unit. In comparison, more than 58 percent of the PEDOT sites registered at least 1 quality unit, a nearly 40 percent improvement (p<0.001). PEDOT sites recorded an average of 0.75 ± 0.1 quality units from day to day, whereas uncoated sites recorded an average of 0.56 ± 0.1 quality units (p<0.001).

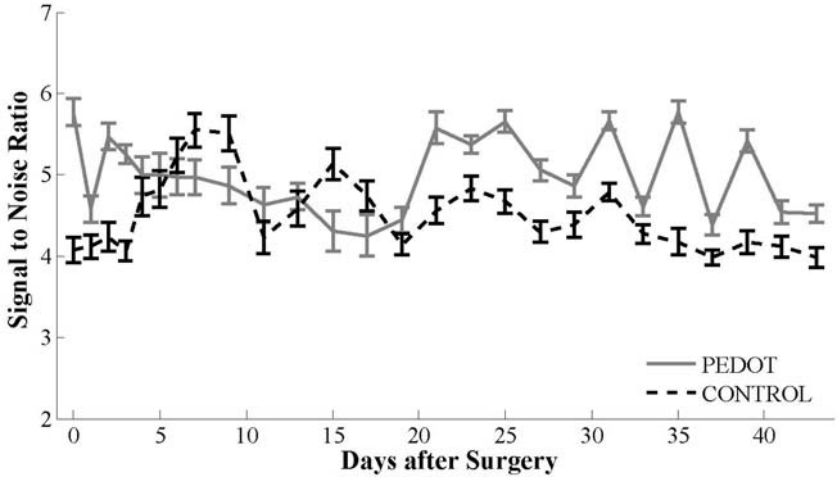

Figure 3.6: Average SNR over Time. The bars denote standard error of the data set on a given day (n=64). Average SNR was calculated using units with a SNR of greater than 3, as PEDOT sites typically registered both more low and high quality units. On average, PEDOT sites recorded units with greater SNR than control sites for the first three days after implantation, and from day 15 until the end of the study (p<0.001). Between day 3 and day 15 post-implantation, individual unit recordings varied on day to day (and even hour to hour) basis. No significant difference in average SNR between PEDOT and control sites was noted during this timeframe (p>0.05)

Signal to Noise over Recording Sessions

Calculating an average signal-to-noise ratio (SNR) of unit recordings was complicated by the fact that PEDOT sites registered a larger number of poor, moderate, and quality units. For purposes of calculating the SNR of unit recordings, only units of moderate or better

quality (SNR>3.0) were used. The SNR of recorded units of moderate or better quality over time also can be separated into 3 time periods (Figure 3.6). During the two days following surgery, the average SNR of the units recorded on PEDOT sites was 5.1 ± 1.2 while the average SNR of the units recorded on the control sites was 4.1 ± 1.1 ($p<0.001$). Over the period spanning days three to fifteen following surgery, the average SNR of units recorded on PEDOT and uncoated sites was roughly the same, 4.8 ± 1.8 and 4.9 ± 1.7 respectively ($p>0.05$). After day 15, the SNR of unit recordings for PEDOT and uncoated sites began to diverge again; the average SNR of units recorded on PEDOT sites was 5.1 ± 1.2, while the average SNR of units recorded on uncoated sites was 4.3 ± 1.0 ($p<0.001$).

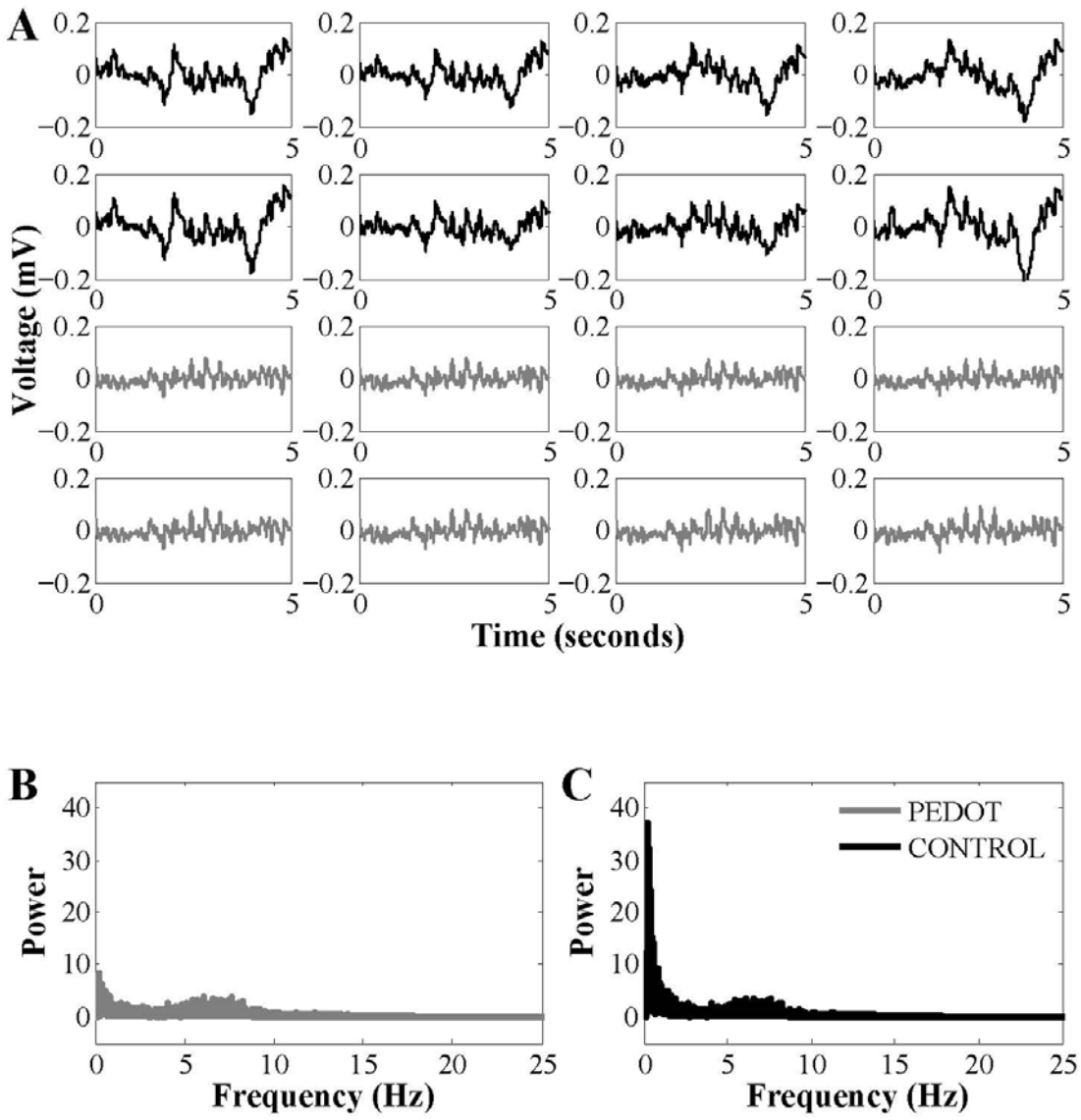

Figure 3.7: Local Field Potential Recordings. (a) Five-second segment of local field potential recordings for one subject on day 41. The top two rows are local field potential recordings from control sites. The bottom two rows are local field potential recordings from sites deposited with a PEDOT film over the same timeframe. Sites deposited with a PEDOT film registered considerably less low frequency artifact (0.1 to 1 Hz) than control sites. (b) Average Power versus Frequency (Resolution=0.001 Hz) of PEDOT sites for same subject on day 41. (c) Average Power versus Frequency (Resolution=0.001 Hz) of control sites for same subject on day 41.

Local Field Potential Recordings

Local field potentials recordings (LFPs), typically ranging from 3-90 Hz, are routinely recorded using Michigan probes. Over the course of taking chronic LFP recordings, an

undesirable low frequency artifact often becomes evident. LFP recordings were taken at the end of the six week study in order to investigate the possibility that sites deposited with a PEDOT film would reduce low frequency artifact in LFP recordings. Figure 3.7 depicts a sample of LFPs recorded on PEDOT and control sites. Low frequency artifact was intermittently evident on the control recording sites that was not apparent on the PEDOT sites. The magnitude of the average power in the band from 0.1 to 1 Hz is indicative of the extent of low frequency artifact. Across all subjects, the average power in the frequency band from 0.1 to 1 Hz for the control sites was 4.3 ± 0.8 times larger than the average power across the same band for PEDOT sites ($p<0.001$). For both types of sites, the low frequency artifact was sufficient in amplitude to register despite the use of a second order band-pass filter with a cutoff frequency of 3 Hz.

Histological Evaluation

Although detailed histological evaluation was not a focus of this study, cursory hematoxylin and eosin (H&E) staining was performed on the implanted cortical tissue from six of the subjects at the end of the experiment (data not shown) (47). Since the probes were inserted by hand, the insertion angle of the probe relative to the surface of the brain could not be guaranteed. As a result, determining the precise location of a specific recording site relative to a coronal section was impossible, and therefore no specific comparison between immune response at PEDOT and control sites could be made. Coronal sections were instead visually inspected for any abnormally large immune response. In general, the coronal sections were consistent with the modest

global tissue reaction to implanted silicon probes reported elsewhere (Biran et al. 2005; Szarowski et al. 2003; Vetter et al. 2004).

Discussion

Trend in Recordings with Respect to Progression of the Immune Response

There have been a number of excellent studies monitoring the progression of the immune response to an implanted silicon probe over time (Biran et al. 2005; Schmidt et al. 1993; Szarowski et al. 2003; Turner et al. 1999). In addition, Liu and McCreery have investigated the stability of single unit neural recordings at different points in time after implantation (Liu et al. 1999). In order to place the comparative results of PEDOT and control recording sites into proper context, a discussion of the trends in recording site impedance, recorded signal amplitude, and recorded noise amplitude over the six weeks following implantation is necessary. The trends found in this study follow logically from the known progression of the immune response to an implanted silicon probe, and are consistent with results from similar microelectrode studies (Vetter et al. 2004; Williams et al. 1999; Williams 2001).

Immediately upon implanting the modified probes, the measured impedance on all recording sites increased by 70-100 kΩ. This impedance increase may be attributed to immediate protein adsorption on the recording sites coupled with the change in the surrounding medium from 0.1 M phosphate buffered saline to cortical tissue. As the individual shanks of the Michigan probe are small in comparison to other recording technologies, a minimal amount of tissue should be disrupted during their insertion. As a

result, recordings with the Michigan probe immediately after surgery tend to be strong (Polikov et al. 2005; Schwartz 2004).

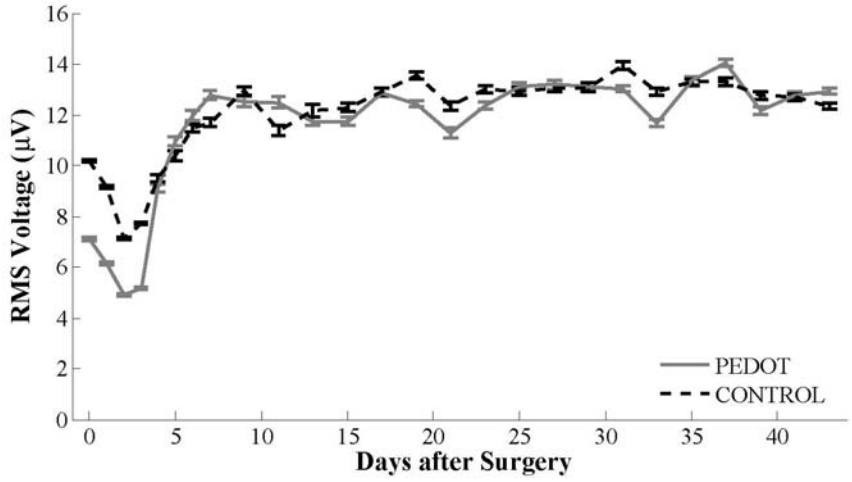

Figure 3.8: Average Noise over Time. The bars denote standard error of the data set on a given day (n=64). The recorded noise level for PEDOT sites was significantly lower than control sites over the first 3 days following implantation, presumably a result of a reduced thermal noise (p<0.001). The recorded noise level for both PEDOT and control sites increased dramatically after day 3, reaching a maximum value at the one week mark. The increase in impedance on both PEDOT and control sites apparent after day 3 should also cause an increase in thermal noise. By day 15 post-implantation, the average RMS noise on PEDOT and control sites was not significantly different (p>0.05).

According to literature, swelling of the tissue surrounding an implanted biomaterial occurs not long after implantation (Black 1999). Swelling around an implanted probe could cause neurons near the recording sites to be "pushed away". As a result of swelling, the neural sources of signal could be moved to a more distant location, theoretically causing a decrease in signal amplitude. Similarly, the noise amplitude would decrease as the distal neural sources that generate the biological component of measured noise are also pushed away from the recording site. Consistent with this hypothesis, both measured signal amplitude as well as recorded noise amplitude in this study decreased following surgery. In general, swelling subsides between three and six

days after a biomaterial is implanted (Black 1999), theoretically allowing displaced neurons to return to the area around the recording site. In this study, both signal and noise amplitude increased during days three to seven, which is consistent with neurons returning to the region near the recording site as swelling subsides (Figures 3.8 and 3.9).

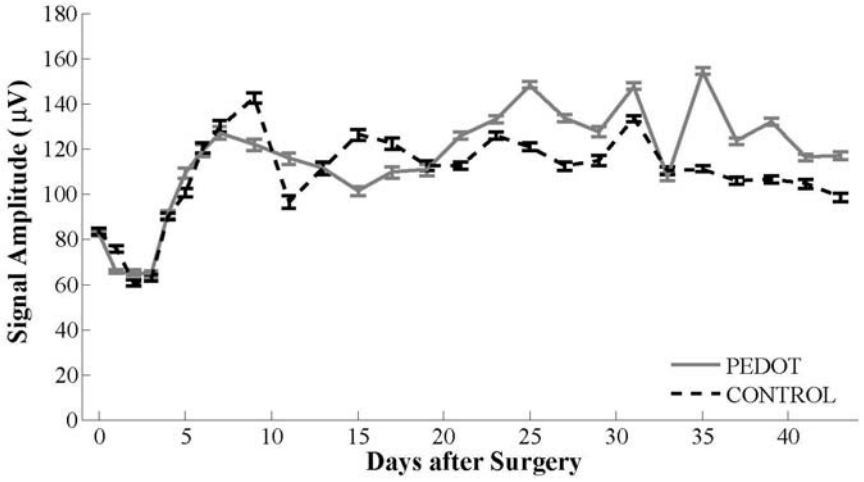

Figure 3.9: Average Signal Amplitude over Time. The bars denote standard error of the data set on a given day (n=64). During the first 3 days after implantation, swelling around the recording sites may have pushed neurons away from the recording, causing an apparent reduction in signal amplitude. Average signal amplitude was not significantly different between PEDOT and control sites during this timeframe ($p>0.05$). Signal amplitude increased until seven days post-surgery. At the two week point day to day recordings stabilized, and the average signal amplitude of units recorded on PEDOT sites became significantly larger in comparison to control sites ($p<0.001$).

Biran *et al*. report that there is a comparable reduction in neuronal cell density in the tissue surrounding an implanted probe at two and four weeks post insertion (Biran et al. 2005). Data tracking neuronal cell density surrounding a probe over the two weeks following implantation is not currently available; however, it may be possible that this reduction in neuronal cell density develops immediately after a probe is inserted and remains relatively constant for the life of the implant. A reduction in neuronal cell

density should result in an overall decrease in measured signal and biological noise, and therefore could also account for the reduction in recorded signal and noise amplitude that occurred after the first day after implantation. The reduction in recorded signal and noise amplitude as a result of decreased neuronal cell density should be a relatively constant bias over time, and therefore does not account for the dramatic increase in recorded signal and noise apparent after day 3 in this study.

Unit recordings over the two weeks following surgery were unstable. Individual units changed on a daily, and sometimes hourly, basis. Unit recordings are unstable during the early reactive response timeframe because the tissue surrounding the recording sites is in a constant state of flux (Liu et al. 1999; Turner et al. 1999). During this period, a loose sheath of cells consisting of microglia and reactive astrocytes begins to form around the shanks of the recording electrodes (Turner et al. 1999). The impedance of the electrode recording sites at 1 kHz in this study increased up to the two week mark (Figure 3.3), presumably as a result of the formation of a cellular sheath.

Researchers have shown that the encapsulation around the electrode shanks becomes more defined at the two week mark, and the immune response begins a transition into the chronic phase (Turner et al. 1999). Around the two week point in this study, impedance magnitude and variability at 1 kHz began to settle (Figure 3.3) (Vetter et al. 2004). Unit recordings became more stable; individual unit recordings changed primarily on a week to week basis. Liu and McCreery suggest that the encapsulation of the electrode shank anchors the recording site in position with respect to the surrounding tissue, and therefore stabilizes the day to day recordings (Liu et al. 1999).

By the sixth week after surgery, a well-defined encapsulating sheath of microglia and reactive astrocytes has formed around typical implanted silicon devices, and the immune response has transitioned into the long-term chronic response (Turner et al. 1999). Presumably as a result of this encapsulating sheath, the 1 kHz impedances at six weeks for all recording sites in this study were between 500 to 1000 kΩ larger than initial *in vitro* impedance measurements (Figure 3.3) (Vetter et al. 2004). Consistent with the findings of Liu and McCreery, unit recordings at six weeks became even more stable (Liu et al. 1999).

Effect of Reduced Impedance on Recorded Signal and Noise Amplitude

Lowering the impedance of recording sites is purported to enhance neural recordings by reducing noise and minimizing signal loss through shunt pathways (Kovacs 1994; Robinson 1968; Schmidt and Humphrey 1990; Shoham and Nagarajan 2003). Noise in neural recordings is primarily comprised of thermal (Johnson) noise and small amplitude signals from diffuse neural sources (Kovacs 1994; Schmidt and Humphrey 1990; Shoham and Nagarajan 2003). *In vitro*, the largest component of recorded noise is thermal noise. The thermal noise for a recording site can be computed as follows:

$$V_{Noise} = \sqrt{4kTZ\Delta F}$$

Where k is Boltzman's constant, T is temperature, ΔF is the frequency band of interest, and Z is the impedance at the frequency band of interest (Kovacs 1994; Schmidt and Humphrey 1990; Shoham and Nagarajan 2003). As long as the thermal noise remains the largest portion of the measured noise, the recorded noise should vary proportionately

with the measured impedance over the frequency band of interest. The average *in vitro* noise amplitude for PEDOT recording sites was 2.1 ± 0.3 μV, compared to 5.5 ± 0.3 μV for control sites ($p<0.001$). A reduction in the impedance of an electrode site should not only decrease thermal noise, but increase both measured signal as well as measured biological noise, due to a reduction in measured potential loss through shunt pathways.

The ratio of impedance at 1 kHz between uncoated sites and PEDOT sites was approximately 7.5 to 1 over the first two days following surgery. Consequently, the average measured noise was 8.0 ± 0.4 μV for uncoated sites and 5.3 ± 0.3 μV for PEDOT sites ($p<0.001$) (Figure 3.8). This increase in measured noise amplitude for PEDOT and control sites with respect to *in vitro* values is attributable to a 70 kΩ increase in impedance after implantation across all sites coupled with the addition of biological sources of noise. Over the same timeframe, the average signal amplitude for units recorded on PEDOT sites was not significantly different from the average signal amplitude of units recorded on control sites ($p>0.05$) (Figure 3.9). Therefore, the difference in SNR between PEDOT and uncoated sites over the first two days was attributable to diminished thermal noise (Figure 3.6). Swelling around the recording site during this timeframe likely increased the distance from the recording site to signal sources and sources of biological noise, mitigating the benefit of decreased signal loss through the shunt pathway. The increased SNR attributable to decreased thermal noise related directly to an increase in the resolvable number of neurons (Figure 3.5).

From day 3 to day 15, the impedance magnitude at 1 kHz increased on both uncoated and PEDOT sites, presumably as a result of the early reactive response to the implants.

Similarly, the average noise voltage for uncoated and PEDOT sites increased to 11.9 ± 0.6 μV and 11.4 ± 0.5 μV respectively (p>0.05). As the ratio of impedance at 1 kHz between uncoated and PEDOT sites diminished, the average noise amplitude for both types of sites converged. The average signal amplitude for units recorded between day 3 and day 15 increased to 112 ± 15 μV for PEDOT sites and to 115 ± 17 μV for control sites (p>0.05).

As discussed earlier, the dramatic increase in both measured noise and measured signal amplitude was likely related to the return of neurons to the area surrounding the recording site after the insertion trauma subsided. As neurons returned, the contribution of the diffuse activity of neurons nearby the recording sites to the ambient noise level began to approach and even surpass the contribution of thermal noise. Moreover, the thermal noise presumably increased in proportion to the increase in impedance over all sites. Because neither the average signal amplitude nor recorded noise for PEDOT and uncoated sites was markedly different between days 3 and 15, the SNR for both PEDOT and control sites was approximately the same. Although more units were evident on PEDOT sites during this period (Figure 3.5), the unit recordings were very unstable on a day to day (and sometimes hour to hour) basis during this timeframe, complicating statistical analysis.

After day 15, the impedance magnitude at 1 kHz settled for both PEDOT and uncoated sites. Action potentials recorded from individual neurons became consistent on a week to week basis. The difference in average noise amplitude between PEDOT and uncoated sites remained negligible (PEDOT: 12.7 ± 0.8 μV, uncoated: 13.1 ± 0.9 μV, p>0.05).

However, the average signal amplitude of units recorded on PEDOT sites increased to 129 ± 15 μV after day 15, while the average signal amplitude of units recorded on uncoated sites did not change significantly (113 ± 13 μV, $p<0.001$). Consequently, the SNR of units recorded on PEDOT sites after day 15 was higher than the SNR of units recorded on uncoated sites, correlating directly to an increased number of sorted units (Figure 3.5).

The increase in signal amplitude on PEDOT sites after day 15 is most likely a function of decreased signal loss through the shunt impedance[5]. Similarly, a decrease in signal loss through the shunt impedance should increase the amplitude of measured biological noise. As a result, the noise amplitude across PEDOT sites approached the noise amplitude across control sites; the expected decrease in thermal noise caused by reduced impedance was compensated for by an increase in measured biological noise.

Functional Significance of Reduced Initial Impedance on Single Unit Recordings

Prior to implantation and over the first three days following surgery, every PEDOT site in this study registered a lower measured noise amplitude than the lowest measured noise amplitude for a control site. This result is likely attributable to the large difference in 1 kHz impedance seen between PEDOT and control sites during this period. After day 3, there was an equivalent increase in impedance on both PEDOT and control sites,

[5] Additionally, conductive polymer coatings grow outward from the normally planar recording site to create a hemispherical electrode site, enhancing the site's ability to detect neurons in the periphery (Cui et al, 2001). The rough topography of a conductive polymer film has also been hypothesized to promote neural growth in comparison to planar sites (Cui et al, 2001). Over multiple animals, these effects may create an additional increase in both average signal amplitude as well as the average measured amplitude of biological noise sources.

indicating a global immune response affecting the electrical characteristics of PEDOT and control sites equally. As site impedances increased by 0.5 - 1 MΩ with the encapsulation of the probe, the ratio of average impedance at 1 kHz between control and PEDOT sites decreased from the 10 to 1 *in vitro* value to 2 to 1. Consequently, the benefit of electrochemically depositing PEDOT films in order to improve single-unit recordings was mitigated. This result is not surprising considering that the expected difference in thermal noise and signal loss through shunt impedance between PEDOT and control sites depends on the magnitude of this ratio.

Although a statistically significant increase in signal to noise and number of recorded units was evident using a large number of recording sites over an extended period of time, the improvement in recordings for individual subjects on specific days was not always significant. Alternative methods intended to reduce the initial impedance of neural recording electrodes will also likely have their efficacy diminished by the contribution of encapsulation to recording site impedance. Reducing initial impedance is of some benefit, but these results suggest that the single largest determinant in effectively isolating a single-unit potential in a chronic setting is distance from recording site to neuronal source.

Artifact in LFP Recordings

Low frequency noise in LFP recordings is often the result of either motion artifact or thermal noise. As noted earlier, thermal noise is proportional to the square root of impedance across a frequency band. Standard iridium electrodes are designed to transduce ionic current into electronic current via the formation of a non-faradaic

capacitive double layer. The impedance of this capacitive double layer at a given frequency is $1/j\omega C$, where ω is the frequency and C is the double layer capacitance. LFP recordings typically have frequency components in the 3-90 Hz range, much lower than the 350-5000 Hz range of action potentials. Not surprisingly, the impedances of iridium microelectrodes at frequencies relevant for LFP recordings are substantially higher than their impedances at 1 kHz (Figure 3.4).

Recording sites deposited with PEDOT films in this study routinely exhibited much lower impedances than iridium control sites at low frequencies (Figure 3.4). As noted earlier, ions can more effectively infiltrate the porous PEDOT at lower frequencies, creating a larger accessible interfacial area, and therefore reducing low frequency impedance by increasing recording site capacitance and lowering charge transfer resistance (Cui et al. 2001). At the six week mark, the ratio in average impedance at low frequency between control and PEDOT sites was still quite large. A large decrease in low frequency impedance should correlate directly to a reduction in thermal noise across lower frequency bands. However, the relative magnitude of thermal noise in proportion to the magnitude of the desired LFP signal of interest is unknown. Furthermore, thermal noise should be random in nature, whereas the low frequency artifact visually evident across control sites was highly correlated (Figure 3.7).

Artifact that is highly correlated across multiple sites suggests one outside source of artifact influencing the recordings on all of those sites, such as motion artifact. Motion artifact is often the result of a disturbance in the established capacitive double layer at the interface between the recording site and the tissue. One possible source of motion

artifact is movement of the electrode shanks with respect to the surrounding tissue (Subbaroyan et al. 2005). Movement of the electrode shanks can cause a disturbance in the ionic layer at multiple recordings sites simultaneously. Because the impedance of iridium electrode sites at low frequencies is quite high, disturbing the ionic interface could result in large variations in measured potential. PEDOT coated recording sites, having considerably reduced low frequency impedance, would therefore register smaller variations in measured potential when the ionic interface is disturbed.

Unlike non-faradaic noble metal microelectrodes, PEDOT films are designed to transduce ionic current into electronic current via a reversible faradaic redox reaction. The increased impedance of the non-faradaic capacitive double layer at low frequencies may cause a bias towards a faradaic mechanism of conduction for PEDOT films. Faradaic electrode reactions are governed by the concentration of product and reactants species and the mobility of electrons and ions in their respective mediums. Porous PEDOT films are designed to promote fast ion exchange at the interface between recording site and surrounding tissue (Cui et al. 2001; Yang et al. 2005). As a result, motion of the electrode with respect to the surrounding tissue may not significantly disturb the local concentration of product and reactants. Consequently, LFPs taken with PEDOT sites may be more resistant to motion artifact.

Reducing the amount of low frequency artifact in LFP recordings has a number of potential benefits. First, removing artifact closer to the source is always preferential to digital filtering. Second, digital filtering of the low frequency artifact may not be an option for real-time applications. Third, large low frequency artifact can cause the

recording amplifier to saturate, preventing any viable signal from being registered. Finally, recording electrode low frequency drift is often a limiting consideration in device design.

Conclusions

Over the course of the study, recording sites deposited with a PEDOT film registered almost 40 percent more quality units than control sites, while minimizing the amount of low frequency artifact evident in LFP recordings. The modest tissue response, typical of cortical implants, resulted in an average 700 kΩ increase in impedance magnitude at 1 kHz across both PEDOT and control recording sites at six weeks. Consequently, the benefit of reduced noise and decreased signal loss through the shunt impedance as a function of lower initial impedance for PEDOT films was diminished. The dominating contribution to site impedance of the encapsulating sheath should similarly affect alternative methods of reducing initial recording site impedance. The results of this study indicate that surfactant-templated ordered PEDOT films remain suitable for obtaining high quality neural recordings out to six weeks. Future studies will investigate the long-term effectiveness of seeding PEDOT films with drugs tailored to alleviate the immune response and induce neural growth towards the electrode in order to maximize recording performance.

Acknowledgements

The authors of this paper would like to acknowledge all of members of the Neural Engineering Laboratory at the University of Michigan for their assistance in this study.

Specific thanks go to Elizabeth Nunamaker and Erin Purcell for histological assistance, Rachel Miriani and Jey Subbaroyan for surgical assistance, and Rio Vetter, Matt Johnson, and Nick Langhals for invaluable advice throughout the course of the study. David C. Martin acknowledges partial support provided by NIH NINDS-N01-NS-1-2338 and NSF DMR 0084304, NSF DMR 0518079.

References

Abbott LF, and Salinas E. Vector Reconstruction from Firing Rates. *Journal of Computational Neuroscience* 1: 89–107, 1994.

Anderson DJ, Najafi K, Tanghe SJ, Evans DA, Levy KL, Hetke JF, Xue XL, Zappia JJ, and Wise KD. Batch-fabricated thin-film electrodes for stimulation of the central auditory system. *IEEE Trans Biomed Eng* 36: 693-704, 1989.

Beck F, Braun P, and Oberst M. Organic Electrochemistry in the Solid State-Overoxidation of Polypyrrole. *Berichte Der Bunsen-Gesellschaft-Physical Chemistry Chemical Physics* 91: 967-974, 1987.

Beiko J, and Cain DP. The effect of water maze spatial training on posterior parietal cortex transcallosal evoked field potentials in the rat. *Cereb Cortex* 8: 407-414, 1998.

Bezdek JC. *Pattern recognition with fuzzy objective function algorithms*. New York: Plenum Press, 1981, p. xv, 256.

Biran R, Martin DC, and Tresco PA. Neuronal cell loss accompanies the brain tissue response to chronically implanted silicon microelectrode arrays. *Exp Neurol* 195: 115-126, 2005.

Black J. *Biological Performance of Materials: Fundamentals of Biocompatibility (3RD, REVISED & EXPANDED)* New York: Marcel Dekker 1999, p. 463.

Bobacka J, Lewenstam A, and Ivaska A. Electrochemical impedance spectroscopy of oxidized poly(3,4-ethylenedioxythiophene) film electrodes in aqueous solutions. *Journal of Electroanalytical Chemistry* 489: 17-27, 2000.

Brown EN, Frank LM, Tang D, Quirk MC, and Wilson MA. A statistical paradigm for neural spike train decoding applied to position prediction from ensemble firing patterns of rat hippocampal place cells. *J Neurosci* 18: 7411-7425, 1998.

Burke LD, and Shannell RA. An Investigation of Hyrdous Oxide Growth on Iridium in Base. *Journal of Electroanalytical Chemistry* 119-141, 1984.

Carmena JM, Lebedev MA, Crist RE, O'Doherty JE, Santucci DM, Dimitrov DF, Patil PG, Henriquez CS, and Nicolelis MAL. Learning to Control a Brain-Machine Interface for Reaching and Grasping by Primates. *PLoS Biology* 1: e42, 2003.

Craighead HG, Hames C D and Turner A M P. Chemical and topographic patterning for directed cell attachment. *Curr Opoin Solid State Mater Sci* 177-184, 2001.

Cui X, and Martin DC. Electrochemical deposition and characterization of poly(3,4-ethylenedioxythiophene) on neural microelectrode arrays. *Sensors and Actuators* B 89: 92-102, 2003.

Cui XY, Hetke JF, Wiler JA, Anderson DJ, and Martin DC. Electrochemical deposition and characterization of conducting polymer polypyrrole/PSS on multichannel neural probes. *Sensors and Actuators a-Physical* 93: 8-18, 2001.

Dobelle WH. Artificial vision for the blind by connecting a television camera to the visual cortex. *Asaio Journal* 46: 3-9, 2000.

Donoghue JP, Suner S, and Sanes JN. Dynamic organization of primary motor cortex output to target muscles in adult rats. II. Rapid reorganization following motor nerve lesions. *Exp Brain Res* 79: 492-503, 1990.

Dowell-Mesfin NM, Abdul-Karim MA, Turner AM, Schanz S, Craighead HG, Roysam B, Turner JN, and Shain W. Topographically modified surfaces affect orientation and growth of hippocampal neurons. *J Neural Eng* 1: 78-90, 2004.

Drake KL, Wise KD, Farraye J, Anderson DJ, and BeMent SL. Performance of planar multisite microprobes in recording extracellular single-unit intracortical activity. *IEEE Trans Biomed Eng* 35: 719-732, 1988.

Dunn JC. A Fuzzy Relative of the ISODATA Process and Its Use in Detecting Compact Well Compact Well-separated Clusters. *Journal of Cybernetics* 3: 32-57, 1974.

Fan Y W CFZ, Chen L N, Zhai Y, Xu Q Y, and Lee I S. Adhesion of neural cells on silicon wafer with nano-topographical surface. *Appl Surf Sci* 313-318, 2002.

Gerstein GL, Bloom MJ, Espinosa IE, Evanczuk S, and Turner MR. Design of a Laboratory for Multineuron Studies. *IEEE Trans Sustems, Man Cybern* 13: 668-676, 1983.

Glaser EM. *Separation of neuronal activity by waveform analysis*. New York: Academic, 1971, p. 77-136.

Glaser EM, and Marks WB. On-line separation of interleaved neuronal pulse sequences. *Data Acquisition Process Biol Med* 5: 137-156, 1968.

Harris KD, Henze DA, Csicsvari J, Hirase H, and Buzsaki G. Accuracy of tetrode spike separation as determined by simultaneous intracellular and extracellular measurements. *J Neurophysiol* 84: 401-414, 2000.

Henze DA, Borhegyi Z, Csicsvari J, Mamiya A, Harris KD, and Buzsaki G. Intracellular features predicted by extracellular recordings in the hippocampus in vivo. *J Neurophysiol* 84: 390-400, 2000.

Hitoshi Yamato MO, Wolfgang Wernet. Stability of polypyrrole and poly(3,4-ethylenedioxythiphene) for biosensor application. *Journal of Electroanalytical Chemistry* 397: 163-170, 1995.

Johnson MD, Otto KJ, and Kipke DR. Repeated voltage biasing improves unit recordings by reducing resistive tissue impedances. *IEEE Trans Neural Syst Rehabil Eng* 13: 160-165, 2005.

Karkkainen I, and Franti P. Dynamic Local Search for Clustering with Unknown Number of Clusters. In: *Int Conf on Pattern Recognition*. Quebec, Canada: August 2002, p. 240-243.

Kovacs GTA. Introduction to the theory, design, and modeling of thin-film microelectrodes for neural interfaces. In: *Enabling Technologies for Cultured Neural Networks*, edited by Academic) DASaTML1994, p. 121–165.

Kuffler SW. *A Cellular Approach to the Function of the Nervous System*. Sunerland, MA: Sinauer Associates, 1976.

Lewicki MS. A review of methods for spike sorting: the detection and classification of neural action potentials. *Network-Computation in Neural Systems* 9: R53-R78, 1998.

Liu X, McCreery DB, Carter RR, Bullara LA, Yuen TG, and Agnew WF. Stability of the interface between neural tissue and chronically implanted intracortical microelectrodes. *IEEE Trans Rehabil Eng* 7: 315-326, 1999.

Paik SJ, Park Y, and Cho DI. Roughened polysilicon for low impedance microelectrodes in neural probes. *Journal of Micromechanics and Microengineering* 13: 373-379, 2003.

Polikov VS, Tresco PA, and Reichert WM. Response of brain tissue to chronically implanted neural electrodes. *J Neurosci Methods* 148: 1-18, 2005.

Robinson DA. The electrical properties of metal microelectrodes. *Proceedings of the IEEE* 56: 1065, 1968.

Schlenoff JB, and Xu H. Evolution of Physical and Electrochemical Properties of Polypyrrole During Extended Oxidation. *Journal of the Electrochemical Society* 139: 2397-2401, 1992.

Schmidt CE, Shastri VR, Vacanti JP, and Langer R. Stimulation of neurite outgrowth using an electrically conducting polymer. *Proc Natl Acad Sci U S A* 94: 8948-8953, 1997.

Schmidt E, and Humphrey DR. Extracellular Single-unit Recording Methods. In: *Neurophysiological techniques*. Clifton, N.J.: Humana Press, 1990, p. 1-64.

Schmidt S, Horch K, and Normann R. Biocompatibility of silicon-based electrode arrays implanted in feline cortical tissue. *J Biomed Mater Res* 27: 1393-1399, 1993.

Schwartz AB. Cortical neural prosthetics. *Annu Rev Neurosci* 27: 487-507, 2004.

Selim Suner MRF, Carlos Vargas-Irwin, Kenji Nakata, and John P. Donoghue. Reliability of Signals from a Chronically Implanted, Silicon-based Electrode Array in Non-human Primate Primary Motor Cortex. *Submitted to IEEE* 2005.

Serruya MD, Hatsopoulos NG, Paninski L, Fellows MR, and Donoghue JP. Instant neural control of a movement signal. *Nature* 416: 141-142, 2002.

Shahriari K. Safe and effective techniques for surgically inserting flexible microelectrode arrays into the cortex. 2001, p. xv, 135 leaves.

Shoham S, and Nagarajan S. The Theory of Central Nervous System Recording. In: *Neuroprosthetics: Theory and Practice*, edited by Horch KW, and Dhillon GS. Singapore: World Scientific Publishing, 2003, p. 448-465.

St John PM, Kam L, Turner SW, Craighead HG, Issacson M, Turner JN, and Shain W. Preferential glial cell attachment to microcontact printed surfaces. *J Neurosci Methods* 75: 171-177, 1997.

Subbaroyan J, Martin DC, and Kipke DR. A finite-element model of the mechanical effects of implantable microelectrodes in the cerebral cortex. *Journal of Neural Engineering* 2: 103-113, 2005.

Szarowski DH, Andersen MD, Retterer S, Spence AJ, Isaacson M, Craighead HG, Turner JN, and Shain W. Brain responses to micro-machined silicon devices. *Brain Res* 983: 23-35, 2003.

Turner JN, Shain W, Szarowski DH, Andersen M, Martins S, Isaacson M, and Craighead H. Cerebral astrocyte response to micromachined silicon implants. *Exp Neurol* 156: 33-49, 1999.

Vetter RJ, Williams JC, Hetke JF, Nunamaker EA, and Kipke DR. Spike recording performance of implanted chronic silicon-substrate microelectrode arrays in cerebral cortex. *IEEE Transactions on Neural Systems and Rehabilitation Engineering* 52: 2004.

Wernet W. Freidburg: 1985.

Williams J, Rennaker R, and Kipke D. Long-term neural recording characteristics of wire microelectrode arrays implanted in cerebral cortex. *Brain Res Brain Res Protocol* 4: 303–313, 1999.

Williams JC. Performance of chronic neural implants: measurement, modeling and intervention strategies. 2001.

Yang J, Kim DH, Hendricks JL, Leach M, Northey R, and Martin DC. Ordered surfactant-templated poly(3,4-ethylenedioxythiophene) (PEDOT) conducting polymer on microfabricated neural probes. *Acta Biomaterialia* 1: 125-136, 2005.

Zouridakis G, and Tam DC. Identification of reliable spike templates in multi-unit extracellular recordings using fuzzy clustering. *Computer Methods and Programs in Biomedicine* 61: 91-98, 2000.

CHAPTER 4
COMMON AVERAGE REFERNCING

Abstract

In this study, we propose and evaluate a technique known as common average referencing (CAR) to generate a more ideal reference electrode for microelectrode recordings. CAR is a computationally simple technique, and therefore amenable to both on-chip and real-time applications. CAR is commonly employed in electroencephalography (EEG), where it is necessary to identify small signal sources in very noisy recordings. In order to investigate the efficacy of common average referencing, we compared CAR to both referencing with a stainless steel bone-screw, and a single microelectrode site. Data consisted of *in vivo* chronic recordings in anesthetized Sprague Dawley rats drawn from prior studies, as well as previously unpublished data. By combining the data from multiple studies, we have generated and analyzed one of the more comprehensive chronic neural recording datasets to date. Reference types were compared in terms of noise level, signal-to-noise ratio, and number of neurons recorded across days. Common average referencing was found to drastically outperform standard types of electrical referencing, reducing noise by more than 30 percent. As a result of the reduced noise floor, arrays referenced to a CAR yielded almost 60 percent more discernible neural units than traditional methods of electrical referencing. CAR should impart similar benefits to other microelectrode recording technologies – for example,

chemical sensing – where similar differential recording concepts apply. In addition, we provide a previously unpublished mathematical justification for CAR using Gauss-Markov theorem, and therefore help place the application of CAR into a theoretical context.

Introduction

Individual unit recordings from cortical neurons are dependent on separating the recorded extracellular action potential of a neuron from ambient sources of noise. These sources of noise can be correlated or uncorrelated across the electrode array, and include motion artifact, 60 Hz noise, instrumentation noise, thermal noise, and biological sources of noise (Horsch and Dhillon 2004; Kovacs 1994; Schmidt and Humphrey 1990; Shoham and Nagarajan 2003; Webster 1998). As cortical recording experiments move away from closed environments designed to reduce noise (e.g. Faraday cages) to more real-world situations (e.g. neuroprosthetic devices), these sources of noise become increasingly problematic (Horsch and Dhillon 2004; Kovacs 1994; Schmidt and Humphrey 1990; Shoham and Nagarajan 2003; Webster 1998).

Recording useful signal is dependent upon minimizing sources of noise through the use of an appropriate reference electrode (Horsch and Dhillon 2004; Kovacs 1994; Schmidt and Humphrey 1990; Shoham and Nagarajan 2003; Webster 1998). Typically either an additional microelectrode, or a large electrode such as a stainless steel bone-screw or stripped wire, is placed in a location with minimal cortical activity and used as a reference to subtract out correlated sources of noise (Blanche et al. 2005; Henze et al. 2000; Ludwig et al. 2006; Nelson et al. 2008; Vetter et al. 2004; Webster 1998; Williams

et al. 1999). Both microelectrode and large electrode references have their own specific advantages and disadvantages.

A large electrode is often preferred as a reference to minimize impedance (Horsch and Dhillon 2004; Kovacs 1994; Schmidt and Humphrey 1990; Shoham and Nagarajan 2003; Webster 1998). Thermal noise is proportional to impedance; therefore, less thermal noise is 'subtracted into' the recordings when using a low-impedance reference electrode (Horsch and Dhillon 2004; Kovacs 1994; Schmidt and Humphrey 1990; Shoham and Nagarajan 2003; Webster 1998). Unfortunately, there is a significant size and impedance mismatch between the reference and the recording sites on the microelectrode array when using a large reference electrode (Horsch and Dhillon 2004; Kovacs 1994; Schmidt and Humphrey 1990; Shoham and Nagarajan 2003; Webster 1998). Consequently, the representation of correlated sources of noise (such as motion artifact and 60 Hz noise) is different between the reference and the microelectrode sites, and therefore is not fully removed by reference subtraction (Horsch and Dhillon 2004; Webster 1998).

Due to the sheer size of the large electrode, the reference is typically placed on top of the dural surface, as opposed to implantation in cortical tissue (Ludwig et al. 2006; Vetter et al. 2004). By placing the reference in a location distal from the microelectrode sites, the difference between the voltage representation of correlated sources of noise at the reference and the microelectrode sites is increased (Horsch and Dhillon 2004; Webster 1998). In addition, there remains the possibility of the reference adding an ECoG (electrocorticogram) signal at the dural surface into the recordings.

As opposed to a large reference electrode, the use of an additional microelectrode implanted in cortical tissue as a reference presents alternative problems. Microelectrodes have greater impedance than their large counterparts, and therefore 'subtract in' more thermal noise to the recordings when used as a reference (Horsch and Dhillon 2004; Kovacs 1994; Ludwig et al. 2006; Schmidt and Humphrey 1990; Shoham and Nagarajan 2003). This problem is exacerbated in chronic applications, where the microelectrode reference becomes encapsulated in fibrous tissue, further increasing its impedance (Hochberg et al. 2006; Ludwig et al. 2006; Nicolelis et al. 2003; Otto et al. 2006; Polikov et al. 2005; Rennaker et al. 2007; Seymour and Kipke 2007; Spataro et al. 2005; Suner et al. 2005; Szarowski et al. 2003; Turner et al. 1999; Vetter et al. 2004).

When placed on the electrode array itself, a microelectrode reference may actually record neural signal, or uncorrelated biological noise caused by the activity of distal neural sources; this uncorrelated activity is then subtracted into the recordings (Horsch and Dhillon 2004; Webster 1998). If placed in a location to minimize the probability of recording neural activity (e.g. Corpus Callosum), the increased physical separation of the reference electrode from the microelectrode array decreases the correlation between noise at these two locations, and therefore decreases the utility of the reference (Horsch and Dhillon 2004; Webster 1998).

In this study, we introduce a technique known as common average referencing (CAR) to generate a more ideal electrode reference for single unit neural recordings. CAR is commonly employed in electroencephalography (EEG), where it is necessary to identify small signal sources in very noisy recordings (Cooper et al. 2003; Offner 1950; Osselton

1965). Unlike more complex methods of de-noising recorded signals *post-hoc* (Aminghafari et al. 2006; Bierer and Andersen 1999; Oweiss and Anderson 2001), common average referencing is a computationally simple technique, and therefore amenable to both on-chip and real-time applications. As the name implies, an average of all the recordings on every electrode site is taken and used as a reference (Cooper et al. 2003; Offner 1950; Osselton 1965). Through the averaging process, only signal/noise that is common to all sites (correlated) remains on the CAR[6]. Signal that is isolated on one site (single unit activity) does not appear on the CAR, unless the signal is so large as to dominate the average[7] (Cooper et al. 2003; Offner 1950; Osselton 1965). Uncorrelated random noise with a zero mean is minimized through the averaging process[8]. As the CAR provides an accurate representation of correlated noise at the location of the microelectrode array, but minimizes the contribution of uncorrelated noise sources, we hypothesize that common average referencing will improve neural recording quality with respect to both large and microelectrode references.

In order to investigate the efficacy of common average referencing, we compared CAR to both referencing with a stainless steel bone-screw and a single microelectrode site, using *in vivo* chronic recordings from a prior study (Ludwig et al. 2006) as well as previously unpublished data. By combining the data from multiple studies, we have generated and analyzed one of the largest chronic neural recording datasets to date. Reference types were compared in terms of peak-to-peak noise, signal-to-noise ratio, and number of units

[6] For example, 60 Hz noise and motion artifact.
[7] Given *n* electrodes, this occurs if the signal is *n* times larger than the peak-to-peak value of the noise floor.
[8] For example, thermal noise and distal neural sources.

recorded across days. Moreover, we provide a previously unpublished mathematical justification for common average referencing based on Gauss-Markov theorem, and therefore build a theoretical context for future CAR applications.

Methods

Microelectrodes

Twenty-one male Sprague-Dawley rats were implanted with twenty-six 16-channel chronic silicon 'Michigan' microelectrode arrays, using experimental procedures outlined previously (Ludwig et al. 2006; Vetter et al. 2004). Arrays consisted of four shanks, each with four evenly spaced iridium electrodes. Site and shank spacings were sufficient (100 μm or greater) to limit the probability of an individual neuron being recorded from multiple sites (Henze et al. 2000). All of the electrodes on a specific array were the same site size; electrode site sizes on an individual array were either 703 or 1250 μm^2.

The data for this study was drawn from previous (Ludwig et al. 2006) and ongoing studies aimed at evaluating the efficacy of the conductive polymer poly(3,4-ethylenedioxythiophene) (PEDOT) for improving neural recording quality. Towards that end, eight of the sites on each array were coated with PEDOT using various deposition methods and counter-ions, the details of which are beyond the scope of this study (Ludwig et al. 2006). The remaining eight sites were left uncoated as controls. Sites were stagger coated to prevent bias due to cortical depth or location (Ludwig et al. 2006).

Overall, PEDOT sites perform similarly to control sites in recording neural activity, with one exception. As noted in other studies, sites coated with PEDOT recorded activity

from a slightly larger number of neurons, primarily as a result of reduced thermal noise (Cui and Martin 2003; Ludwig et al. 2006; Yang et al. 2005). These slight differences in recording performance did not affect the results in this paper (See Results and Discussion for details).

Surgical Techniques

All of the arrays in this study were implanted in motor cortex, targeting cortical layer V. Initial anesthesia was administered via intra-peritoneal injections of a mixture of 50 mg/ml ketamine, 5 mg/ml xylazine, and 1 mg/ml acepromazine at an injection volume of 0.125 ml/100g body weight. Updates of 0.1 ml ketamine (50 mg/ml) were delivered as needed to maintain anesthesia during the surgery. Animals were secured to a standard stereotaxic frame, and three stainless steel bone-screws were inserted into the skull. The electrode connector was grounded to a bone-screw over parietal cortex using a stainless steel wire.

A craniotomy approximately 3 mm by 2 mm was made over the target area (target location 3.0 mm anterior to bregma, 2.5 mm lateral from bregma, and 1.4 mm deep from the surface of the brain). Two incisions were made in the dura mater to create four flaps, which were subsequently folded back over the edge of the craniotomy. The electrodes were then hand inserted into the approximate target cortical area. Cortical depth was estimated using the known location of the electrode sites on the individual shanks in conjunction with the known length of the individual shanks. Next, the surface of the brain was covered with GelFoam® (Henry Schein, Inc., Miami, FL) for protection. The

silicon cable connector was covered with either remaining Gelfoam or Kwik-Sil silicone polymer (World Precision Instruments, Inc). The entire assembly excluding the connector was then enclosed using dental acrylic (Co-Oral-Ite, Dental Mfg. Co., Santa Monica, Ca). Finally, sutures were used to close the skin around the acrylic and triple-antibiotic ointment was applied. All procedures complied with the United States Department of Agriculture guidelines for the care and use of laboratory animals and were approved by the University of Michigan Animal Care and Use Committee.

Neural Recordings & Data Analysis

For eight of the animals in this study, recorded neural signals were acquired using a Plexon Multi-channel Neural Acquisition Processor (MNAP; Plexon Inc, Dallas, TX). For the remaining animals, signals were acquired using a TDT multi-channel acquisition system (Tucker-Davis Technologies, Gainesville, FL). Neural electrophysiological recordings for all sixteen channels were amplified and bandpass filtered; single and multi-unit recordings were sampled at either 40 kHz (Plexon), or 24414 Hz (TDT), and bandpass filtered from 450-5000 Hz. During recording sessions, animals were placed in an electrically shielded recording booth and multiple 30-second segments of continuous neural recordings were taken.

Neural recording segments were analyzed offline using custom automated MatLab (Mathworks Inc., MA) software, as described in detail elsewhere (Ludwig et al. 2006). In summary, an amplitude threshold window was set 3.5 standard deviations above and below the mean of the sample distribution. For each peak exceeding the threshold window, a 2.4 ms candidate waveform snippet centered on the absolute minimum of the

waveform was removed from the recorded segment and stored. The amplitude of the noise voltage for every recording site in each recorded segment was calculated after all candidate waveforms had been removed.

After initial principal component analysis and fuzzy C-means clustering (Ludwig et al. 2006), waveforms with a cluster membership index of greater than 0.8 were used to determine a mean waveform for a cluster. An interspike interval histogram for each cluster was generated and visually inspected for an obvious absolute refractory period as an additional measure of noise rejection. Signal amplitude for a cluster was defined as the peak-to-peak amplitude of the mean waveform for each cluster.

The signal-to-noise ratio (SNR) for a given cluster was defined as follows:

SNR = Signal Amplitude / (Peak-to-Peak Amplitude of the Noise Floor)

The peak-to-peak amplitude of the noise on a given site was calculated as six times the standard deviation of the recording after thresholded waveforms were removed, spanning approximately 99.7 percent of normally distributed noise data (Blanche et al. 2005). By using this method, the calculated signal-to-noise ratio and peak-to-peak noise amplitude on a given site was more consistent with a visual inspection of the recorded voltage traces (See Figures 4.2 and 4.3). For example, an SNR of 2 would indicate that the mean peak-to-peak amplitude of the signal was twice as large as the peak-to-peak amplitude of the noise floor. As the peak-to-peak amplitude of the noise floor for neural recordings is typically between six and ten times larger than the root mean square (RMS) value of the

noise floor (Blanche et al. 2005), SNR calculations for neural recordings based on the RMS of the noise floor non-intuitively inflate SNR values.

Clusters with a mean SNR of 1.1 or greater were considered discriminable units, as the signal amplitude of these clusters was sufficient to be reliably differentiated from the noise floor. Conversely, clusters generated by random outlying perturbations from sources of noise had mean SNR values of 0.9 or less. Although normally distributed noise sources will occasionally exceed the 3.5 standard deviation threshold by random chance, the average waveform generated by these noise sources returns to zero after crossing threshold (instead of exhibiting an immediate opposing peak). Consequently, the mean waveform of a noise cluster spans less than six standard deviations of the noise floor, resulting in a calculated SNR of less than 1. When adjusted for the difference between calculating SNR using peak-to-peak amplitude of the noise floor instead of RMS, an SNR of 1.1 or greater corresponded well with observations of 'moderate or better' unit quality based on SNR values from similar recording studies (Henze et al. 2000; Ludwig et al. 2006; Suner et al. 2005).

Isolating action potentials from an individual neuron using an individual recording site is inherently prone to classification errors (Harris et al. 2000; Lewicki 1998). The methodology employed in this study was intended to minimize these errors, and should accurately parallel the true number of underlying neural sources (Ludwig et al. 2006). The sorting routine produces similar results to manual sorting performed by experienced researchers over the same data sets, but with the advantage of being objective and automated (Ludwig et al. 2006).

Referencing Techniques

As noted previously, all recordings in this study were initially referenced to a stainless steel bone-screw (Screw) located over parietal cortex. Both the microelectrode reference and the common average reference (CAR) were implemented digitally after this initial reference subtraction.

Common Average Reference (CAR)

The most intuitive implementation of a CAR would be to reference a specific site to the sample by sample average of all of the remaining sites on the array. Unfortunately, this approach presents two problems with respect to real-time cortical recordings. First of all, each of the sixteen sites would have a unique reference, instead of a global reference shared by all sites. This presents an additional layer of complication in translating a CAR from a digital reference to an on-chip analog reference. Second, individual sites on a microelectrode array occasionally fail to function properly. Consequently, these bad sites must be identified and removed from the data set prior to generating a CAR.

To address these problems, the common average reference for each array was generated by taking the sample by sample average of *all* 'good' recording sites, creating one global reference for all sites (CAR-16). For a site to be considered 'good', the RMS of the noise floor on the site was required to be between 0.3 and 2 times the average RMS of the noise floor across all sixteen sites on the array. Sites identified as 'bad' through impedance spectroscopy (Ludwig et al. 2006) typically exhibited noise floors with an RMS value three to six times larger than the average RMS of the noise floor on good sites. This

simple methodology for eliminating 'bad' channels proved sufficient for removing the occasional 'bad' site from further analysis in an automated fashion.

As each 'good' recording site contributes to the average calculated for the 'global' CAR, the amplitude of all samples on a 'good' site is slightly decreased when referenced to the CAR. More specifically, given *n* good sites, the amplitude of each sample will be (*n-1)/n* times the original value (Cooper et al. 2003; Offner 1950; Osselton 1965). As *n* becomes larger, this scale factor approaches a value of 1. Since this scale factor affects both signal and noise equally, it does not affect the calculated signal-to-noise ratio on each site[9]. For comparison with other types of referencing, all CAR peak-to-peak noise values denoted in this study have been appropriately adjusted to compensate for this scale factor.

In order to assess the contribution of recording sites electrochemically deposited with a conductive polymer to the overall data, two additional common average references were created and applied to all data sets. One CAR was generated from only the conductive polymer sites on a given array, and the second CAR from only the control iridium sites. The CAR generated from conductive polymer sites was only applied as a reference to the conductive polymer sites; the CAR generated from control sites was only applied as a reference to the control sites. In this paper, data obtained using this secondary method is referred to as CAR-8.

---

[9] Although SNR is not affected by this scale factor, CAR improves SNR by removing noise common to all sites without adding uncorrelated noise.

Single-Best Microelectrode Reference

Cortical recordings are often taken in reference to an individual microelectrode site; consequently, we implemented an algorithm to identify the single-best microelectrode reference on an array to compare with common average referencing. As a single microelectrode may pick up single-unit activity, we first used our automated sorting algorithm in conjunction with CAR to identify candidate sites with no discernible unit activity[10]. Each of the candidate sites were then employed as a reference for the entire array on the *original* data set. The candidate microelectrode reference that created the lowest average noise floor across the array on a given day was selected as the single-best microelectrode reference. By identifying the single-best microelectrode reference for each array on a daily basis, we created a conservative comparison for common average referencing.

Statistical Analysis

Because the four types of referencing in this study were performed digitally on the same data sets, these data sets are highly correlated, precluding the use of standard ANOVA techniques. To accommodate the correlations between comparison groups, correlated t-tests were performed; a Bonferroni correction was applied to the tests for each group pair to control for experimentwise error rate. The Bonferroni correction is regarded as a very strict/conservative test of significance when comparing multiple groups. At an alpha

[10] Employing a common average reference was necessary to identify sites without unit activity, as the noise floor using the ground screw as a sole reference was sufficient to mask unit activity on many days.

value of .01, the Bonferroni correction required a *p*-value of less than .0017 for significance. Equality of variance was verified by the Levene statistic.

Results

Noise

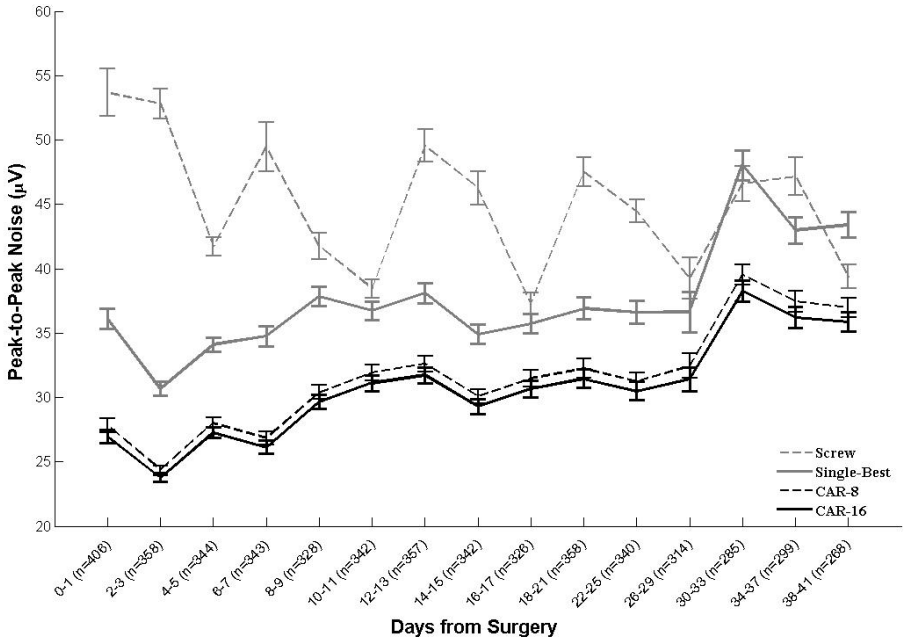

Figure 4.1: Noise across Days. Bars denote standard error of the data set on a given block of days. Number of sites on a given block of days, *n*, is listed on the x-axis. Over the course of the study, sites referenced to a common average reference exhibited 30 percent less noise than standard methods of referencing ($p < 10^{-20}$). Sites referenced to a ground screw placed over parietal cortex exhibited increased noise floor variability in comparison to referencing with CAR or the single-best microelectrode site. Noise floor amplitude calculated using CAR or single-best microelectrode site references decreased immediately following surgery and then increased afterwards, consistent with the trend in noise level found in prior studies (Williams, Rennaker et al. 1999; Schwartz 2004; Vetter, Williams et al. 2004; Ludwig, Uram et al. 2006).

Over the course of this study, the average peak-to-peak noise floor across all sites using CAR was 32.5 μVs (Figure 4.1), a significant improvement over referencing to either a stainless steel ground screw (45.9 μVs, $p < 10^{-20}$) or to the single-best microelectrode site on the array (40.7 μVs $p < 10^{-20}$). More specifically, every single recording site in the

study (*n = 5010)* exhibited a lower noise floor when referenced to the CAR in comparison to the single-best microelectrode reference. In all but three instances, the noise floor employing CAR was lower than referencing to a ground screw.

Using either CAR or single-best references, the trend in the average noise floor across sites following surgery paralleled the results of other microelectrode recording studies. The noise floor typically decreased over the days immediately following surgery, and then gradually increased over time. An increase in noise over time is expected, as the impedances of electrode sites are known to increase over time due to fibrous encapsulation, increasing the thermal noise on a site (Ludwig et al. 2006; Vetter et al. 2004; Williams et al. 1999).

In contrast to CAR or single-best references, the noise floor using the ground screw as a sole reference was considerably more variable. This variability can be explained by separating the recordings into two distinct cases. In the first case, the ground screw recordings were contaminated by one or more large sources of correlated noise (Figure 4.2). Both the CAR and single-best reference minimize the contribution of correlated noise sources, and therefore exhibit lower noise floors and more distinct unit activity than ground screw referencing when large sources of correlated noise are evident. As the ground screw is a poor match for the implanted microelectrode in terms of location, impedance, and geometry, it does not lower the contribution of correlated noise sources as effectively. The noise floor on electrode sites was larger when employing the single-best electrode reference as opposed to the CAR, as the single-best electrode subtracts in the uncorrelated noise from the single electrode site. Conversely, uncorrelated sources of

noise with a zero mean tend towards zero when averaged over all the sites on an array using CAR.

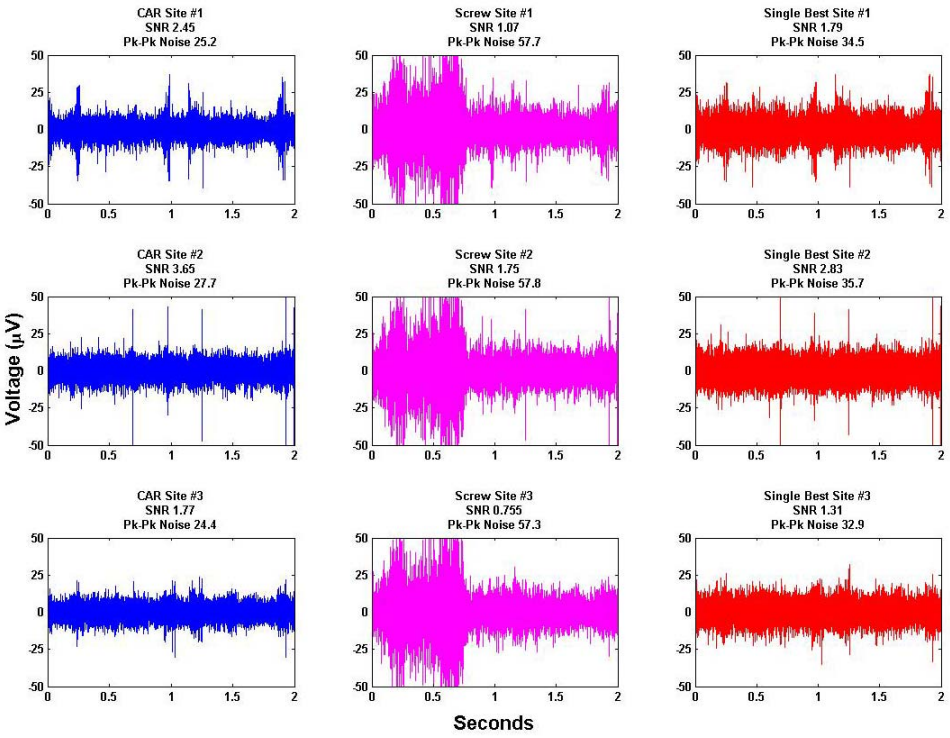

Figure 4.2: Representative Example of Recordings Contaminated by Correlated Noise. Column one depicts two seconds of high speed recordings, taken simultaneously across three sites on the same array, referenced to a common average reference (CAR). Column two depicts the same data set, referenced only to a stainless-steel screw placed above parietal cortex. Column three also depicts the same data set, but referenced to the single-best microelectrode reference on the array. Sites referenced to CAR exhibit a lower noise floor and higher signal-to-noise ratio than standard electrical references. When sites are referenced to the ground screw, an intermittent correlated noise source is evident that does not appear when employing either the CAR or single best microelectrode reference. This noise source is sufficient to completely obscure unit activity. Also note that despite the presence of large action potentials on site 2, traces of this signal are not evident on sites 1 and 3 when reference to CAR (See sites 1 and 3 screw and single best references over the same data set for comparison).

In the second case, the recordings were only minimally contaminated by correlated noise (Figure 4.3). In this case, the ground screw reference actually lowered the noise floor with respect to the single-best microelectrode reference. Ground screws used in this

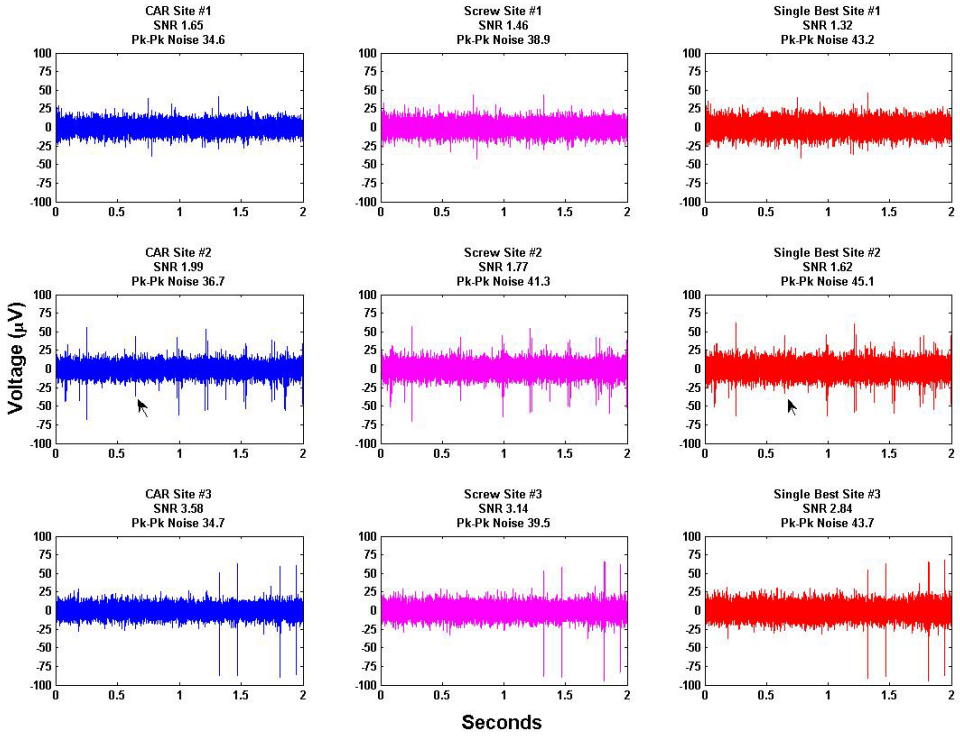

Figure 4.3: Example of Recordings with Low Correlated Noise. Column one depicts two seconds of high speed recordings, taken simultaneously across three sites on the same array, referenced to a common average reference (CAR). Column two depicts the same data set, referenced only to a stainless-steel screw placed above parietal cortex. Column three also depicts the same data set, but referenced to the single-best microelectrode reference on the array. Sites referenced to CAR exhibit a lower noise floor and higher signal-to-noise ratio than standard electrical references. In cases where large sources of correlated noise are not evident, the ground screw reference routinely outperformed the single-best reference in terms of noise level, signal-to-noise, and number of discriminable units. In these cases, common average referencing still outperformed referencing to either a ground screw or the single-best microelectrode site on the array. Arrows denote a neural signal evident on Site 2 when referenced to either CAR or single-best microelectrode reference. Note that the waveform has been distorted on the voltage axis, presumably a result of the increased noise floor when using the single-best microelectrode reference. Even if a neural unit is discernible from the noise, an increased noise floor means more waveform variability, limiting the efficacy of common sorting algorithms (Lewicki 1998).

study had impedances that were multiple orders of magnitude lower than implanted microelectrodes, and consequently subtracted less thermal noise into the recordings[11].

[11] Many students in our lab were surprised to note that digitally referencing an individual electrode site would often *increase* the noise floor across the array, and initially attributed this result to an equipment malfunction.

As only recordings referenced to the ground screw were significantly altered by the absence or presence of correlated noise, recordings referenced to the ground screw were considerably more variable[12]. The CAR, which minimized both correlated and uncorrelated sources of noise, dramatically outperformed the single-best and ground screw references in both cases.

Signal-to-Noise and Unit Activity

Calculating a meaningful average signal-to-noise ratio (SNR) of unit recordings for comparison between reference types was complicated by the fact that sites registered an overall greater number of discernible units with CAR (See end of Section). More specifically, the reduction in noise on CAR sites was sufficient to separate previously unapparent signals from the noise floor - instead of just increasing the SNR of already discriminable units. Therefore, comparing the 'average' SNR of all discriminable units was not representative of the true difference in SNR between reference types.

In order to calculate the 'true' difference in SNR between CAR and other types of referencing, we first used CAR in conjunction with our automated sorting algorithm to identify the location in time of all unit activity. The known location in time of unit activity was then used to calculate the mean signal amplitude for all reference types. Through this methodology, we were able to identify the location of signal that was previously obscured by the noise floor when not using CAR.

---

[12] **Note:** Within array variances when employing all types of referencing in this study were equivalent, as verified by the Levene statistic. Ground screw peak-to-peak noise values varied greatly between arrays, depending upon the presence of correlated noise sources.

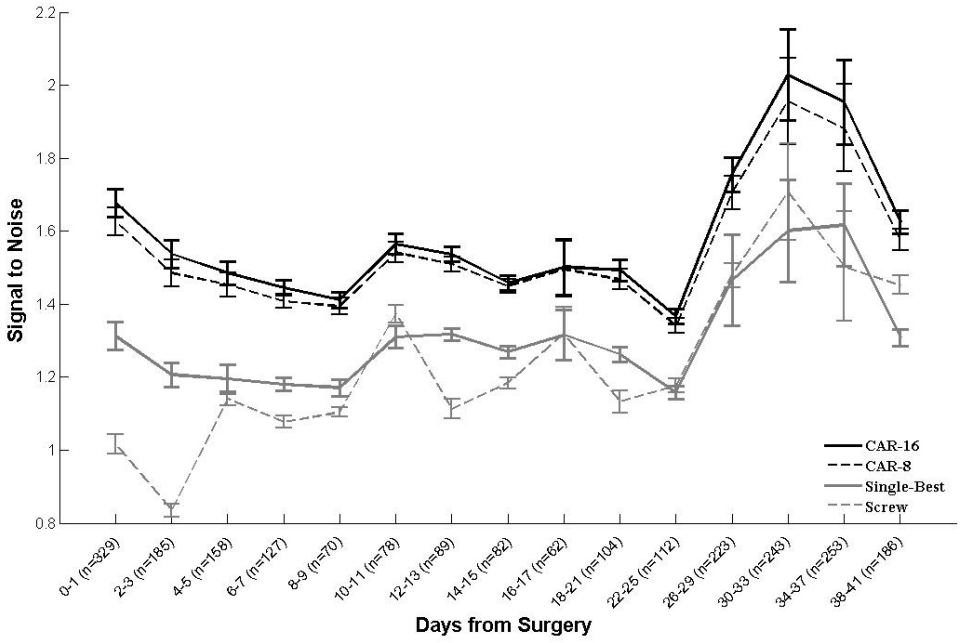

Figure 4.4: Signal to Noise across Days. Bars denote standard error of the data set on a given block of days. Number of units recorded on a given block of days, *n*, is listed on the x-axis. Over the course of the study, sites referenced to CAR exhibited a signal-to-noise ratio of 1.59, a significant improvement over referencing to either the single-best microelectrode site (1.31, $p < 10^{-10}$) or ground screw (1.24, $p < 10^{-10}$). Variability in signal to noise ratio across all types of reference increased towards the end of the study, concurrent with an increase in number of units recorded across all arrays. An increase in number of units recorded starting at six weeks post implantation has been noted in prior studies (Schwartz 2004; Ludwig, Uram et al. 2006).

Over the course of this study, sites referenced to CAR exhibited a higher signal-to-noise ratio than sites referenced to either a ground screw or single-best microelectrode reference ($p < 10^{-10}$, See Figure 4.4). The average SNR on CAR sites was 1.59, in comparison to 1.31 for sites referenced to the single-best microelectrode reference and 1.24 for sites referenced to a ground screw. As CAR does not alter the relative size of signal on a given site, this improvement in performance is attributable to the decreased CAR noise floor.

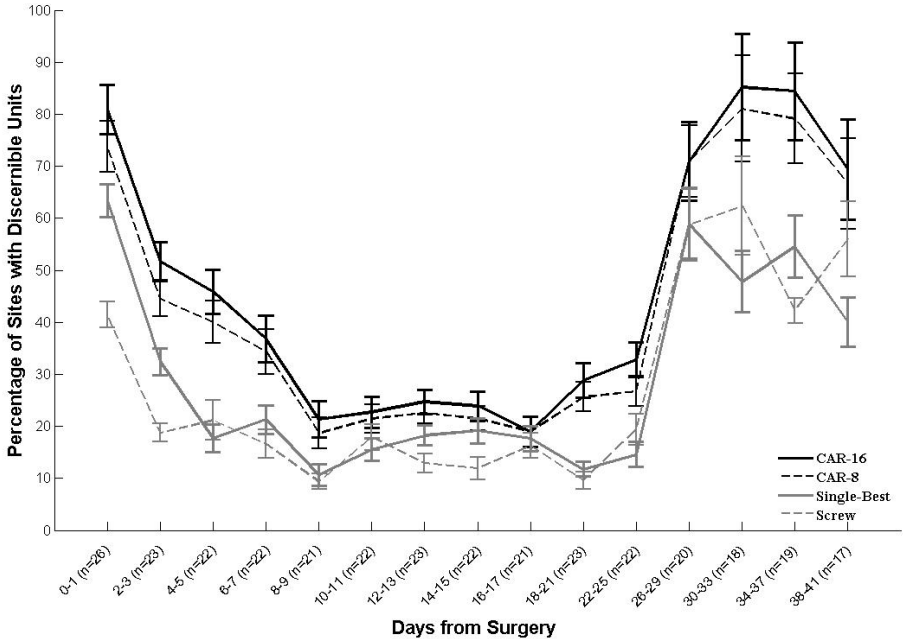

Figure 4.5: Percentage of Sites with Units over Days. Bars denote standard error of the data set on a given block of days. Number of arrays included in analysis, *n*, is listed on the x-axis. Over the course of the study, sites referenced to a common average reference yielded almost 60 percent more discernible units than when reference to standard electrical references. This increase in performance is attributable to a reduced noise floor, enhancing signal-to-noise ratio, and therefore increasing the number of discernible units. Unit recordings were strong initially, dipped dramatically in the days following surgeries, and returned to initial levels after the four week point. This trend in recording performance has been noted in previous recording studies (Schwartz 2004; Ludwig, Uram et al. 2006; Santhanam, Linderman et al. 2007).

Referencing with CAR both a) increased the signal-to-noise ratio of units already evident when referencing to the single-best microelectrode reference or the ground screw, and b) decreased the noise floor sufficiently to reveal units that were previously obscured when referencing to the single-best microelectrode or the ground screw. Consequently, there was a greater number of discernible units when referencing to CAR in comparison to a ground screw or single-best microelectrode reference ($p < 10^{-10}$, See Figure 4.5). Over the course of the study, an average of 46.5 percent of CAR sites exhibited discriminable unit activity, in comparison to 29.6 percent of the single-best sites and 27.46 percent of the ground screw sites. As with the improvement in SNR, this improvement is

attributable to the markedly decreased CAR noise floor. Consistent with previous studies (Ludwig et al. 2006; Santhanam et al. 2007; Schwartz 2004; Vetter et al. 2004; Williams et al. 1999), there was a notable decrease in unit activity in the days immediately following surgery, followed by an increase in unit activity after day fifteen.

Local Field Potential Recordings

Comprehensive quantification of the effects of CAR on local field potential recordings (LFPs) is beyond the scope of this study because of the difficulties in separating true LFP signal from noise. In general, LFPs referenced to a CAR were qualitatively 'cleaner' than LFPs referenced to a ground screw, with a marked reduction in 60-Hz noise. These results are not unexpected, as LFPs are similar in amplitude and frequency content to EEG signals, and common average referencing is commonly used to eliminate noise in EEG recordings (Cooper et al. 2003). As LFPs are routinely obtained using higher impedance microelectrodes than used for EEG recordings, common average referencing should create a larger reduction in noise for local field potential recordings. Care should be taken when using CAR for LFPs, however, as a common average reference will affect standard coherency analyses.

Discussion

Theoretical Justification of CAR Using Gauss-Markov Theorem

Multi-channel neural recordings can be described as an observed noisy signal, Y, which is composed of an unknown true signal, X, and an unknown noise, N. This general situation can be described by the following equation (Albert 1972; Stark and Woods 2002):

$$Y = AX + N, \qquad (1)$$

where Y is the $n \times 1$ vector of observed neural recordings across n channels, X is a $k \times 1$ vector representing the true signal, A is an $n \times k$ matrix ($n > k$) which maps X onto Y, and N is an $n \times 1$ normally distributed random noise vector with zero mean and covariance matrix K.

One useful approach for obtaining a 'good' estimate, $\grave{X}$, of X from the observed values of Y is to restrict $\grave{X}$ to be a linear function of Y:

$$\grave{X} = BY \qquad (2)$$

In this formulation, we want to determine the matrix B, a spatial filter that provides the *best linear unbiased estimate (BLUE)* of X based on Y.

The filter, B_i, for each channel, i, can be calculated as follows (Albert 1972; Stark and Woods 2002):

$$B_i = (A_i' K^{-1} A_i)^{-1} A_i' K^{-1} \qquad (3)$$

There are two simplifications that align this general solution with the present study.

1. Site spacing is sufficiently large to ensure that neurons are expressed on only one site. Consequently, A_i for each channel has the form [1, 0, 0, …, 0].

2. The noise model for each channel is identical, producing a covariance matrix K with equal diagonal values (1) and equal off-diagonal components (c).

Consequently, B for each channel has the form:

$$B_i = [1, \alpha, \alpha, \ldots, \alpha], \quad (4)$$

where $\alpha = - c/(1+(n-2)c)$.

As n increases, α approaches $-1/(n-1)$, leaving B_i as:

$$B_i = [1, -1/(n-1), -1/(n-1), \ldots, -1/(n-1)] \quad (5)$$

Placing this result into equation 2, obtaining the best linear unbiased estimate of X is equivalent to subtracting the average of all other channels from the current channel – in other words, use a common average reference. This formulation is generally true even if the diagonal and off-diagonal values vary across channels. Note that when c is large (near 1), c approaches $-1/(n-1)$ more quickly. This result is intuitive; when there is high-amplitude correlated noise across channels, referencing is particularly effective. When there is very little or no correlated noise across channels, employing a reference only 'subtracts in' uncorrelated noise from the reference to the other channels. Although common average referencing minimizes uncorrelated noise as a function of n, it does not remove it entirely. Consequently, referencing becomes counter-productive when there is no correlated noise between the reference and recordings sites.

Conductive Polymer Common Average Reference

As noted in the methods, two additional common average references were created and applied to all data sets in order to assess the contribution of recording sites electrochemically deposited with a conductive polymer to the overall data. One CAR was generated from only the conductive polymer sites on a given array, and the second CAR from only the control sites (CAR-8). The CAR generated from conductive polymer

sites was only applied as a reference to the conductive polymer sites; the CAR generated from control sites was only applied as a reference to the control sites.

If the noise between conductive polymer sites was more correlated than the noise between conductive polymer and control sites, one would expect the noise floor to decrease by generating separate CARs for conductive polymer and control sites. Instead, creating separate CARs marginally *increased* the noise floor (See Figure 4.1). This increase in noise is a result of using only eight sites to calculate the CAR, instead of sixteen. As shown ealier, employing CAR more closely approximates the best linear unbiased estimate of the signal as the number of channels increases. The average of uncorrelated sources of noise with a zero mean tends towards zero; the contribution of uncorrelated sources of noise becomes closer to zero when more sites are included to generate the average. Consequently, decreasing the number of sites used to calculate the CAR increases the contribution of uncorrelated noise sources.

Application of CAR to Tetrodes

Under certain circumstances, there is a possibility of registering neural signal on a single site so large that it dominates the average of all sites, and therefore appears on the common average reference (Cooper et al. 2003; Offner 1950; Osselton 1965). Accordingly, this neural signal would appear as a small false unit on all sites referenced to the CAR. For this to occur, given *n* recording sites, the average amplitude of the signal on a given site must be *n* times larger than the peak-to-peak amplitude of the noise floor (Cooper et al. 2003; Offner 1950; Osselton 1965). In this study, the signal amplitude on one site was never sufficient to dominate the average (See Figure 4.4); given sixteen

recordings sites on every array, the signal on a single site would have to regularly exceed sixteen times the peak-to-peak amplitude of the noise floor (Figures 4.2 and 4.3). As sites were separated by more than 100 microns in this study, the probability of recording signal from an individual neuron on multiple sites simultaneously was low (Henze et al. 2000).

For some neural recording applications, microelectrodes are manufactured with groups of four recording sites closely spaced to deliberately detect neural activity from an individual neuron simultaneously, known commonly as a tetrode configuration (Gray et al. 1995). As a result, the probability of signal from an individual neuron dominating the CAR average becomes much greater. If *m* sites out of *n* total electrodes record similar signal from an individual neuron, the average signal across *m* electrodes needs only to exceed *n*/*m* times the peak-to-peak amplitude of the noise floor to dominate the CAR average. One solution to this problem would be to increase *n*, the number of electrode sites used to calculate the CAR. In addition, a site or sites recording aberrantly large signal could simply be removed when calculating the common average reference (Cooper et al. 2003; Offner 1950; Osselton 1965).

When using a CAR, the potential contribution from a neural source on one electrode in a tetrode could diminish the measured potential from the neural source on the three remaining electrodes in the tetrode. This distortion should be constant across all four electrodes, and therefore should not adversely affect standard amplitude-based tetrode clustering techniques (Gray et al. 1995). The distortion could be problematic, however, when employing mathematical techniques to locate the neural source in space.

Additional Benefits of Reducing Noise

In some cases in this study, common average referencing provided a significant improvement in recording performance, in other cases CAR salvaged recordings that would have otherwise been unusable. Decreasing the noise floor not only increases the total number of units recorded across an array, but also decreases the variability of those units. Additional noise can alter the instantaneous shape of an action potential, potentially distorting the recorded waveform in principal component analysis space (PCA), deleteriously affecting common sorting techniques (Lewicki 1998) (Figure 4.3).

Perhaps even more significant, common average referencing mitigates the contribution of intermittent sources of correlated noise (Figure 4.2), such as motion artifact. These noise sources distort the relationship between neural firing rates and underlying physiological processes. This is especially problematic in real-time applications such as brain-machine interfaces, where intermittent artifact cannot be removed through *post-hoc* analysis. Reducing variability in the noise floor can also be critical for comparison studies of electrode performance. Significant differences in electrode performance as a function of electrode design or a drug treatment could potentially be masked by the large variance in noise floor from day to day.

Conclusions

According to standard differential recording theory, the reference electrode and the recording electrode must be matched as closely as possible in terms of geometry, electrode material, location, and electrical characteristics (Kovacs 1994; Schmidt and Humphrey 1990; Shoham and Nagarajan 2003; Webster 1998). These requirements

would seem to suggest the use of a single microelectrode as a reference, instead of an unmatched larger electrode. Unfortunately, due to the small size of a microelectrode, coupled with fibrous encapsulation endemic to long-term cortical implants (Edell et al. 1992; Johnson et al. 2005; Ludwig et al. 2006; Polikov et al. 2005; Schmidt et al. 1993; Szarowski et al. 2003; Turner et al. 1999; Vetter et al. 2004; Williams et al. 1999; Xindong et al. 1999), the impedance of a microelectrode reference adds significant uncorrelated thermal noise to cortical recordings (Kovacs 1994; Schmidt and Humphrey 1990; Shoham and Nagarajan 2003; Webster 1998). Moreover, the microelectrode reference could potentially register neural signal as well as uncorrelated biological noise – adding both to neural recordings. In contrast, a common average reference minimizes uncorrelated sources of signal and noise through averaging, while eliminating sources of noise common to all sites. Therefore, a common average reference more closely approximates the theoretical differential recording ideal.

Not surprisingly, common average referencing was found to drastically outperform standard types of electrical referencing over the course of this study, reducing noise by more than 30 percent. As a result of the reduced noise floor, arrays referenced to a CAR yielded almost 60 percent more discernible units than traditional methods of electrical referencing. However, these results need to be considered in context of the experimental methodology; recordings in this study were taken from anesthetized animals placed in a Faraday cage designed to reduce ambient noise. Recordings taken from awake and behaving animals in non-shielded environments would have much more noise. Consequently, the non-idealities of either single microelectrode or large electrode references would be further exacerbated. Under these circumstances the common

average reference would likely exhibit an even more dramatic increase in recording performance. Common average referencing may impart similar benefits to other microelectrode recording technologies – for example, chemical sensing (Burmeister and Gerhardt 2001; Dressman et al. 2002; Johnson et al. 2007) – where similar differential recording concepts apply.

Acknowledgements

The authors of this paper would like to acknowledge all of the members of the Neural Engineering Laboratory at the University of Michigan for their assistance in this study. Specific thanks go to Sarah Richardson-Burns for coating some of the probes used in this study, and to Erin Purcell, John Seymour, Matt Gibson and Hirak Parikh for invaluable advice and manuscript review. This work was supported by the NIH P41 Center for Neural Communications Technology (EB002030), Biotectix, LLC and the Whitaker Foundation.

References

Albert AE. *Regression and the Moore-Penrose pseudoinverse*. New York,: Academic Press, 1972, p. xiii, 180 p.

Aminghafari M, Cheze N, and Poggi JM. Multivariate de-noising using wavelets and principal component analysis. *Computational Statistics & Data Analysis* 50: 2381-2398, 2006.

Bierer SB, and Andersen DJ. Multi-channel spike detection and sorting using an array processing technique. *Neurocomputing* 26-27: 947-956, 1999.

Blanche TJ, Spacek MA, Hetke JF, and Swindale NV. Polytrodes: High-Density Silicon Electrode Arrays for Large-Scale Multiunit Recording. *J Neurophysiol* 93: 2987-3000, 2005.

Burmeister JJ, and Gerhardt GA. Self-Referencing Ceramic-Based Multisite Microelectrodes for the Detection and Elimination of Interferences from the Measurement of L-Glutamate and Other Analytes. *Analytical Chemistry* 73: 1037-1042, 2001.

Cooper R, Binnie CD, Osselton JW, Prior PF, and Wisman T. EEG, paediatric neurophysiology, special techniques and applications. In: *Clinical Neurophysiology Vol 2*, edited by Cooper R, Mauguiere F, Osselton JW, Prior PF, and Tedman BM. Amsterdam: Elsevier B.V, 2003, p. 8-103.

Cui X, and Martin DC. Electrochemical deposition and characterization of poly(3,4-ethylenedioxythiophene) on neural microelectrode arrays. *Sensors and Actuators* B 89: 92-102, 2003.

Dressman SF, Peters JL, and Michael AC. Carbon fiber microelectrodes with multiple sensing elements for in vivo voltammetry. *Journal of Neuroscience Methods* 119: 75-81, 2002.

Edell DJ, Toi VV, McNeil VM, and Clark LD. Factors influencing the biocompatibility of insertable silicon microshafts in cerebral cortex. *IEEE Trans Biomed Eng* 39: 635-643, 1992.

Gray CM, Maldonado PE, Wilson M, and McNaughton B. Tetrodes markedly improve the reliability and yield of multiple single-unit isolation from multi-unit recordings in cat striate cortex. *J Neurosci Methods* 63: 43-54, 1995.

Harris KD, Henze DA, Csicsvari J, Hirase H, and Buzsaki G. Accuracy of tetrode spike separation as determined by simultaneous intracellular and extracellular measurements. *J Neurophysiol* 84: 401-414, 2000.

Henze DA, Borhegyi Z, Csicsvari J, Mamiya A, Harris KD, and Buzsaki G. Intracellular features predicted by extracellular recordings in the hippocampus in vivo. *J Neurophysiol* 84: 390-400, 2000.

Hochberg LR, Serruya MD, Friehs GM, Mukand JA, Saleh M, Caplan AH, Branner A, Chen D, Penn RD, and Donoghue JP. Neuronal ensemble control of prosthetic devices by a human with tetraplegia. *Nature* 442: 164, 2006.

Horsch KW, and Dhillon GS. *Neuroprosthetics theory and practice*. River Edge, N.J.: World Scientific, 2004, p. xxv, 1261 p.

Johnson MD, Kao OE, and Kipke DR. Spatiotemporal pH dynamics following insertion of neural microelectrode arrays. *Journal of Neuroscience Methods* 160: 276-287, 2007.

Johnson MD, Otto KJ, and Kipke DR. Repeated voltage biasing improves unit recordings by reducing resistive tissue impedances. *Neural Systems and Rehabilitation Engineering, IEEE Transactions on [see also IEEE Trans on Rehabilitation Engineering]* 13: 160-165, 2005.

Kovacs GTA. Introduction to the theory, design, and modeling of thin-film microelectrodes for neural interfaces. In: *Enabling Technologies for Cultured Neural Networks*, edited by Academic) DASaTML1994, p. 121–165.

Lewicki MS. A review of methods for spike sorting: the detection and classification of neural action potentials. *Network-Computation in Neural Systems* 9: R53-R78, 1998.

Ludwig KA, Uram JD, Yang J, Martin DC, and Kipke DR. Chronic neural recordings using silicon microelectrode arrays electrochemically deposited with a poly(3,4-ethylenedioxythiophene) (PEDOT) film. *Journal of Neural Engineering* 3: 59, 2006.

Nelson MJ, Pouget P, Nilsen EA, Patten CD, and Schall JD. Review of signal distortion through metal microelectrode recording circuits and filters. *Journal of Neuroscience Methods* 169: 141-157, 2008.

Nicolelis MAL, Dimitrov D, Carmena JM, Crist R, Lehew G, Kralik JD, and Wise SP. Chronic, multisite, multielectrode recordings in macaque monkeys. *P Natl Acad Sci USA* 100: 11041-11046, 2003.

Offner FF. The EEG as potential mapping: The value of the average monopolar reference. *Electroencephalography and Clinical Neurophysiology* 2: 213-214, 1950.

Osselton JW. Acquisition of EEG data by bipolar unipolar and average reference methods: a theoretical comparison. *Electroencephalography and Clinical Neurophysiology* 19: 527-528, 1965.

Otto KJ, Johnson MD, and Kipke DR. Voltage pulses change neural interface properties and improve unit recordings with chronically implanted microelectrodes *Biomedical Engineering, IEEE Transactions on* 53: 333-340, 2006.

Oweiss KG, and Anderson DJ. Noise reduction in multichannel neural recordings using a new array wavelet denoising algorithm. *Neurocomputing* 38-40: 1687-1693, 2001.

Polikov VS, Tresco PA, and Reichert WM. Response of brain tissue to chronically implanted neural electrodes. *J Neurosci Methods* 148: 1-18, 2005.

Rennaker RL, Miller J, Tang H, and Wilson DA. Minocycline increases quality and longevity of chronic neural recordings. *Journal of Neural Engineering* 4: 2007.

Santhanam G, Linderman MD, Gilja V, Afshar A, Ryu SI, Meng TH, and Shenoy KV. HermesB: a continuous neural recording system for freely behaving primates. *IEEE Trans Biomed Eng* 54: 2037-2050, 2007.

Schmidt E, and Humphrey DR. Extracellular Single-unit Recording Methods. In: *Neurophysiological techniques*. Clifton, N.J.: Humana Press, 1990, p. 1-64.

Schmidt S, Horch K, and Normann R. Biocompatibility of silicon-based electrode arrays implanted in feline cortical tissue. *J Biomed Mater Res* 27: 1393-1399, 1993.

Schwartz AB. Cortical neural prosthetics. *Annu Rev Neurosci* 27: 487-507, 2004.

Seymour JP, and Kipke DR. Neural probe design for reduced tissue encapsulation in CNS. *Biomaterials* 28: 3594-3607, 2007.

Shoham S, and Nagarajan S. The Theory of Central Nervous System Recording. In: *Neuroprosthetics: Theory and Practice*, edited by Horch KW, and Dhillon GS. Singapore: World Scientific Publishing, 2003, p. 448-465.

Spataro L, Dilgen J, Retterer S, Spence AJ, Isaacson M, Turner JN, and Shain W. Dexamethasone treatment reduces astroglia responses to inserted neuroprosthetic devices in rat neocortex. *Exp Neurol* 194: 289-300, 2005.

Stark H, and Woods JW. *Probability and random processes with applications to signal processing*. Upper Saddle River, N.J.: Prentice Hall, 2002, p. xv, 689 p.

Suner S, Fellows MR, Vargas-Irwin C, Nakata GK, and Donoghue JP. Reliability of signals from a chronically implanted, silicon-based electrode array in non-human primate primary motor cortex. *Neural Systems and Rehabilitation Engineering, IEEE Transactions on [see also IEEE Trans on Rehabilitation Engineering]* 13: 524-541, 2005.

Szarowski DH, Andersen MD, Retterer S, Spence AJ, Isaacson M, Craighead HG, Turner JN, and Shain W. Brain responses to micro-machined silicon devices. *Brain Res* 983: 23-35, 2003.

Turner JN, Shain W, Szarowski DH, Andersen M, Martins S, Isaacson M, and Craighead H. Cerebral astrocyte response to micromachined silicon implants. *Exp Neurol* 156: 33-49, 1999.

Vetter RJ, Williams JC, Hetke JF, Nunamaker EA, and Kipke DR. Spike recording performance of implanted chronic silicon-substrate microelectrode arrays in cerebral cortex. *IEEE Transactions on Neural Systems and Rehabilitation Engineering* 52: 2004.

Webster JG. *Medical Instrumentation - Application and Design*. New York: John Wiley and Sons, Inc., 1998.

Williams J, Rennaker R, and Kipke D. Long-term neural recording characteristics of wire microelectrode arrays implanted in cerebral cortex. *Brain Res Brain Res Protocol* 4: 303–313, 1999.

Xindong L, McCreery DB, Carter RR, Bullara LA, Yuen TGH, and Agnew WF. Stability of the interface between neural tissue and chronically implanted intracortical microelectrodes. *Rehabilitation Engineering, IEEE Transactions on [see also IEEE Trans on Neural Systems and Rehabilitation]* 7: 315-326, 1999.

Yang J, Kim DH, Hendricks JL, Leach M, Northey R, and Martin DC. Ordered surfactant-templated poly(3,4-ethylenedioxythiophene) (PEDOT) conducting polymer on microfabricated neural probes. *Acta Biomaterialia* 1: 125-136, 2005.

CHAPTER 5
CONCLUSIONS AND FUTURE DIRECTIONS

Conclusions

The work presented in this dissertation was focused on the neural interface – bridging the gap between the true information content of neural coding useful for controlling a neuroprosthetic device (NPD), and the incomplete representation of this information received through extracellular recordings. In order to quickly translate the initial promise of neuroprosthetic studies into a practical clinical device, decoding algorithms need to be predicated on assumptions that are easily met outside of an experimental setting. Given present technology limitations, a low number of potentially unstable neuronal units must be assumed from day to day, driving a need for decoding algorithms which a) are not dependent upon a large number of neurons for control, b) are adaptable to alternative sources of neuronal input such as local field potentials, and c) require only marginal training data for day to day calibrations. Moreover, practical decoding algorithms must be able to recognize and eliminate poor training data, as well as when the user is not intending to generate a control output. Finally, every effort must be made to improve the quality and quantity of neural information sources used as an input to the decoding algorithm. The three studies which comprise this dissertation represent a significant advance in addressing all of the above issues.

Chapter 2 describes a Bayesian Maximum Likelihood Estimation strategy to isolate quality training data for a neuroprosthetic device. Simulation and *in vivo* results demonstrate that the standard eight-state center out task can be accomplished using as little as two neurons as input, and require as few as eight trials for training. In addition, untrained animals could quickly obtain accurate neuroprosthetic control using local field potentials and neurons in cingulate cortex – two neuronal sources not known to have a linear relationship to a movement parameter. Finally, the algorithm successfully recognized segments of 'No Control', and did not generate training data or a control output during these segments.

In Chapter 3, standard iridium electrodes were modified with the conductive polymer poly(3,4-ethylenedioxythiophene) (PEDOT) and evaluated *in vivo* for six weeks. PEDOT sites were found to outperform unmodified sites in terms of number of units recorded, noise levels, and artifact in local field potential recordings. However, the benefit obtained by minimizing initial electrode impedance through PEDOT application was mitigated over time by contribution of the foreign body response to impedance.

Chapter 4 details an *in vivo* comparison of common average referencing (CAR) to standard electrical referencing techniques used for single-unit neural recordings. CAR was found to reduce noise levels by over 30 percent in comparison to standard referencing strategies. This reduction in noise led to a 60 percent improvement in number of units recorded. CAR may impart similar benefits to similar microelectrode recording technologies – for example, chemical sensing. The benefits of CAR over

alternative referencing strategies should be even more dramatic in real-world environments where ambient noise sources are more prominent.

Future Directions and Preliminary Results

Using the bMLE Classifier to Isolate Training Data for a Kalman Filter

The work presented in Chapter 2 tested the utility of a bMLE classifier in isolating quality training data for a standard MLE decoding scheme. MLE provides discrete control output, instead of continuous analog control. To address the issue of continuous control, preliminary studies have been conducted using the bMLE classifier to isolate training data for a Kalman filter (Gage et al. 2005; Maybeck 1979; Wu 2002).

Briefly, the Kalman filter is a mathematical procedure that provides an efficient computational means to estimate the state of a process based on noisy Gaussian observations (Gage et al. 2005; Maybeck 1979; Wu 2002). The observations are the binned neuronal firing rates, which can be assumed to be Gaussian distributed provided that unit firing rates are sufficiently high. The position of the output device is modeled as a system state variable x_k, where k is an index of time (k = 1, 2, . . . , K; where K is the number of 200 ms time steps in a trial). The position x_k is assumed to propagate in time according to the following equation:

$$x_k = \mathbf{A}x_{(k-1)} + w_{(k-1)}, \qquad (1)$$

where **A** relates the prior output position of the device to the current position, and w is a white noise term that is assumed to have a normal probability distribution, i.e $w_k \sim N(0,\mathbf{W})$.

Neuronal firing rates are collected in 200 ms bins and modeled as an observed noisy response to the unobserved state process. The linear relationship between the output position of the device (x_k) and the observed firing rates of the recorded neurons (z_k) is

$$z_k = \mathbf{H}x_k + q_k, \qquad (2)$$

where z_k is a C x 1 vector of firing rates from C neurons, **H** is a C x 1 vector that linearly relates the output position of the device to z_k. Again, the noise in the observation is assumed to have zero mean and is normally distributed, i.e $q_k \sim N(0,\mathbf{Q})$.

The Kalman filter predicts the current position of the device x_k, by determining which x_k would minimize the least squared error in these two equations (Maybeck 1979; Wu 2002). Unlike standard linear filters, a standard Kalman filter also utilizes the last known position, velocity, and acceleration of a subject's arm in motion – in conjunction with the previously determined linear relationship between these three variables - to refine the current prediction of arm position. Whereas the positional output generated by standard linear filters can jump dramatically from neural observation to neural observation, the Kalman filter output is reasonably governed by the previously determined kinematic restrictions of arm movement.

Our earlier work explored the possibility of creating a 'naïve' Kalman filter – a Kalman filter not predicated on *a priori* movement measurements (Gage et al. 2005). In this setup, the animal was always assumed to be attempting to generate neural control during a response window (Gage et al. 2005). Training data for the Kalman filter on each trial was chosen by selecting an appropriate time lag in the response window (Gage et al. 2005). The optimum time lag for each trial was determined as the time where a single

neuronal unit evidenced the largest correlation to the expected device movement over each trial (Gage et al. 2005). This study was novel in that it was the first demonstration of rudimentary cortical control without the need for movement measurements for algorithm calibration. Unfortunately, the decoding methodology was sub-optimal in that a) noise induced false correlations, generating bad training data, b) periods of No-Control generated bad training data, and c) the **A** matrix was assumed to be the identity matrix, as no prior positional measurements were available from which to calculate **A**, violating a basic assumption of the Kalman filter (Gage et al. 2005).

In order to improve upon these non-idealities, the bMLE classifier was substituted for the *ad-hoc* correlation methodology used to identify training data for the Kalman filter. In addition, estimates of **A** and **W** were obtained using pre-recorded movements of the neural output device driven by a human controlled joystick (mouse). This methodology was analogous to incorporating the real movement restrictions of a prosthetic arm to limit the predictions of the neuronal output signal, instead of translating the kinematic restrictions of real movement to the movement of the prosthetic. Preliminary tests were conducted using the *in vivo* neural unit data detailed in Chapter 2 as an input to this modified Kalman filter, and off-line performance on the center-out task employing the modified Kalman was simulated. Initial analysis indicates that the output performance of the modified Kalman on the center-out task almost exactly mimics the performance of the Maximum Likelihood Estimator, given the same neural data sets as an input.

PEDOT Coatings to Facilitate Smaller Electrode Sites

The utility of implantable microelectrode arrays is currently limited by the size of the individual electrode sites for a number of reasons. First, smaller electrode sites would facilitate the development of more densely packed microelectrode arrays. At present, researchers are limited to sampling from a few neurons out of the billions of neurons which execute function in the brain. As a result, the study of how large networks of neurons interact to produce biologically relevant behaviors is severely hampered. In order to produce statistically significant conclusions about the neurological underpinnings of behavior, the ability to record reliably from larger numbers of neurons over smaller volumes is of paramount importance. Second, smaller electrode sites facilitate the design of smaller arrays, which in turn cause less damage upon implant. Recent studies indicate that probe dimensions which are smaller than 12 microns may minimize the reactive cell responses which negatively impact long-term neural recordings (Bernatchez et al. 1996; Sanders et al. 2000; Seymour and Kipke 2007). However, decreasing the size of an electrode site proportionally increases the impedance, which can degrade recordings. Typically, electrodes with impedances of 5 MΩ or greater have levels of thermal noise and shunt loss that make recording from individual neurons problematic (Hetke et al. 1994; Najafi et al. 1990; Robinson 1968).

In a preliminary study, we investigated the potential of using PEDOT to lower the impedance of small, gold recording electrodes with initial impedances outside of the effective range. Three rats were implanted with 4-shank, 16-channel arrays with sites of alternating PEDOT coatings, and neural recordings were monitored over 7 days. Control

site 1-kHz impedances ranged between 6-10 MΩ, whereas the sites coated with PEDOT

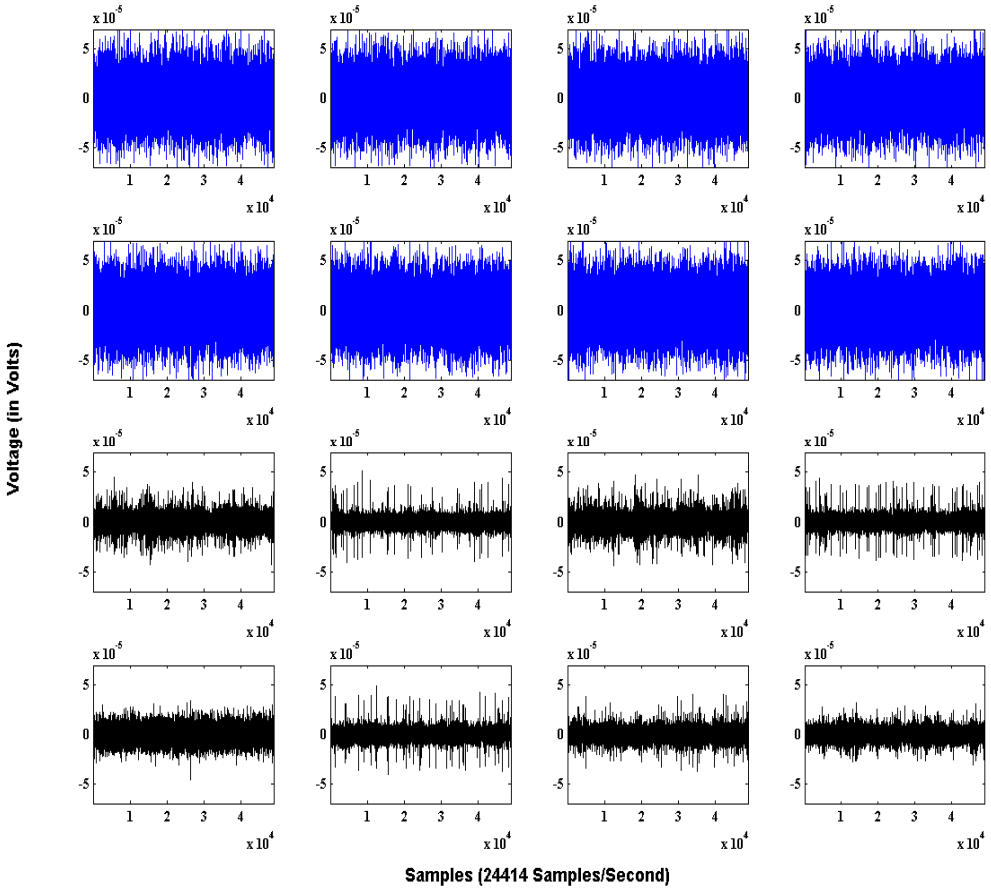

Figure 5.1: Representative Recordings from PEDOT and Control Small Sites on the Same Array. Control sites are in blue, and consisted of gold 177 μm^2 sites with initial impedances in the 6-10 MΩ range. Eight of the control sites were modified with surfactant templated PEDOT (denoted in black), bringing site impedances down to the 0.4-0.6 range. The noise floor on the control sites is sufficient to obscure all neural activity, whereas the PEDOT sites exhibit a much lower noise floor, as well as obvious spiking activity across many of the sites.

ranged between 0.3-0.6 MΩ. As expected, control sites were unable to record well-isolated unit activity, primarily as a result of a dramatically increased noise floor. Conversely, sites coated with PEDOT were able to consistently record high-quality neural activity, and exhibited a much lower noise floor than controls (Figure 5.1). These results indicate that PEDOT coatings can be used to reduce the impedances of small electrode sites into effective recording ranges.

Concluding Remarks

For neuroprosthetic devices to provide a robust clinical benefit, researchers must move away from 'proof of concept' experiments and towards developing a well-engineered end- product. Despite the amazing successes predicated upon microelectrode recording technology, the underlying electrode – along with our understanding of the electrode – has remained virtually unchanged over the last fifty years. In essence we are still placing a partially stripped insulated wire into the brain to register the electric field generated by neuronal action potentials. In proof of concept experiments, electrodes only needed to provide stable neural recordings for enough time to complete the experiment. Consequently, there was no drive to improve the underlying electrode technology; inconsistent performance was sufficient to conduct the experiment.

Electrodes that perform inconsistently are not sufficient, however, to realize a clinically useful neuroprosthetic device. This point was aptly demonstrated in the first human neuroprosthetic study by Hochberg et al, where neural recordings vanished after ten months, rendering the neuroprosthetic device inert (Hochberg et al. 2006). Even prior to losing neural recordings, the utility of the neuroprosthetic device was not sufficient to satisfy the expectations of the patient.

Transitioning from 'proof of concept' experiments to fully realized clinical products will require a renewed dedication to understanding the basic theory behind electrode technology. Neural unit recordings, local field potential recordings, and even impedance spectroscopy are theoretically based on an underlying stable electrode open circuit potential. Moreover, the open circuit potential of the microelectrode needs to match the

open circuit potential of the electrical ground to prevent a dc offset. However, it is well known that protein deposition on a metal creates an unstable open circuit potential. In addition, the pulsatile motion of the brain resulting from breathing and blood pressure changes constantly disturbs the electrode/electrolyte equilibrium condition. The ramifications of these facts on traditional electrode performance have yet to be explored in an acute setting, much less a long-term *in-vivo* environment. For non-traditional electrodes, such as conductive polymers coatings seeded with biomolecules to mitigate the immune response, basic open circuit potential measurements are rarely performed *in-vitro* – much less *in-vivo*.

A similar return to basics is necessary to understand how the foreign body response to the implanted electrode influences electrophysiogical recording measurements. While it is know that a glial scar forms around the implanted array, and neuronal death occurs in the vicinity of the electrode, these histological measurements have not been directly correlated to neuronal signal, the noise floor, or recorded local field potentials. To understand the failure modes of these electrodes, histological performance metrics must be evaluated in terms of electrophysiological performance metrics, otherwise the true relevance of these histological findings remains unknown.

Along with a renewed dedication to basic theory, a push towards more clinical data must be made before we can manufacture neuroprosthetic devices that are well-engineered to a patient's design requirements. There have only been a handful of human patients implanted with microelectrodes successful in achieving neural control of a neuroprosthetic device. Moreover, this control was limited in terms of utility of

movement and longevity. Current generation neuroprosthetic devices are focused on making incremental improvements based off of the expected limitations inherent in transitioning from an experimental environment to a functioning clinical device. However, until more of these devices are tested in a clinical setting, practical feedback from the end-user is severely limited. Only through large scale day-to-day testing in a clinical setting can the current issues with neuroprosthetic devices be clearly defined, and eventually rectified. One thing is certain, however – neuroprosthetic devices are dependent upon the quality and stability of neuronal inputs. Electrodes which reliably provide stable neural recordings for periods of greater than two years are an absolute necessity before a clinically useful neuroprosthetic device can be realized.

References

Bernatchez SF, Parks PJ, and Gibbons DF. Interaction of macrophages with fibrous materials in vitro. *Biomaterials* 17: 2077-2086, 1996.

Gage GJ, Ludwig KA, Otto KJ, Ionides EL, and Kipke DR. Naive coadaptive cortical control. *J Neural Eng* 2: 52-63, 2005.

Hetke JF, Lund JL, Najafi K, Wise KD, and Anderson DJ. Silicon ribbon cables for chronically implantable microelectrode arrays. *Biomedical Engineering, IEEE Transactions on* 41: 314-321, 1994.

Hochberg LR, Serruya MD, Friehs GM, Mukand JA, Saleh M, Caplan AH, Branner A, Chen D, Penn RD, and Donoghue JP. Neuronal ensemble control of prosthetic devices by a human with tetraplegia. *Nature* 442: 164, 2006.

Maybeck PS. *Stochastic Models, Estimation and Controls*. New York: Academic, 1979.

Najafi K, Ji J, and Wise KD. Scaling limitations of silicon multichannel recording probes. *Biomedical Engineering, IEEE Transactions on* 37: 1-11, 1990.

Robinson DA. The electrical properties of metal microelectrodes. *Proceedings of the IEEE* 56: 1065, 1968.

Sanders JE, Stiles CE, and Hayes CL. Tissue response to single-polymer fibers of varying diameters: evaluation of fibrous encapsulation and macrophage density. *J Biomed Mater Res* 52: 231-237, 2000.

Seymour JP, and Kipke DR. Neural probe design for reduced tissue encapsulation in CNS. *Biomaterials* 28: 3594-3607, 2007.

Wu W, Black, M. J., Gao, Y., Bienenstock, E., Serruya, M., Shaikhouni, A., Donoghue, J. P. Neural decoding of cursor motion using a Kalman filter. *Neural Information Processing Systems, NIPS Vancouver, BC* 2002.

APPENDIX A
TRANSLATING CURRENT NEURAL STATE INTO A FEEDBACK TONE

In order to generate the frequency and intensity of the auditory cursor representative of the subject's present neural state R, equation 4 (Chapter 1) was used to generate the probability of baseline and each of the target tones based on R. The location of the auditory cursor on the two-dimensional plane defined by frequency and intensity (see Figure 2.1) was determined by the following equations:

$$Cursor_{freq} = \rho(Base|R) * Base_{freq} + \sum_{i=1}^{i=8} \left(\rho(Target\ Tone_i|R) * Target\ Tone_{i\ freq}\right) Cursor_{intensity}$$

$$= \rho(Base|R) * Base_{intensity} + \sum_{i=1}^{i=8} \left(\rho(Target\ Tone_i|R) * Target\ Tone_{i\ intensity}\right)$$

Notice that as the probability of a specific target tone given the observed response R approached one, the frequency and intensity of the auditory cursor approached the frequency and intensity of that target tone.

APPENDIX B
ADJUSTING THE LENGTH OF THE MLE HISTORY

The number of observed response vectors, R, stored in the history for each target tone was adjusted based on the subject's performance over the last twenty presentations of the target tone using the following equation:

$$Number\ of\ R_{Target\ Tone\ i} = 5 * ceil(20 * Percent\ Correct_{Target\ Tone\ i})$$

For example, if the percent correct over the last twenty presentations of target $tone_2$ was 54, the number of observed responses R stored in the history for target $tone_2$ would be 55. The mean neural response for target $tone_2$, M_2, was then calculated as the mean of all R stored in the history for target $tone_2$.

This strategy was adopted to allow the subject to adopt new neural classes quickly during periods of poor performance for a given tone, while keeping the neural class for each target tone consistent during periods of strong performance.